# ENHANCEMENT OF CEDIRANIB ANTI-ANGIOGENIC/ANTI-TUMOR EFFICACY IN INTRACRANIAL MOUSE GLIOMA

By

Merryl Roland Lobo

A DISSERTATION

Presented to the Department of Biomedical Engineering
of the Oregon Health & Science University
School of Medicine
in partial fulfillment of
the requirements for the degree of

Doctor of Philosophy
in Biomedical Engineering

September 2013

Department of Biomedical Engineering
School of Medicine
Oregon Health & Science University

---

CERTIFICATE OF APPROVAL

---

This is to certify that the Ph.D. dissertation of
Merryl Roland Lobo
has been approved

---

Martin M. Pike, Ph.D.
Associate Scientist, Thesis Advisor

---

Charles S. Springer, Ph.D.
Senior Scientist

---

Owen J. T. McCarty, Ph.D.
Associate Professor

---

Monica T. Hinds, Ph.D.
Associate Professor

---

Leslie L. Muldoon, Ph.D.
Associate Professor

# TABLE OF CONTENTS

# List of Figures

**Chapter 1: Introduction**



**Chapter 2: Quinacrine enhanced cediranib anti-glioma efficacy *in-vitro***

**Chapter 3: Quinacrine enhances cediranib anti-angiogenic/anti-tumor efficacy in intracranial mouse glioma**



**Chapter 4: Dynamic MRI investigation of cediranib anti-angiogenic/anti-tumor efficacy when combined with proteasome inhibition**

**Chapter 5: Conclusions and future directions**

# List of Abbreviations

| | |
|---|---|
| 3-MA | 3-methyladenine |
| AIF | arterial input function |
| ATP | adenosine triphosphate |
| AV | autophagic vacuole |
| BSA | bovine serum albumin |
| C | contrast agent concentration |
| CBF | cerebral blood flow |
| CBV | cerebral blood volume |
| CD31 | cluster of differentiation 31 |
| c-kit | stem cell factor receptor |
| CML | chronic myelogenous leukemia |
| CNS | central nervous system |
| $C_p$ | contrast agent concentration in plasma compartment |
| $C_t$ | contrast agent concentration in tissue space |
| DCE-MRI | dynamic contrast-enhanced magnetic resonance imaging |
| DMEM | Dulbecco's modified Eagle's medium |
| DSC-MRI | dynamic susceptibility-contrast magnetic resonance imaging |
| DTPA | diethylene triamine pentaacetic acid |
| EGFR | epidermal growth factor receptor |
| ER | endoplasmic reticulum |
| FA | flip angle |

| | |
|---|---|
| FBS | fetal bovine serum |
| FDA | U.S. Food and Drug Administration |
| FGF | fibroblast growth factor |
| FLASH | fast low angle shot |
| GBM | glioblastoma multiforme |
| Gd | gadolinium |
| h | transport functions |
| H&E | hematoxylin and eosin |
| HER2 | human epidermal growth factor receptor 2 |
| $IC_{50}$ | half maximal inhibitory concentration |
| k | proportionality constant |
| $K_{ep}$ | flux rate constant between tissue and plasma compartments |
| $k_h$ | correction factor |
| $K^{trans}$ | microvascular permeability surface area product |
| LC3 | microtubule associated light chain 3 |
| M | DCE T1 weighted image |
| $M_0$ | fully relaxed image |
| MRI | magnetic resonance imaging |
| mTOR | mammalian target of rapamycin |
| MTT | mean transit time |
| MVD | mean vessel density |
| NF-κB | nuclear factor -κB |
| p53 | protein 53 |

| | |
|---|---|
| PBS | phosphate buffered saline |
| PDGF | platelet derived growth factor |
| PDGFR | platelet derived growth factor receptor |
| PI3K | phosphatidylinositol 3-kinase |
| PP2A | protein phosphatase 2A |
| PTEN | phosphatase and tensin homolog |
| R | residual function |
| $r_1$ | relaxivity of contrast agent |
| $R_1$ | longitudinal relaxation rate constant |
| $R_{10}$ | preconstrast longitudinal relaxation rate constant |
| $R_2$*,$R_2$ | transverse relaxation rate constants |
| RARE | rapid acquisition with relaxation enhancement |
| Rb | retinoblastoma |
| rCBF | relative cerebral blood flow |
| rCBV | relative cerebral blood volume |
| RF | radio frequecy |
| RFP | red fluorescence protein |
| rMTT | relative mean transit time |
| ROI | region of interest |
| ROS | reactive oxygen species |
| RTK | receptor tyrosine kinase |
| S | signal intensity on DSC image |
| SDS | sodium dodecyl sulfate |

| | |
|---|---|
| SEM | standard error of the mean |
| SPIO | super paramagnetic iron oxide |
| $T_1$ | longitudinal relaxation time constant |
| $T_2$*, $T_2$ | transverse relaxation time constant |
| TE | echo time |
| TEM | transmission electron microscopy |
| TR | repetition time |
| TRIS | trisaminomethane |
| V-ATPase | vacuolar H+ ATPase |
| $V_e$ | extracellular extravascular volume fraction |
| VEGF | vascular endothelial growth factor |
| $V_i$ | intracellular volume fraction |
| $V_p$ | plasma volume fraction |
| WHO | World Health Organization |
| α | excitation flip angle |

# Acknowledgements

First and foremost, I want to express my sincere appreciation and gratitude to my advisor, Dr. Martin Pike for being such a tremendous mentor to me in the past 5 years. His enthusiasm, patience, ideas and knowledge have had a huge impact on my research and career. I will always be grateful for the guidance he gave me and also the freedom, to pursue research topics of my interest, allowing me to think independently and grow as a scientist. I am also thankful for all the stimulating research conferences in the country I was encouraged to attend. My participation in the development of his laboratory at OHSU has been a valuable learning experience and I hope for its success and growth in the future.

I thank the other valuable members of my committee: Dr. Charles Springer, Dr. Owen McCarty and Dr. Monica Hinds for their support and encouragement throughout my graduate study. Their ideas and suggestions have helped me produce a stronger piece of work for my thesis. I am also grateful to Dr. Leslie Muldoon for kindly agreeing to serve on my defense committee.

An important advantage of being a part of Dr. Pike's laboratory was the opportunity to collaborate and exchange ideas with highly qualified people across a range of research areas. I want to extend my special thanks to Dr. Randall Woltjer and members of his laboratory, Sarah Green and Huong Tran, for helping with histological studies and educating me on techniques such as western blotting. I am thankful to Dr. Matthias Schabel for his advice and help with the analysis of my DCE-MRI data. I am grateful to

Dr. Yancey Gillespie (University of Alabama at Birmingham) for providing me with the 4C8 glioma cell line used for all the studies in my thesis. Xiaoyan Wang from the Rosalie Sears laboratory, Keri Forquer from the OHSU histopathology core and Dr. Stefanie Kaech Petrie also had important contributions to my research, and I am thankful to them. I also thank all other collaborators including Dr. Peter Kurre and Dr. Mary Stenzel Poore for kindly allowing me to implement some of my research work at their laboratory.

It has been an honor to be a part of the Advanced Imaging Research Center (AIRC) team at OHSU and have the opportunity to work and exchange thoughts with some of the best minds in the MR field including Dr. Charles Springer, Dr. Bill Rooney, Dr. Tom Barbara, Dr. Mark Woods, Dr. Wei Huang and Dr. Xin Li. I am thankful to all of them and also to my dear colleagues and friends Audrey Seltzer, Erin Taber, Jim Pollaro and Ian Tagge.

I am very grateful for the love and support of my friends including Sandra Castor, Arunav Sikder, Ramesh Bhaskar, Sangeet Lal, Tanu Singhal, Shashank Govind, Ravi Samatham, Sushil Kumar and Aravind Penmatsa. I also want to extend my thanks to Matt Silva, Jack Hoppin and Patrick McConville for their encouragement during the final year of my graduate study.

Lastly, none of this would have been possible without the undying support, love and encouragement from my family. The belief my parents, Roland and Leena, have in me, has been an immense source of strength and courage and I am thankful to them, especially my mother, for being my best friend.

# Abstract

## Enhancement of cediranib anti-angiogenic/anti-tumor efficacy in intracranial mouse glioma

Merryl R. Lobo

Department of Biomedical Engineering
School of Medicine
Oregon Health & Science University

September 2013
Thesis Advisor: Martin M. Pike, Ph.D.

Glioblastoma Multiforme is the most aggressive manifestation of glioma, affecting ~12000 people/year in the United States alone, with an average survival of just 12-14 months. Despite robust vascularization in malignant gliomas, anti-angiogenic therapy has failed to induce durable responses. This can be attributed, at least in part, to the upregulation of resistance mechanisms such as the pro-survival Akt pathway and its downstream effects on autophagy and cell growth.

This dissertation aims at improving the anti-tumor and anti-angiogenic efficacy of the receptor tyrosine kinase inhibitor, cediranib (targets include vascular endothelial growth factor (VEGF) and platelet derived growth factor (PDGF) receptors) in the treatment of glioblastoma. Studies were focused on two novel therapeutic combinations with cediranib, which have the potential to modulate the Akt pathway and its downstream targets and create a synergistic anti-glioma effect.

Because autophagy (a cellular catabolic pathway) can promote tumor cell survival and resistance, the first therapeutic strategy involved a combination of cediranib with the late stage autophagy inhibitor, quinacrine. A combination of biophysical techniques and magnetic resonance imaging revealed enhanced glioma cytotoxicity *in vitro* and a potent reduction in tumor growth and vascularization *in vivo*, accompanied by increased tumor necrosis and median survival.

The second therapeutic strategy involved a novel combination of cediranib with proteasome inhibitor, SC68896. Results described in this thesis demonstrate a significant improvement in anti-glioma efficacy for this combination, and also a possible normalizing effect on the tumor vasculature.

Collectively, this thesis provides insights into the potential for two innovative treatment strategies for malignant glioma and warrants further exploration in the clinical setting.

# Chapter 1: Introduction

## 1.1 Gliomas

Malignant gliomas are the most common and fatal primary brain tumors. These tumors are intrinsic to the brain and arise from glial cells such as astrocytes, oligodendrocytes and ependymal cells. Depending on the cell of origin, gliomas are characterized as astrocytomas, oligodendrogliomas and ependymomas, respectively. Based on the pathology of the tumor, the World Health Organization (WHO) has categorized gliomas into 4 different grades: Grade I and II are low grade gliomas that are slow-growing, less aggressive and composed of well differentiated cells. Grade III and grade IV tumors, on the other hand, are characterized by a higher proliferation rate and loss of differentiation, with grade IV tumors being associated with the presence of hypoxia, necrotic tissue and angiogenic activity (Westphal*, et al.* 2011, Lim*, et al.* 2011).

Grade IV astrocytoma, called Glioblastoma Multiforme (GBM) is the most aggressive manifestation of glioma, affecting around 12000 people in the US every year, with an average survival of just 12 to 14 months (Westphal*, et al.* 2011, Preusser*, et al.* 2011, Van Meir*, et al.* 2010). Most cases of glioblastoma are primary tumors that develop with a clinical history of just a few weeks (de novo), whereas a smaller fraction of glioblastomas are secondary tumors that progress from a lower grade glioma (Preusser*, et al.* 2011). Currently, there is no real cure for this deadly disease and treatment of patients remains

only palliative (Westphal, *et al.* 2011). Upon diagnosis of GBM, surgical resection will be the first therapeutic option, the success of which is hugely compromised by the infiltrative characteristics of glioblastoma cells (Preusser, *et al.* 2011). This is accompanied by radiotherapy with concomitant and adjuvant chemotherapy with the alkylating agent, Temozolomide. In 2009, the anti-angiogenic agent, Bevacizumab (Genentech, San Francsico, CA) was also approved by the U.S. Food and Drug Administration (FDA) for the treatment of recurrent glioblastoma (Van Meir, *et al.* 2010).

There is a wide array of genetic events that contribute to the malignant transformation required for gliomagenesis, and they are mostly related to a negative regulation of cell death and apoptotic pathways and/or a constitutive activation of growth factor receptor signaling (Lim, *et al.* 2011). Some of the most common changes seen in glioblastomas to downregulate cell death are the loss of p53 and retinoblastoma (Rb) signaling which are critical to tumor suppressor pathways. These are altered in over 70% glioblastomas. Deregulation of growth receptor pathways in glioma is achieved through the overexpression of genes encoding the epidermal growth factor receptor (EGFR) and platelet derived growth factor receptor (PDGFR) or through the constitutive activation of these pathways via mutations in specific components of the downstream signaling cascade described later, in Section 1.4 (Lim, *et al.* 2011, Preusser, *et al.* 2011, Van Meir, *et al.* 2010).

## 1.2 Angiogenesis

One of the most prominent features of glioma progression is the abundant presence of abnormal neovasculature. Glioblastomas, particularly, are one of the most vascularised solid tumors, characterized by a high degree of endothelial cell proliferation (Hardee*, et al.* 2012). A series of events co-ordinated by multiple signaling molecules is involved in the process.

At the absolute initial stages of glioma growth, vascular co-option enables tumor cells to take advantage of the host's vasculature for their needs of nutrients and oxygen. This process involves the arrangement of tumor cells around normal blood vessels. (Hardee*, et al.* 2012). Up to a volume of ~2 $mm^3$, the needs of tumor cells are fulfilled through mere diffusion from the host's nearby vasculature. At this stage there is a balance between pro- and anti-angiogenic molecules in the tumor microenvironment. Beyond this tumor size, an angiogenic phenotype is adopted, which is considered to be a key step in tumor progression. The main driver of angiogenic signaling is hypoxia and nutrient deprivation that develops as the tumor grows in the avascular state (Eichhorn*, et al.* 2007). These stresses induce tumor cells to release proangiogenic molecules including vascular endothelial growth factor (VEGF), platelet-derived growth factor (PDGF) and fibroblast growth factor (FGF) (Eichhorn*, et al.* 2007, Rahman*, et al.* 2010). These angiogenic factors bind to receptors on the endothelial cells and initiate the process of angiogenesis. Growth factor signaling in endothelial cells stimulates them to proliferate and secrete proteases to digest the basement membrane surrounding the vessel. The junctions between the endothelial cells become leaky, which allows them to form tubular structures

or vessel sprouts that grow toward the source of stimulus - the tumor (Eichhorn*, et al.* 2007).

The VEGF family of growth factors and receptors play the most significant role in the process of glioma angiogenesis. VEGF ligands include VEGF-A, VEGF-B, VEGF-C, VEGF-D and placental growth factor. These ligands interact with VEGF receptors, VEGFR-1, VEGFR-2 and VEGFR-3. Specifically, VEGF-A is primarily upregulated in glioblastoma and triggers endothelial cell survival, proliferation and migration through its activation of VEGFR-2 (Hardee*, et al.* 2012, Eichhorn*, et al.* 2007, Rahman*, et al.* 2010). This signaling pathway is also well known for its ability to induce vascular leakage and VEGF is therefore also called vascular permeability factor. Similar to VEGF, FGF also triggers endothelial cell proliferation. PDGF signaling, through interactions between factors: PDGF-A, PDGF-B, PDGF-C and PDGF-D, and receptors: PDGFR-α and PDGFR-β, triggers the recruitment of pericytes to the walls of the newly formed vessels and contributes to maintaining blood vessel integrity (Rahman*, et al.* 2010).

A critical part of the angiogenic process is the maturation and stabilization of newly formed microvasculature through the buildup of pericyte coverage and basement membrane re-establishment. The constant stimulus for endothelial cells to proliferate and form new vessels within tumors results in an incomplete maturation phase, leading to vessels that are irregular and tortuous with discontinuous endothelial linings, defective basement membrane and poor pericyte coverage. This contributes to the increased vascular permeability and blood-brain barrier disruption in the glioma setting which plays

a role in limiting the survival of diseased patients (Hardee*, et al.* 2012, Eichhorn*, et al.* 2007). This chapter will briefly describe some of the approaches that have been developed over the years to curb angiogenesis and discuss ways in which tumors resist the effects of treatment, thus presenting possible avenues for combination therapy.

## 1.3 Anti-angiogenic therapy

### *1.3.1 Overview of anti-angiogenic therapy*

Research on tumor angiogenesis and anti-angiogenic molecules effectively kick-started in the 1970's when the surgeon Judah Folkman hypothesized that tumors secrete diffusible substances which trigger endothelial cell proliferation in the host's capillary blood vessels. Through a series of experiments, Folkman and colleagues showed that tumor growth is angiogenesis dependant and that the inhibition of this process could be therapeutic (Cao*, et al.* 2008, Ribatti 2008). Anti-angiogenic treatment strategies have a number of advantages compared to conventional cytotoxic chemotherapy directed against tumor cells. Angiogenesis inhibitors do not have to cross an endothelial barrier to reach their target, since they are directed towards to tumor blood vessel walls which are accessible through systemic circulation. Angiogenesis in adults is only required in certain situations such as wound healing and the reproductive ovarian cycle, which ensures that there are minimum off target effects. Also, since angiogenesis is critical to the growth of most solid tumors, these treatment strategies can be extended to a wide variety of tumor types (Eichhorn*, et al.* 2007).

Most anti-angiogenic agents target the VEGF signaling pathway, thus inhibiting endothelial proliferation and migration (Figure 1.1). One of the most prominent agents is Bevacizumab which is a humanized monoclonal antibody against VEGF and was the first anti-angiogenic agent to be approved by the FDA for colorectal carcinoma, 2004. Since then, Bevacizumab has also gained FDA approval in 2009 for other tumor types including recurrent GBM. A similar approach to Bevacizumab is VEGF-Trap, which is a soluble decoy receptor with a high affinity for VEGF-A. Antibodies against VEGFR-2 have also been developed. More recently, a number of receptor tyrosine kinase (RTK) inhibitors targeting specific components of the angiogenic pathways have found their way into clinical use as well (as reviewed by Rahman, *et al.* 2010).

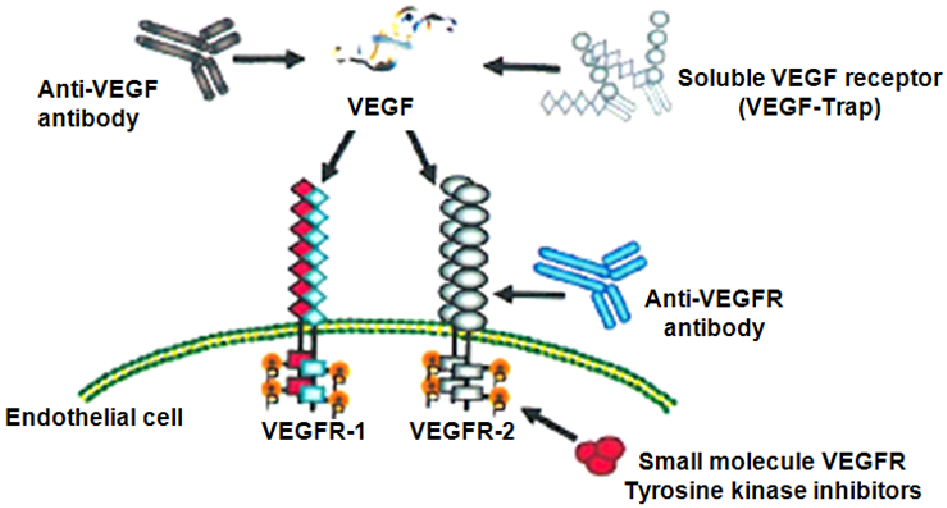


**Figure 1.1. Therapeutic strategies designed to combat VEGF-induced tumor angiogenesis.** Most anti-angiogenic treatments have been developed to target the VEGF pathway which is known to play a central role in tumor vascularization. Anti-VEGF antibodies such as Bevacizumab and VEGF decoy receptors work by targeting VEGF secreted by tumor cells. Antibodies and RTK inhibitors that target the VEGF receptors on the endothelial cells have also been developed. Figure adapted and reprinted with permission from Springer Science and Business Media, Langenbeck's Archives of Surgery (Eichhorn, *et al.* 2007).

*1.3.2 RTK inhibition*

Tyrosine kinases are enzymes which transfer a phosphate group from ATP (adenosine triphosphate) to the tyrosine residues on specific protein substrates that results in functional changes in those proteins. Tyrosine kinases can either be associated with receptors where they are responsible for transduction of extracellular signals into the cell or they can be non-receptor tyrosine kinases, accomplishing intracellular signaling (Gotink*, et al.* 2010).

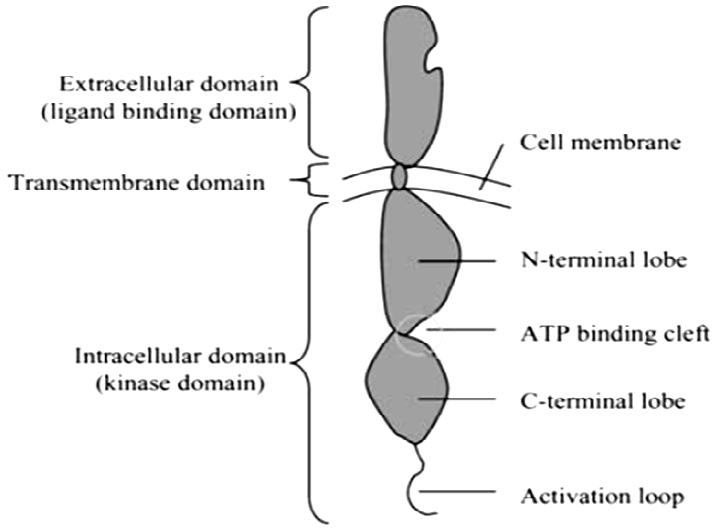


**Figure 1.2. Structure of a receptor tyrosine kinase.** A receptor tyrosine kinase is responsible for transducing signals from extracellular stimuli into the cell. It consists of an extracellular ligand binding domain, a transmembrane domain and an intracellular tyrosine kinase domain. The tyrosine kinase domain has an ATP cleft where the phosphorylation of various downstream signaling substrates takes place. Figure adapted and reprinted with permission from Springer Science and Business Media, Angiogenesis (Gotink*, et al.* 2010).

A RTK monomer consists of an extracellular ligand binding domain, a transmembrane domain and an intracellular domain with tyrosine kinase activity (Figure 1.2). The kinase domain has a bi-lobar structure, consisting of an adenosine triphosphate (ATP) binding cleft located between the two domains. When the ligand binds to the extracellular domain of the receptor, the receptors dimerize, followed by autophosphorylation of tyrosine

residues in the intracellular kinase domain and subsequent phosphorylation of other proteins that contribute to the signaling cascade (Gotink*, et al.* 2010). Most RTK inhibitors developed so far compete with ATP, through their similarity in structure to the adenine ring in the ATP molecule. The selectivity of these RTK inhibitors is engineered through parts of the molecular structure that is not similar to the ATP molecule. The VEGFR tyrosine kinase is an important target to anti-angiogenic RTK inhibitors since it is critical to the process of angiogenesis. RTK inhibitors such as Sunitinib (Pfizer, La Jolla, CA, targets include VEGFR, PDGFR) and Sorafenib (Bayer, West Haven, CT and Onyx, Richmond, CA, targets include Raf, VEGFR and PDGFR) have already been clinically approved for the treatment of certain tumor types (Eichhorn*, et al.* 2007).

*1.3.3 Cediranib*

An important RTK inhibitor that has been in numerous clinical trials for GBM and other tumor types is Cediranib (AZD2171, Astra-Zeneca, London, UK) which inhibits tyrosine kinase receptors associated with all VEGF receptor subtypes (VEGFR-1, -2, -3), PDGFR and c-kit (Figure 1.3) (Rahman*, et al.* 2010).

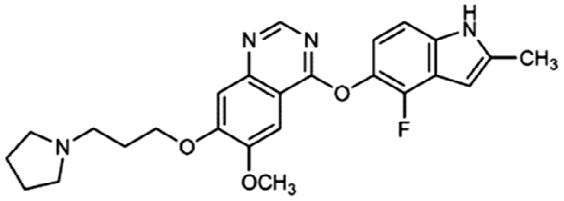


**Figure 1.3. Chemical structure of Cediranib.** Cediranib is an RTK inhibitor which targets VEGFR-1, -2 and -3with strong activity against PDGF receptors and c-kit as well. Figure adapted and reprinted with permission from Elsevier, Journal of Chromatography (Wang*, et al.* 2011).

Cediranib effectively inhibits VEGF induced angiogenesis *in vitro* at subnanomolar concentrations (Wedge*, et al.* 2005). Recent preclinical studies using various mouse GBM models show that although cediranib reduces tumor blood vessel diameter and permeability *in vivo*, it fails to have any effect on tumor growth (Kamoun*, et al.* 2009). Reduction in vessel permeability contributes to an alleviation of edema which has been shown to improve survival in these studies as well as in patients (Batchelor*, et al.* 2007, Kamoun*, et al.* 2009, Farrar*, et al.* 2011). A phase II trial of the agent for the treatment of recurrent glioblastoma showed a radiological response rate of 56% and an increase in 6-month progression free survival to 26% (Rahman*, et al.* 2010). An added advantage of RTK inhibitors like cediranib is that glioma cells frequently possess autocrine or paracrine PDGF signaling which contributes to cell growth. Cediranib treatment thus can directly affect glioma cells and has been shown to do so at micromolar concentrations (Wedge*, et al.* 2005).

### *1.3.4 Vascular normalization and devascularization*

Traditionally, anti-angiogenic inhibitors were developed to restrict the growth of tumors by causing an extensive destruction of tumor vessels or devascularization. The resultant inadequacy of oxygen and nutrients in the tumors was proposed to trigger tumor cell death (Figure 1.4) (Fukumura*, et al.* 2007). Although the development of resistance has greatly limited such efficacy in glioblastomas, a number of studies have shown that anti-angiogenic therapy can transiently "normalize" the tumor vasculature. Such normalization is brought about by the pruning of immature and permeable tumor vessels and a remodeling of the remaining vessels into a more efficient vascular network (Figure

1.4) (Winkler, *et al.* 2004). This normalization lasts only for a finite time window which seems to be 6 days in animal models, but can last up to 1 - 4 months in patients (Fukumura, *et al.* 2007, Winkler, *et al.* 2004). The normalizing effect has been proposed to offer many advantages such as the reduction of peritumor edema, hypoxia and metastatic spread of the disease through intravasation of cancer cells. The restricted permeability of normalized vasculature also helps reduce interstitial fluid pressure, allowing an improved delivery of cytotoxic agents (Fukumura, *et al.* 2007). In a recent phase II trial, Cediranib was shown to normalize the tumor vasculature in patients with recurrent GBM within 1 day of treatment, which lasted up to 28 days (Batchelor, *et al.* 2007). Thus, vascular normalization and devascularization present two therapeutically advantageous outcomes of anti-angiogenic therapy, and depend on the severity of the effects.

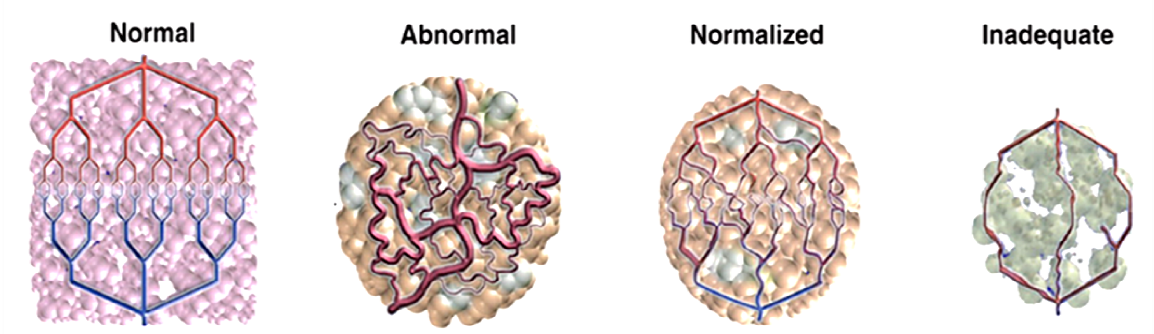


**Figure 1.4. Changes in tumor vasculature with anti-angiogenic therapy.** The tumor vascular network is structurally and functionally abnormal and highly inefficient. Although anti-angiogenic therapy was proposed to trigger tumor cell necrosis (grey) by blocking the supply of oxygen and essential nutrients through devascularization, it has been shown that such agents are more effective in transiently normalizing the vasculature, thus improving the delivery of drugs and oxygen. Figure adapted and reprinted with permission from Elsevier, Microvascular Research (Fukumura, *et al.* 2007).

## 1.4 Resistance to anti-angiogenic therapy

### *1.4.1 Overview of mechanisms of resistance to anti-angiogenic therapy*

Although the clinical approval of multiple anti-angiogenic inhibitors either as monotherapy or in combination with chemotherapy has validated Dr. Folkman's initial hypothesis about the need for angiogenesis in the manifestation and progression of cancer, many preclinical and clinical studies have revealed that the therapeutic benefits of such agents are mostly transitory, followed by tumor revascularization and growth (Grepin*, et al.* 2010, Rahman*, et al.* 2010). Emerging data suggest that tumors adapt by acquiring changes which help functionally evade the blockade of angiogenesis. Such evasive resistance is brought about by a number of mechanisms including the upregulation of alternative angiogenic signaling factors like FGF (Bergers*, et al.* 2008). This was validated by a recent clinical trial involving Cediranib treatment in patients with GBM which showed that relapsing patients had higher levels of FGF compared to others (Batchelor*, et al.* 2007). Hypoxic conditions exacerbated by anti-vascular treatments also tend to promote the recruitment of bone marrow-derived cells such as endothelial and pericyte progenitor cells that differentiate into endothelial cells lining the blood vessel walls and pericytes enveloping the vessels, respectively. Hypoxic conditions have also shown to increase invasiveness among tumor cells, contributing to metastatic spread of the disease in response to anti-angiogenic treatment (Bergers*, et al.* 2008, Grepin*, et al.* 2010, Loges*, et al.* 2010). More recently, studies have reported the involvement of certain critical survival pathways in tumor cells such as the phosphatidylinositol 3-kinase (PI3K)/Akt/mammalian target of rapamycin (mTOR) pathway, in contributing to

resistance against anti-angiogenic therapy (Izuishi, *et al.* 2000, Jiang, *et al.* 2000, Zhao, *et al.* 2011).

### *1.4.2 The Akt signaling pathway*

The Akt signaling pathway plays a central role in tumor cell survival, proliferation and angiogenesis, and is a pathway that is deregulated in 80% of glioblastomas (Joshi, *et al.* 2012, Lim, *et al.* 2011, Van Meir, *et al.* 2010). This pathway shows sensitivity to a range of different conditions such as growth factors, glucose levels and amino acids and has been particularly implicated in enabling hypoxic tumor cells to adopt a more resistant phenotype (Brat, *et al.* 2003, Polytarchou, *et al.* 2011, Populo, *et al.* 2012, Stegeman, *et al.* 2012).

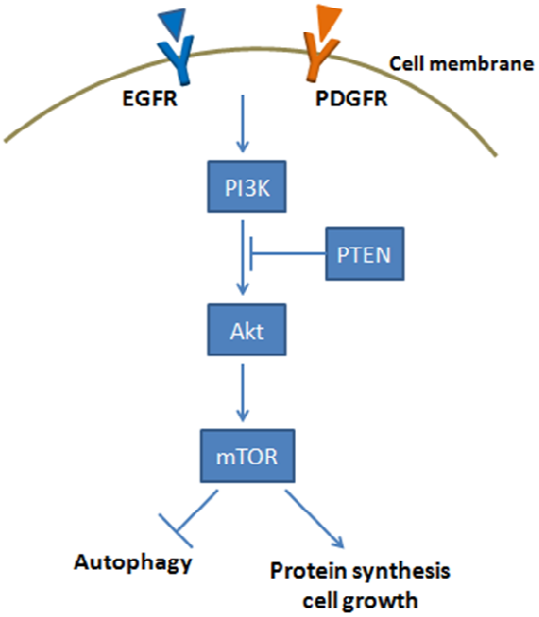


**Figure 1.5. Schematic illustration of the Akt signaling pathway.** The Akt kinase receives signals upstream from critical growth factors like EGFR and PDGFR, through the mediation of PI3K. This pathway plays a central role in maintaining cell growth as well as inhibiting autophagy through mTOR and can significantly contribute to tumor cell survival under conditions of nutrient deprivation, hypoxia and cytotoxic insult.

Upstream of Akt, growth factor RTK signaling leads to the activation of Class I PI3K which in turn phosphorylates and activates the Akt kinase (Figure 1.5). Activated Akt subsequently phosphorylates and activates a number of critical substrates such as nuclear factor-κB (NF- κB) and mTOR, which are involved in cell cycle progression, protein synthesis and cell growth (Populo*, et al.* 2012). Akt activation is regulated by tumor suppressors such as PTEN which is nonfunctional in 37% of glioblastomas. Over-expression of EGFR and PDGFR as well as mutations in genes encoding PI3K also commonly lead to increased activation of Akt in glioblastomas (Joshi*, et al.* 2012). Because of the various pro-survival effects of Akt signaling, an upregulation of this pathway in tumor cells contributes to acquired resistance to anti-cancer therapies and anti-angiogenic agents, and thus, also presents a useful target for combination therapy (Burris 2013, Zhao*, et al.* 2011). Studies have shown that a combination with Akt pathway downregulation improves the therapeutic efficacy of anti-angiogenic agents including RTK inhibitors - this was achieved through the use of specific inhibitors of the Akt pathway (Zhao*, et al.* 2011) or proteasome inhibitors like Bortezomib (Millennium Pharmaceuticals, Cambridge, MA) (Chen*, et al.* 2010, Yeramian*, et al.* 2011, Yu*, et al.* 2006). Another intriguing aspect of the Akt pathway is the control it exercises, through mTOR signaling, over a critical survival mechanism exploited in tumor cells called autophagy (Jung*, et al.* 2010).

### *1.4.3 Autophagy*

The term *autophagy* ("to eat oneself") is the only bulk degradation mechanism present in cells, which allows the digestion and recycling of not just proteins, but also entire

organelles. Autophagy occurs at basal levels in most tissues in the body and plays important homeostatic roles by maintaining protein and organelle quality control. Cancer cells, however, have been shown to exploit this capability for its protective effects against stresses and starvation (Mathew*, et al.* 2007, Shintani*, et al.* 2004).

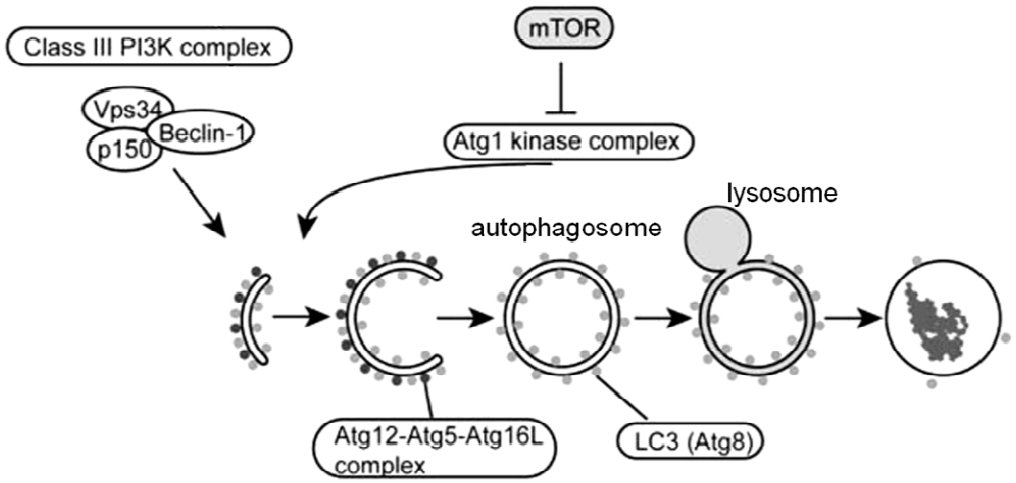


**Figure 1.6. Molecular mechanism of autophagosome formation. .** The Akt pathway excercises control over autophagy through the downstream inhibitory effects of mTOR signaling. When mTOR is inactivated, a series of autophagy related *Atg* proteins work together towards the formation of autophagosomes and the sequestration of cytoplasmic structures for degradation. The Class III PI3K/Beclin-1 and Atg12/Atg5/Atg16 complexes help form the autophagosome membrane whereas the LC3 protein interacts with ubiquitinated substrates. Fusion with the lysosome allows degradation of autophagosomal contents. Figure adapted and reprinted with permission from Nature Publishing Group, Cell Death and Differentiation (Mizushima 2005).

When this catabolic degradation process is activated, a double or multi-membrane-bound vesicle called the autophagosome is formed, to sequester the cytoplasm (Figure 1.6). The cytoplasmic structures could comprise proteins that have been ubiquitinated and targeted for degradation or defective organelles such as mitochondria, which get engulfed through selective or non-selective means (Tschan*, et al.* 2010). This vacuole then fuses with the lysosomes to deliver the internal contents to the lysosomal digestive enzymes for degradation (Figure 1.6) (Shintani*, et al.* 2004). This results in the recycling of macromolecules, producing a supply of critical raw materials such as amino acids and

fatty acids (Rabinowitz*, et al.* 2010). Thus, by providing a temporary supply of biosynthetic substrates and energy, as well as maintaining genomic stability, autophagy could have an important contribution to promoting survival of tumor cells during periods of nutrient deprivation or cytotoxic insult.

On a molecular level, there are a series of autophagy related *Atg* gene products that coordinate the formation of autophagosomes. The Akt pathway can exercise control over autophagy through the inhibitory action of mTOR over the autophagy initiation protein complex which includes Atg1 (Levine*, et al.* 2005, Rabinowitz*, et al.* 2010). When mTOR is inhibited, the initiation complex triggers autophagosome nucleation through the recruitment of Beclin1 and ClassIII PI3K (Figure 1.6). Further elongation of the autophagosomes is mediated through the signaling of a complex of Atg proteins: Atg12, Atg5 and Atg16. Also essential to autophagosome formation is Atg8 or microtubule associated protein 1 light chain 3 (LC3), which is cleaved and then lipidated to form LC3II, that associates with the autophagosome membrane and is commonly used to monitor autophagy experimentally. LC3II plays a critical role in the sequestration of ubiquitinated substrates for degradation (Rabinowitz*, et al.* 2010).

Although autophagy is traditionally characterized as a form of programmed cell death such as apoptosis, the precise role of autophagy in cancer is highly controversial. Most of the evidence shows that autophagy sustains cancer cell survival under conditions of amino acid starvation, glucose and oxygen deprivation, growth factor withdrawal and cytotoxic cellular damage. But, it has also been shown that excessive amounts of

autophagy could lead to tumor cell death (as reviewed by Levine*, et al.* 2005, Mathew*, et al.* 2007, Rabinowitz*, et al.* 2010). The induction of cell death by excessive autophagic flux can possibly be explained by an imbalance between autophagic cellular digestion and the cellular capacity for synthesis (Mathew*, et al.* 2007). Studies show significant levels of cross-talk between autophagy and apoptosis and the accumulation of autophagosomes caused by autophagic inhibition has been shown to trigger cell death in an apoptosis dependant or independent manner (Shingu*, et al.* 2009). Thus, although the exact role of autophagy in tumorigenesis is not fully understood, the modulation of this pathway can help sensitize apoptosis resistant tumor cells to cell death (Mathew*, et al.* 2007). Studies have shown that a possible mitochondrial and lysosomal membrane permeabilitization and the accompanying release of catabolic enzymes may play a role (Boya*, et al.* 2008, Lemasters 2007).

### 1.5 Dynamic magnetic resonance imaging (MRI)

The development of MRI has greatly benefitted the clinical management of a range of diseases, including tumors, by enabling a clear delineation of pathological abnormalities among normal anatomical tissues. Since angiogenesis is a critical component in the development of tumors, the variations in microvascular structure, density, flow and permeability cause temporospatial variations in contrast enhancement patterns on MR images. This provides an excellent basis for a non-invasive investigation of tumor angiogenesis. Dynamic MRI approaches, involving a relaxivity-based technique called dynamic contrast-enhanced MRI (DCE-MRI) and magnetic susceptibility-based technique called dynamic susceptibility contrast MRI (DSC-MRI) are commonly

employed in studies of microvascular permeability/surface area and blood flow/volume, respectively (Jackson*, et al.* 2003, Sorensen 2006, Sourbron*, et al.* 2009). They are widely used clinically in the diagnosis, grading and classification of tumors as well as numerous Phase I and Phase II trials of anti-angiogenic agents (Batchelor*, et al.* 2007, Jackson*, et al.* 2007, O'Connor*, et al.* 2007, O'Connor*, et al.* 2012).

### *1.5.1 DCE-MRI*

A typical DCE-MRI protocol involves an intravenous bolus injection of a gadolinium based contrast agent during the acquisition of several $T_1$-weighted images of the anatomical area of interest. These $T_1$-weighted images are acquired using a spoiled gradient echo sequence with a short repetition time (TR). In an effort to eliminate the $T_2$* weighted signal changes, the echo time (TE) is also minimized. Gadolinium ions are highly paramagnetic and cause a decrease of $T_1$-longitudinal relaxation time constants of the water molecule proton signals they interact with. This causes an increase in the signal intensity on the $T_1$-weighted images (O'Connor*, et al.* 2007). Thus, DCE-MRI exploits the fact that most malignant tumors have an increased vasculaturization which is generally very permeable and will show faster and higher levels of contrast enhancement in comparison to normal tissues (O'Connor*, et al.* 2007). The series of $T_1$-weighted images will track the leakage of contrast agent from the tumor vasculature into the extracellular extravascular space through passive diffusion, as well as the subsequent backflow of contrast agent from the tissue space into the plasma compartment (Figure 1.7).

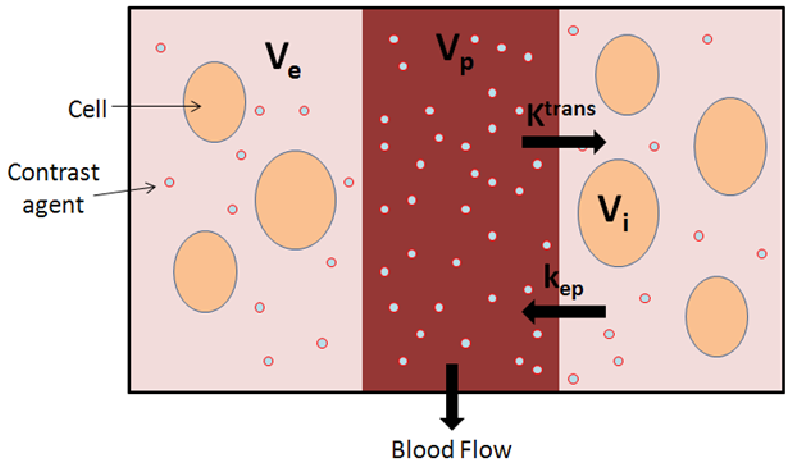


**Figure 1.7. Compartmental modeling of the tumor microvasculature in an MRI voxel.** Contrast agent molecules enter tumor tissue by passive diffusion through the leaky blood vessel walls. The Tofts-Kety pharmacokinetic model assumes uniform contrast agent distribution across two compartments: the plasma compartment with the blood plasma volume fraction $V_p$ and the tissue compartment with the extracellular extravascular volume fraction $V_e$. Contrast agent does not diffuse into intracellular space $V_i$. $K^{trans}$ describes the contrast agent volume transfer between plasma and tissue compartment and $k_{ep}$ describes the rate of backflow into the plasma compartment. Figure design based on review by JPB O'Connor (O'Connor, *et al.* 2007).

To determine the concentration of contrast agent, a knowledge of the precontrast $T_1$ is required. The protocol employed in the subsequent chapters involves acquiring a fully relaxed/ proton density weighted image ($M_0$), using a longer TR and minimum TE (Pike, *et al.* 2009). Signal intensities from various pixels on the postcontrast $T_1$-weighted DCE images ($M$) can then be converted to postcontrast tissue longitudinal relaxation rate constants ($R_1$), which can be further expressed in terms of tissue concentration of contrast agent ($c$).

$$(1.1): \qquad M = M_0 \frac{\left(1 - e^{\left(-\frac{TR}{T_1}\right)}\right)\sin(\alpha)}{1 - e^{\left(-\frac{TR}{T_1}\right)}\cos(\alpha)}$$

$$(1.2): \qquad R_1 = \frac{1}{T_1}$$

$$(1.3): \qquad R_1 = R_{10} + c.r_1$$

where $\alpha$ is the excitation flip angle associated with the $T_1$-weighted DCE sequence, $R_{10}$ is the precontrast longitudinal relaxation rate constant and $r_1$ is the relaxivity of the contrast agent. Once the contrast agent concentration in the tumor tissue ($C_t$) is obtained, the microvascular permeability-surface area product ($K^{trans}$) can be calculated through pharmacokinetic modeling. Although changes in $K^{trans}$ within tumors are mostly related to changes in vascular permeability and/or surface area, they could also be sensitive to flow alterations within a flow-limited regime (Barrett, *et al.* 2007). The pharmacokinetic model used in this thesis is based on the two compartmental Extended Tofts-Kety model (Figure 1.7) (Sourbron, *et al.* 2012, Tofts, *et al.* 1999):

$$(1.4): \qquad C_t(t) = K^{trans}.C_p(t) * e^{(-t.Ktrans/Ve)} + C_p(t).V_p$$

where $C_p$ is the time varying concentration of contrast agent in the plasma compartment, $V_p$ is the volume of the plasma compartment, $V_e$ is the extracellular extravascular volume fraction and * represents the convolution operation. Thus, the approximation of $K^{trans}$ requires an accurate determination of $C_p$ or the Arterial Input Function (AIF) which can be obtained in number of ways including the use of population averaged values, calculating contrast agent concentrations in a nearby arterial vessel or using 'blind estimation' techniques that directly determine the AIF from measured tumor curves (Schabel, *et al.* 2010, Schabel, *et al.* 2010).

A critical limitation of the modeling strategy described above is the assumption that the contrast agent and water molecules are uniformly distributed throughout the tissue compartment (including *Vi*), which equivalent to the assumption that the transcytolemmal

water exchange rate is effectively infinitely fast. This leads to a systematic error in the determination of $K^{trans}$ (Huang, *et al.* 2008). It underestimates $K^{trans}$ specifically in malignant tumors (Huang, *et al.* 2011, Li, *et al.* 2013).

### *1.5.2 DSC-MRI*

DSC-MRI is a technique which exploits the changes in magnetic susceptibility caused by contrast agents using $T_2$*- or $T_2$-weighted imaging sequences. These images are typically acquired with a long TR and TE, using a gradient echo sequence (for $T_2$*-weighting) or spin echo sequence (for $T_2$-weighting) before, during and after the injection of a gadolinium based or iron oxide based (blood pool) contrast agent. Distortions in the magnetic field induced by the passage of contrast agent through the area of interest create a transient drop in the signal intensity on the images, from which information on relative blood flow and volume can be extracted. Since the transit time of the contrast agent bolus through the tissue is only a few seconds, a greater temporal resolution is required compared to DCE-MRI (Akella, *et al.* 2004, Calamante 2005, Thomas, *et al.* 2000).

It has been shown that contrast agent concentration is approximately proportional to the change in the transverse relaxation rate constant $R_2$ or $R_2$*. Assuming that the relationship between signal intensity and $R_2$ is described by a single exponential equation, the time-varying contrast agent concentration in the tissue ($C$) is:

$$(1.5): \qquad C(t) = -\frac{k}{TE}.\ln\left(\frac{S(t)}{S(0)}\right)$$

Where $S(t)$ is the signal intensity measured at time $t$, $S(0)$ is the baseline or precontrast signal intensity and k is the proportionality constant which depends on the tissue, contrast

agent, field strength and pulse sequence parameters (Thomas*, et al.* 2000). Once *C(t)* is calculated, cerebral blood flow (*CBF*) can be obtained:

$$(1.6): \qquad C(t) = CBF.\ AIF(t)*R(t)$$

Where *R(t)* is the residual function, which is related to the fraction of contrast agent still present in the region of interest (ROI) at time *t* following an instantaneous bolus injection at $t = 0$.

$$(1.7): \qquad R(t) = 1 - \int_0^t h(t)dt$$

where h(t) is the probability density function of the transit times through the ROI. The deconvolution of Equation 1.6 isolates *CBF. R(t)* which gives an approximation of *CBF* since $R(t = 0) = 1$.

Cerebral blood volume (CBV) can be calculated using

$$(1.8): \qquad CBV = k_h \frac{\int C(t)dt}{\int AIF(t)dt}$$

where $k_h$ is a correction factor which depends on the hematocrit values in arteries and capillaries.

Mean transit time (MTT) is another parameter which can be approximated using the DSC-MRI technique and is given by the ratio of CBV to CBF. MTT is related to vascular inefficiency.

The DSC-MRI technique described above uses a number of assumptions such as 1) a negligible change in $T_1$ relaxation, 2) CBF is stable during measurement, 3) there is a

negligible recirculation of the contrast agent and 4) there is negligible contrast agent leakage during the first pass (Thomas*, et al.* 2000). The protocol adopted in the subsequent chapters utilizes a blood pool contrast agent, Feridex, to avoid extravasation into the tissue.

### 1.6 Thesis Overview

Glioblastoma Multiforme (GBM) is the deadliest and most aggressive manifestation of glioma, affecting ~12000 people/year in the United States alone. The average survival for the disease has remained 12-14 months over several years and more innovative therapeutic strategies are urgently required. Glioblastomas are known to possess a highly invasive and resistant phenotype which is enabled and supported, to a significant extent, by the development of a dense vascular network through the process of angiogenesis. The dependence of tumors on angiogenesis for maintaining a steady supply of oxygen and nutrients has sparked the development of many anti-angiogenic treatment strategies. Such therapeutic agents have been shown to have only transitory effects in patients with glioblastoma, partly due to changes acquired by tumor cells that help functionally evade the blockade of angiogenesis. The pro-survival Akt signaling pathway has been engineered by tumor cells to sustain tumor growth under a wide variety of stress conditions including hypoxia and nutrient deprivation. This pathway not only supports cell growth through enabling protein translation and transcription of pro-survival genes but also exercises control over an important tolerance mechanism called autophagy.

This thesis centers on developing a rationale for approaches aimed at improving the therapeutic outcome of the anti-angiogenic RTK inhibitor, Cediranib. This has been achieved through a detailed examination of two possible strategies for combination therapy that target the Akt pathway and its downstream effects.

The first treatment strategy involves a combination of Quinacrine, a late stage autophagy inhibitor, with Cediranib for the treatment of glioblastoma cells and has been studied in detail in Chapters 2 and 3. Studies in Chapter 2 assess the synergistic cytotoxic effects of the Quinacrine/cediranib treatment combination on 4C8 glioma cells *in vitro,* and use a range of biophysical techniques such as cell viability assays, western blotting and fluorescence microscopy to explore the mechanistic interactions that may play a role in treatment effects. This approach has revealed that quinacrine significantly enhances the anti-glioma effect of cediranib in hypoxic tumor cells and involves a direct modulation of the Akt pathway and its downstream effects on autophagy.

Studies in Chapter 3 extend the investigation of the Quinacrine/cediranib treatment efficacy to the *in vivo* setting using the 4C8 intracranial mouse glioma model, with quantitative and state-of-the-art MR imaging techniques such as DCE-MRI and DSC-MRI as well as immunohistology. Longitudinal assessment of treatment efficacy using dynamic MRI of key functional vascular parameters such as vascular permeability/surface area, blood flow and volume have revealed a potent tumor devascularization, growth delay and increase in necrosis with the combination treatment. This was also accompanied by an over 2 fold improvement in mouse survival, confirming

that the novel quinacrine/cediranib combination shows great promise not just in glioma cell cultures but also *in vivo*.

Studies in Chapter 4 describe the *in vivo* effects of another novel treatment strategy involving a combination of a proteasome inhibitor, SC68896, and cediranib for the treatment of glioblastoma. Although proteasome inhibitors have not gained much success in the treatment of patients with solid tumors, research has shown that through a combined inhibition of the Akt pathway, proteasome inhibitors could synergistically enhance the efficacy of anti-angiogenic RTK inhibitors. Since these studies have not characterized the *in vivo* effects of such a drug combination for glioblastoma, experiments described in Chapter 4 have been dedicated to providing a detailed evaluation of the potential for this treatment combination in intracranial mouse glioma. Techniques such as DCE-MRI, DSC-MRI and immunohistology have revealed a possible vascular normalizing effect of the treatment combination accompanied by a 2 fold delay in tumor growth, increase in tumor necrosis and a significant improvement in mouse survival.

The studies outlined in Chapters 2-4 provide insights into the potential for two innovative treatment strategies of malignant glioma and provide a rationale for their further exploration in the clinical setting. In Chapter 5, the key findings from my thesis research are summarized and areas of interest for future work are highlighted.

# Chapter 2: Quinacrine enhances cediranib anti-glioma efficacy *in vitro*

*Merryl R. Lobo, Huong Tran, Xiaoyan Wang, Yancey G. Gillespie, Randall L. Woltjer, *Martin M. Pike

*Most of the work described in this Chapter is part of a manuscript in preparation.*

**These authors are the sole contributors to the work.*

## 2.1 Abstract

Despite robust vascularity of malignant gliomas, anti-angiogenic therapy largely fails to induce durable responses. Because autophagy (a cellular catabolic pathway that promotes tumors cell survival under hypoxic/nutrient stress) has been shown to promote treatment resistance among tumors, we investigated the *in vitro* efficacy of a combination of cediranib (a VEGF/PDGF receptor tyrosine kinase (RTK) inhibitor) with quinacrine (a late stage autophagy inhibitor). Cell viability assays and cleaved caspase-3 western blots revealed a greater than additive cytotoxic efficacy under hypoxic conditions. Western blotting for autophagic vacuole (AV) related microtubule associated protein light chain-3 (LC3-II) not only indicated increases with quinacrine, but also with cediranib, suggesting that cediranib increases autophagic flux. The largest AV increases occurred with combined treatment under hypoxic conditions. When AV accumulation was prevented under such conditions using 3-methyladenine (3-MA), an inhibitor of autophagosome formation, tumor cell viability increased. This suggested that AV accumulation plays a

role in the induced cytotoxicity. Probing 4C8 cells for phosphorylation of Akt revealed that both agents potently downregulate Akt activation, and that not only cediranib but also quinacrine could play a role in autophagy induction. Bafilomycin A1, another late-stage autophagy inhibitor, only exhibited additive efficacy with cediranib with substantially lower LC3-II accumulation and no effect on upstream Akt signaling. Our results suggest that the unique cytotoxic efficacy of the quinacrine/cediranib combination is at least partly dependant on increased AV accumulation within hypoxic tumor cells and is associated with potent inhibition of Akt activation.

## 2.2 Introduction

Malignant gliomas are highly aggressive and vascular tumors for which prognosis remains extremely poor and for which novel therapeutic modalities are urgently required. The morbidity and mortality of malignant gliomas, especially the most common type glioblastoma multiforme, can be attributed in part to their robust angiogenesis (Gladson*, et al.* 2010, Norden*, et al.* 2009, Rahman*, et al.* 2010, Rong*, et al.* 2006, Tabatabai*, et al.* 2009). Hence, anti-angiogenic therapy is potentially promising. Most anti-angiogenic treatments developed so far have been designed to target the VEGF pathway which plays a central role in tumor vascularization. Antibodies such as Bevacizumab (Genentech, San Francisco, CA) and decoy receptors such as VEGF-Trap target VEGF molecules whereas RTK inhibitors target the VEGF receptors (Rahman*, et al.* 2010). Most anti-angiogenic RTK inhibitors also have strong activity against the signaling of similar growth factor receptors such as PDGFR. This presents an added advantage in the treatment of glioblastomas since many such tumors express autocrine or paracrine PDGF signaling

which contributes to tumor cell growth (Wedge, *et al.* 2005). Thus, anti-angiogenic RTK inhibitors can have direct cytotoxic effects on tumor cells.

Unfortunately, anti-angiogenic monotherapy largely fails to induce durable responses with malignant glioma, with tumors developing treatment resistance, often through the activation of specific pro-survival signaling pathways (Gotink, *et al.* 2010, Norden, *et al.* 2009, Rahman, *et al.* 2010). Recent studies have shown that autophagy, a cellular degradation pathway, is an important cytoprotective and drug resistance mechanism (Amaravadi 2009, Hoyer-Hansen, *et al.* 2008). Anti-angiogenic RTK inhibitors can activate autophagy through a number of mechanisms including the inhibition of the Akt pathway. The Akt kinase can modulate autophagy through its downstream target, the mammalian target of rapamycin (mTOR), and an inhibition of this pathway by RTK inhibitors could occur through their action on PDGFR (Joshi, *et al.* 2012, Jung, *et al.* 2010). During autophagy, cellular proteins and organelles are sequestered within characteristic double-layered autophagosomes which subsequently fuse with lysosomes for bulk degradation. Activated during metabolic stress, autophagy provides energy and biosynthetic substrates and removes potentially toxic damaged proteins and organelles. However, while autophagy can function as a survival promoting pathway, the incomplete degradation of AVs, and their excessive accumulation, can trigger autophagic cell death, a cell death mechanism exhibiting significant crosstalk with apoptotic signaling (Dalby, *et al.* 2010, Geng, *et al.* 2010, Hoyer-Hansen, *et al.* 2008).The involvement of autophagy in cell death can be therapeutically exploited, as the implementation of late-stage autophagic inhibition when autophagic flux is stimulated can be cytotoxic (Amaravadi

2009, Degtyarev, *et al.* 2008, Mirzoeva, *et al.* 2011). Anti-malarial agents such as chloroquine and quinacrine effectively inhibit late-stage autophagy, through their lysosomotropic action, which enables them to selectively enter and concentrate within AVs (Degtyarev, *et al.* 2008, Geng, *et al.* 2010, Gupta, *et al.* 2010, Mirzoeva, *et al.* 2011). While chloroquine is more commonly employed in cancer treatment, quinacrine is an FDA-approved drug for malaria that is well tolerated, and has superior blood brain barrier penetration to that of chloroquine, a key issue with CNS diseases (Geng, *et al.* 2010, Yung, *et al.* 2004).

Various cancer therapeutics have been shown to activate autophagy, and a number of recent studies in different cancer models have demonstrated increased efficacy via combined autophagy inhibition (Amaravadi 2009, Degtyarev, *et al.* 2008, Gupta, *et al.* 2010, Mirzoeva, *et al.* 2011, Shimizu, *et al.* 2011). However, the combination of anti-angiogenic agents with autophagy inhibitors is a relatively new concept (Hu, *et al.* 2012). Efficacy of the anti-angiogenic RTK inhibitor cediranib, a potent inhibitor of VEGF receptors -1, -2 and -3, PDGF receptors -α and -β and c-Kit (Wedge, *et al.* 2005), has not been investigated in combination with an autophagy inhibitor. Thus, the goal of the studies outlined in this chapter was to assess the cytotoxic effects of cediranib, quinacrine and their combination on glioma cells in culture and determine if quinacrine can significantly enhance the direct anti-glioma effects of cediranib. Furthermore, studies in this chapter also elucidated some of the molecular mechanisms mediating these effects and have revealed that there is a synergistic interaction between the two agents in

hypoxic glioma cells, which depends on AV accumulation and is associated with inhibition of the Akt kinase.

## 2.3 Materials and Methods

### *2.3.1 Cell culture and Tumor Inoculation*

Studies described in this chapter use the 4C8 glioma cell line, which was developed from B6D2F1 mice transgenic for myelin basic protein promoter driven c-neu expression. This cell line (provided by Dr. G. Yancey Gillespie, UAB) was maintained in Dulbecco's modified Eagle's medium/Ham's F-12 50/50 Mix (Invitrogen, Carlsbad, California), supplemented with 7% fetal bovine serum (FBS) (Hyclone, Logan, Utah) and 1% L-glutamine (Sigma-Aldrich, St. Louis, Missouri). To simulate hypoxic conditions of the tumor, cells were incubated in the BioSpherix hypoxic chamber at 0.5% $O_2$. Female C57BL/6 × DBA/2 $F_1$ hybrid mice (B6D2F1) were purchased from *Charles River* Laboratories (Wilmington, MA). Mouse studies were conducted with the approval of the Oregon Health and Science University Institutional Animal Care and Use Committee and under the supervision of the OHSU department of Comparative Medicine. Brain tumors were induced by the intracerebral injection of ~$1 \times 10^6$ 4C8 cells, suspended in DMEM/F12 (5-10µl) using a stereotaxic frame as previously described (Pike*, et al.* 2009).

### *2.3.2 Immunohistochemistry*

For the detection of hypoxic regions within the tumors, mice were injected intravenously with the 2-nitroimidazole hypoxia marker EF5 (30mg/kg), 3 hours prior to sacrifice.

Mouse brains were stored in 10% Formalin. Fixed tissue samples were paraffin embedded and 7 μm sections were mounted on slides. Briefly, sections were deparaffinized in xylene followed by rehydration in decreasing concentrations of ethanol. After heat induced antigen retrieval in citric acid (pH 6.0) for 50 minutes and incubation with blocking agent (3% BSA) for 60 minutes, sections were labeled with Alexa 488 tagged primary antibodies to hypoxia marker EF5. Sections were counterstained with DAPI (Molecular Probes, Inc.) to outline the nuclei.

*2.3.3 Cell viability assays*

Cells were plated in 96-well plates at a density of 3000 cells/well and were exposed to a range of treatment conditions. To assess cell viability in response to treatment, MTS solution (CellTiter 96® AQueous MTS Reagent) was added to cells in 96 well plates (20 μL/well) and left for 1 hour at 37°C. A negative control of MTS solution and medium alone was also included. The absorbance was measured using ELX800 Micro Plate Reader (Bio-Tek Instruments, Inc.) at 490 nm.

*2.3.4 Western blot analysis*

Cells were plated at density of $4.8x10^4$ cells per well in 6-well plates and treated with vehicle or drugs. After the indicated time of treatment, cells were lysed by brief sonication in whole-cell lysis buffer (62.5 mM TRIS, 10% glycerol, 1% SDS, pH 6.8), and cellular proteins were collected in the supernatant fraction after centrifugation at 14,000g for 10 minutes. Proteins were reduced by heating at 100°C for 5 minutes in 50 mM DTT with 0.05 bromphenol blue, and electrophoresed in 4–20% Tris-HCl gels, and

transferred onto nitrocellulose using the NuPage® electrophoresis system (Invitrogen). The membranes were probed with antibodies to LC3, cleaved caspase 3, pan-Akt and phospho-Akt (from Cell signalling, Danvers, MA USA) and actin (from Santa Cruz Biotechnology Company, Santa Cruz, CA). Membranes were treated with appropriate secondary antibody, exposed to enhanced chemiluminescence solutions (Invitrogen) and visualized using the Molecular Imager Gel Documentation System.

*2.3.5 Microscopy for RFP-LC3 expression*

Cells were tranduced with lentiviral particles (*EMD Millipore*, Billerica, MA) to stably express the RFP-LC3 fusion protein. Cells were then treated with the quinacrine/cediranib combination at the concentrations indicated in the legends for Figure 2.3B, for 24 hours. RFP-LC3 expressing cells were then visualized using an EVOS fl fluorescence microscope (AMG).

*2.3.6 Statistical analysis*

Values are expressed as mean ± SEM. Student's t test (*NCSS Statistical Software,* (Kaysville, UT) was employed to test for statistical significance.

**2.4 Results**

*2.4.1 Quinacrine enhances cediranib anti-glioma efficacy under hypoxic conditions*

Glioma growth involves the development of a highly inefficient vascular supply which is largely unable to cope with increasing cellularity, inevitably leading to areas of hypoxia developing within the tumor (Amberger-Murphy 2009). Since hypoxia has been shown to

render tumor cells more resistive to treatment, we sought to determine if hypoxic regions developed with the 4C8 glioma model as well. Tumor sections obtained 2 weeks post tumor growth initiation showed the presence of hypoxic cells through a positive EF5 immunostaining (Figure 2.1). Studies by Evans *et al.* suggest that these areas are most likely under modest (2.5% $pO_2$) to severe (0.1% $pO_2$) hypoxic stress (Evans, *et al.* 2004). Subsequent assessment of treatment efficacy was thus conducted under normoxic and hypoxic (0.5% $pO_2$) conditions.

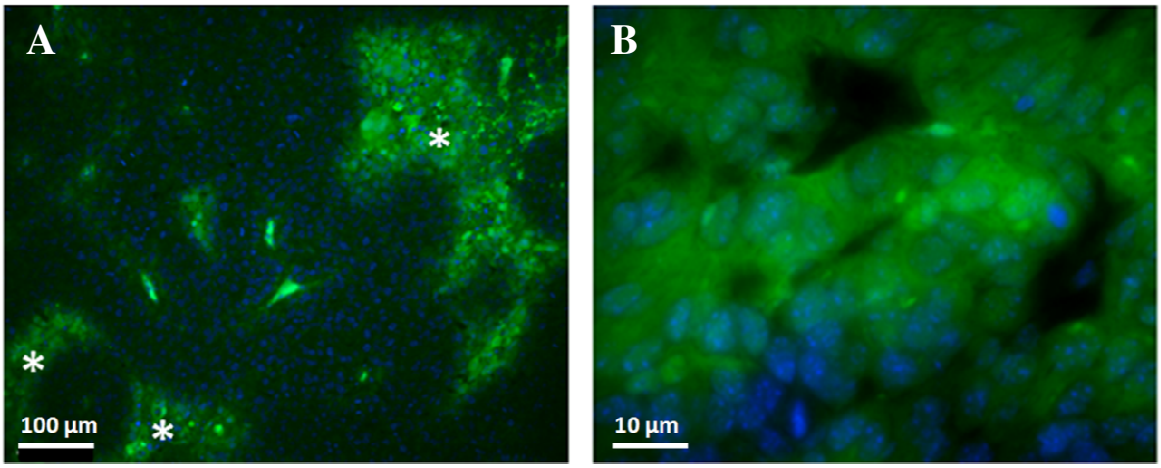


**Figure 2.1. Evidence for the presence of hypoxic regions in 4C8 glioma *in vivo*.**
Representative tumor sections showing immunohistochemical detection of hypoxic regions in 4C8 glioma, shown under A) low and B) high magnification. Sections were obtained from 3 mice, 2 weeks post initiation of tumor growth. Hypoxic cells were identified using Alexa488-labeled anti-EF5 antibody (green). Nuclei were stained with DAPI (blue). Regions marked with * denote positive staining for hypoxia in the low magnification image. Xiaoyan Wang from the Rosalie Sears laboratory implemented the staining of tissue samples.

Figure 2.2A shows the effect of cediranib, quinacrine and their combination on tumor cell viability using MTS assays. Both agents induced dose dependant reductions in cell viability at micromolar concentrations, with mean half maximal inhibitory concentrations ($IC_{50}$): 2.7(±0.1) µM and 3.2(±0.2) µM under normoxic conditions for cediranib and quinacrine respectively. While hypoxia did not affect the cytotoxicity of cediranib, there was a significant decrease in tumor cell viability in response to quinacrine treatment

under hypoxic conditions. The $IC_{50}$ values for cediranib and quinacrine, in the presence of hypoxia, were 2.4(±0.2) μM and 2.4(±0.04) μM respectively. While combined quinacrine/cediranib treatment decreased tumor cell viability in an additive fashion under normoxic conditions, the hypoxic environment significantly potentiated these effects: a combination of 1 μM cediranib with 2.5 μM quinacrine decreased tumor cell viability by 31(±3)% under normoxic conditions and 78(±7)% under hypoxic conditions (Figure 2.2A).

We next determined if the combinatorial effects on cell viability were related to increased apoptotic induction by probing for levels of caspase-3 activation, which is critical to apoptotic cell death. 4C8 glioma cells were exposed to cediranib and quinacrine individually and in combination, under normoxic and hypoxic conditions and revealed a maximum cleavage of caspase-3 under hypoxic conditions, when both agents were combined (Figure 2.2B). Increased apoptosis under these particular conditions correlated well with the greater than additive effects on tumor cell viability (Figure 2.2A). These data demonstrate that quinacrine potently enhances the anti-glioma effects of cediranib under hypoxic conditions.

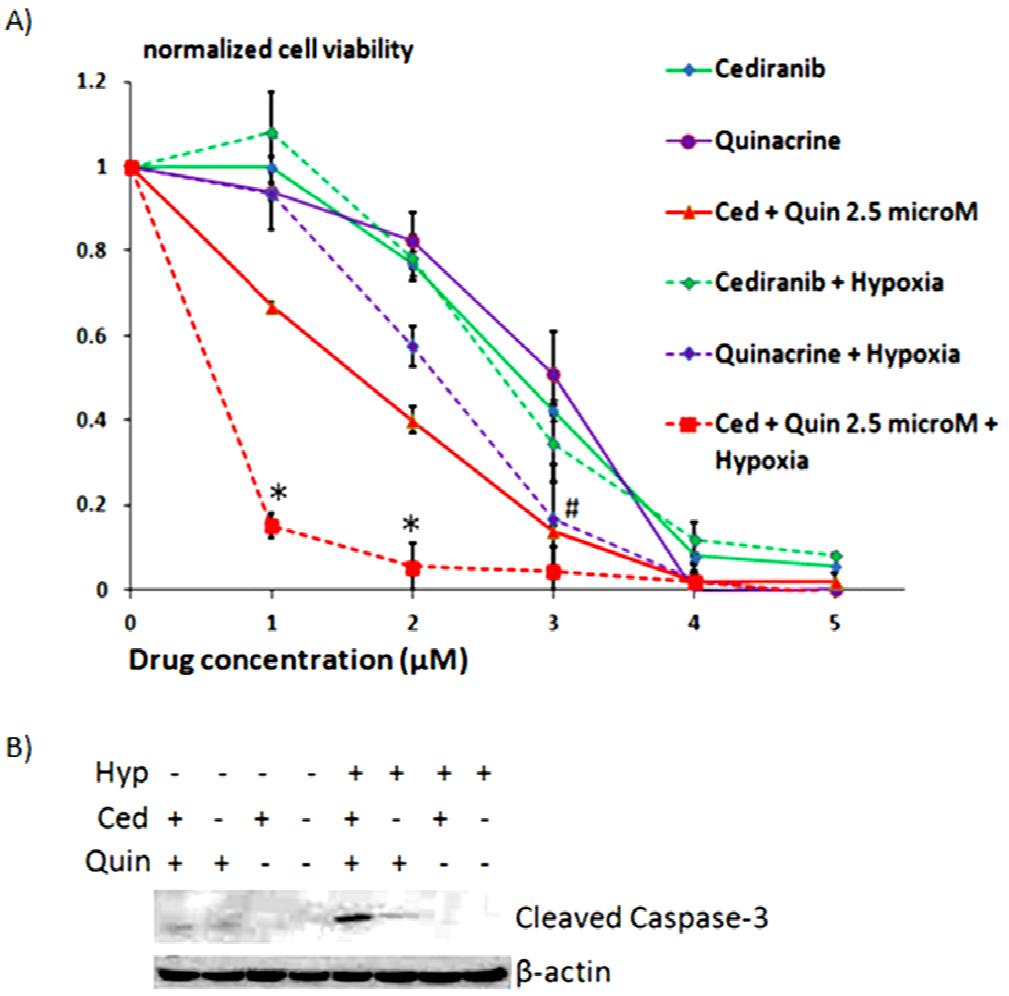


**Figure 2.2. Quinacrine significantly enhances cediranib glioma cytotoxicity under hypoxic conditions.** A) Results from MTS cell viability assays showing mean 4C8 cell viability in response to treatment, normalized to untreated samples. Assays were performed after cells were exposed to treatment for 72 hours, under normoxic or hypoxic (0.5% $O_2$) conditions. Results are mean ± SEM of three independent experiments, performed in triplicate. Significant differences between tumor cell viability results for hypoxic versus normoxic conditions are denoted by # ($p<0.05$) for single agent quinacrine treatment and * ($p<0.05$) for quinacrine/cediranib combination treatment. B) Representative cleaved caspase-3 western blots obtained from 4C8 cells grown under normoxic or hypoxic conditions for 72 hrs while untreated or exposed to cediranib (2 µM), quinacrine (2 µM), or combined quinacrine/cediranib.

*2.4.2 Cediranib and quinacrine have direct modulatory effects on the autophagic pathway in glioma cells*

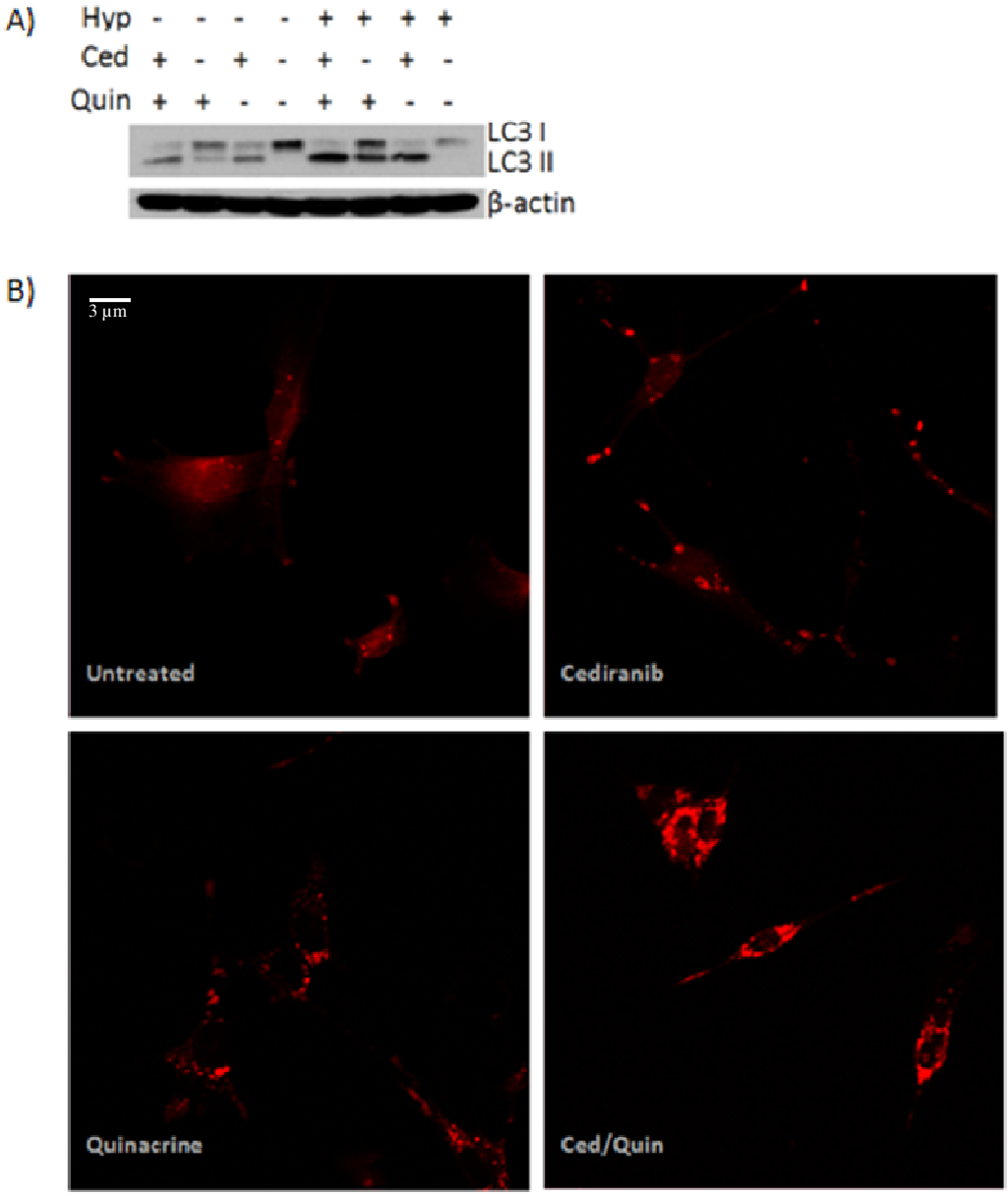


**Figure 2.3. Cediranib and quinacrine modulate the autophagic pathway in glioma cells.** A) Representative LC3 western blots obtained from 4C8 cells grown under normoxic or hypoxic (0.5% $O_2$) conditions for 10 hrs while untreated or exposed to Cediranib (3µM), quinacrine (0.8 µM), or combined quinacrine/cediranib. B) RFP-LC3 expressing 4C8 cells were visualized using Zeiss LSM 780 laser scanning confocal microscope after incubation under hypoxic conditions for 24hr while untreated or exposed to cediranib (2.5µM), quinacrine (2.5 µM), or combined quinacrine/cediranib.

During the process of autophagy, cytoplasmic structures such as proteins and organelles are captured into vesicles called autophagosomes. These autophagosomes are lined with a specific protein called LC3II which plays a role in sequestering ubiquitinated substrates targeted for degradation. As these vesicles get degraded within lysosomes, LC3II will also be degraded. Thus, an increase in LC3II levels in cells could be a result of an increased formation of AVs and/or an inhibition of AV degradation. To assess the effects of cediranib on autophagic induction in hypoxic and normoxic glioma cells, we exposed 4C8 cells to cediranib treatment under both conditions and probed for levels of LC3-II using western blotting. We also studied the effects of quinacrine treatment as well as the combination of the two agents on LC3-II.

Figure 2.3A shows that hypoxia by itself increased LC3-II levels in glioma cells, in agreement with the known induction of autophagy by hypoxia. (Rausch*, et al.* 2012). Cediranib also increased levels of LC3-II in glioma cells compared to untreated, and this effect was potentiated under hypoxic conditions. Additionally, quinacrine treatment resulted in increased LC3-II levels, in agreement with its action as a late stage autophagy inhibitor. Maximum LC3-II accumulation was observed with the combination treatment, under hypoxic conditions (Figure 2.3A). To obtain further evidence for AV accumulation with cediranib and/or quinacrine treatment we sought to observe changes in the spatial localization of LC3-II by using RFP-LC3 transfected 4C8 cells. Figure 2.3B shows a diffuse cytosolic distribution of the LC3-II protein in untreated cells whereas there is an increase in the number of punctae or AVs in response to single agent

treatment. The presence of these vacuoles was much higher in response to combination treatment.

These data suggest that induction of autophagy with cediranib treatment under hypoxic conditions combined with late stage autophagic inhibition with quinacrine resulted in an increased accumulation of AVs. The increased cell death observed (Figure 2.2A and 2.2B) under the same conditions which induced excessive AV accumulation, is consistent with a causal relationship. We further investigated this possibility as discussed in the following section.

*2.4.3 Evidence for a causal relationship between combination treatment induced AV accumulation and tumor cell death.*

We next sought to determine whether the AV accumulation in response to combination treatment under hypoxic conditions is not only associated with but also plays an important role in the anti-glioma effects. To accomplish this, we exposed 4C8 cells to combination treatment under hypoxic conditions with and without the addition of early stage autophagy inhibitor, 3-Methyladenine (3-MA). 3-MA blocks autophagosome formation via the inhibition of type III Phosphatidylinositol 3-kinases (PI-3K).

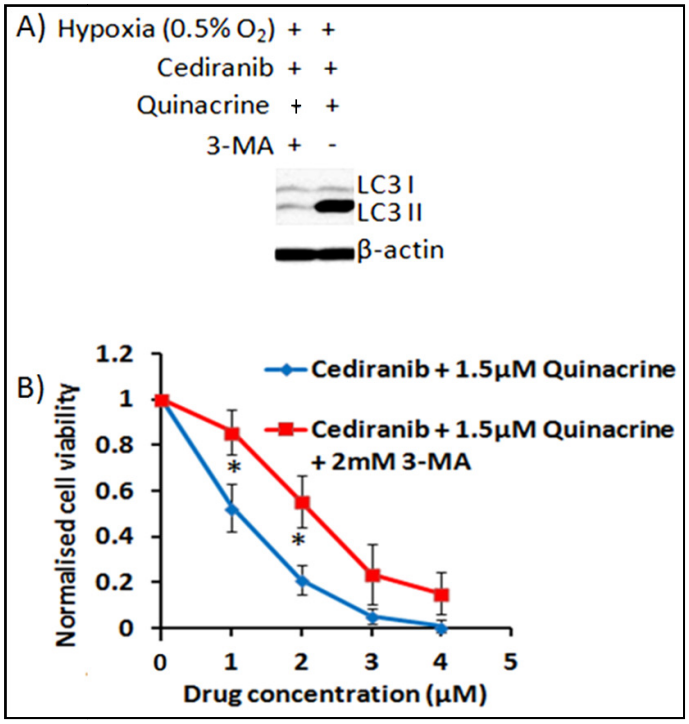


**Figure 2.4. Autophagic vacuole accumulation induced by treatment combination contributes to glioma cell death.** A) Representative LC3 western blots obtained from 4C8 cells grown under hypoxic (0.5% $O_2$) conditions for 24 hrs while exposed to a combination of cediranib (2μM) and quinacrine (1.5μM), either with or without 2mM 3-MA. B) Results from MTS cell viability assays showing mean 4C8 cell viability in response to treatment, normalized to untreated samples. Assays were performed after cells were exposed to treatment for 72 hours, under hypoxic (0.5% $O_2$) conditions. Results are mean ± SEM of three independent experiments, performed in triplicate. Significant differences between tumor cell viability results obtained with and without 3-MA are denoted by * ($p<0.05$).

As expected, when glioma cells were probed for levels of LC3-II, there was an increase in AVs with the combination treatment, but this was largely inhibited in the presence of 3-MA (Figure 2.4A). We next examined whether the glioma cells were spared from the cytotoxicity of the combination treatment when AVs were prevented from forming and accumulating. Figure 2.4B shows that there was a significant increase in 4C8 cell viability in the presence of 3-MA, which provides strong evidence that AV accumulation plays a causal role in the enhanced cytotoxic effects of the combination treatment.

*2.4.4 Cediranib and quinacrine both inhibit Akt kinase activation*

The Akt kinase can strongly affect autophagic flux through its downstream target, mammalian target of rapamycin (mTOR). Inhibitors of the Akt pathway have been shown to potently induce autophagy in tumors (Mirzoeva, *et al.* 2011). Because PDGF signaling can alter the activation of this pathway, we assessed whether cediranib treatment has an effect on the activation of the Akt kinase.

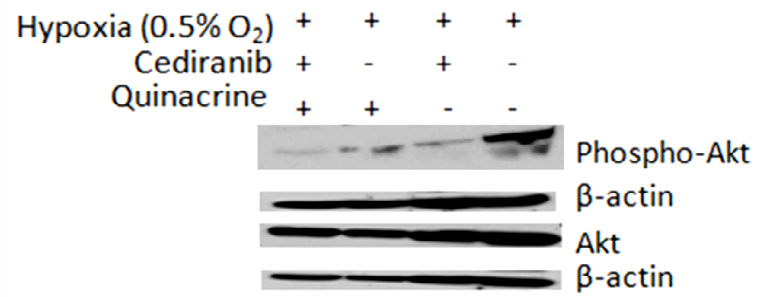


**Figure 2.5. Cediranib and quinacrine inhibit Akt activation.** Western blot analysis of basal Akt and phospho-Akt levels in 4C8 cultures grown under hypoxic (0.5% $O_2$) conditions for 24 hrs while untreated or exposed to cediranib (2.5μM), quinacrine (2.5 μM), or combined quinacrine/cediranib treatement.

Figure 2.5 shows that cediranib strongly inhibited the phosphorylation of the Akt kinase, suggesting a possible mechanism for autophagy induction. Also, because agents structurally related to quinacrine have been reported to have inhibitory effects on Akt activation we determined if quinacrine also possesses such abilities (Guo, *et al.* 2009). Figure 2.5 shows that quinacrine effectively prevents the activation of the Akt kinase, suggesting that apart from inhibiting the degradation of AVs, quinacrine may also be cooperating with cediranib in effectively inducing autophagy in the glioma cells.

*2.4.5 The role of quinacrine treatment in inducing autophagy may be critical to the enhancement of cediranib anti-glioma effect*

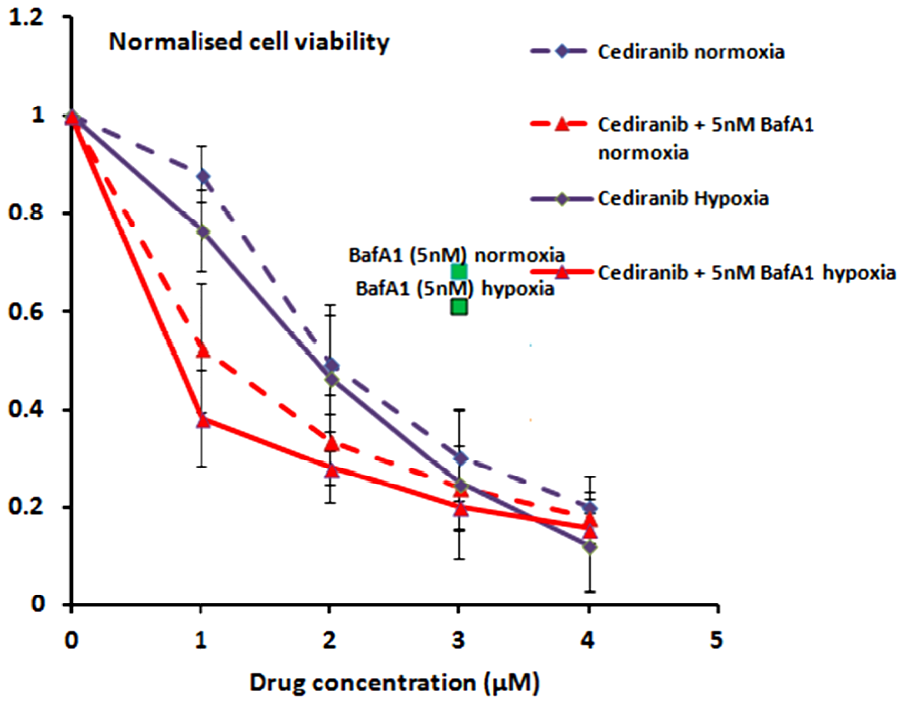


**Figure 2.6. Bafilomycin A1 enhances cediranib glioma cytotoxicity in an additive fashion under hypoxic conditions.** Results from MTS cell viability assays showing mean 4C8 cell viability in response to treatment, normalized to untreated samples. Assays were performed after cells were exposed to cediranib and/or bafilomycin A1 treatment for 72 hours, under normoxic or hypoxic (0.5% $O_2$) conditions. Results are mean ± SEM of three independent experiments, performed in triplicate.

Bafilomycin A1 has been shown to block AV degradation by inhibiting the acidification of lysosomes through its action on the vacuolar H+ ATPase (V-ATPase) enzyme (Yamamoto*, et al.* 1998). Because bafilomycin A1 and quinacrine function as late stage autophagy inhibitors we sought to determine if bafilomycin A1 has the potential to show a similar enhancement of cediranib anti-glioma efficacy. Figure 2.6 shows the results of MTS cell viability assays performed on 4C8 cells exposed to a range of cediranib concentrations in combination with 5nM bafilomycin A1. We observed that bafilomycin A1 cooperated with cediranib in an additive fashion under normoxic and hypoxic

conditions, lending support to the concept that AV accumulation enhances cediranib anti-glioma efficacy. However, the strong potentiation of these effects under hypoxic conditions, as demonstrated with the quinacrine/cediranib combination, was not observed here (Figure 2.6).

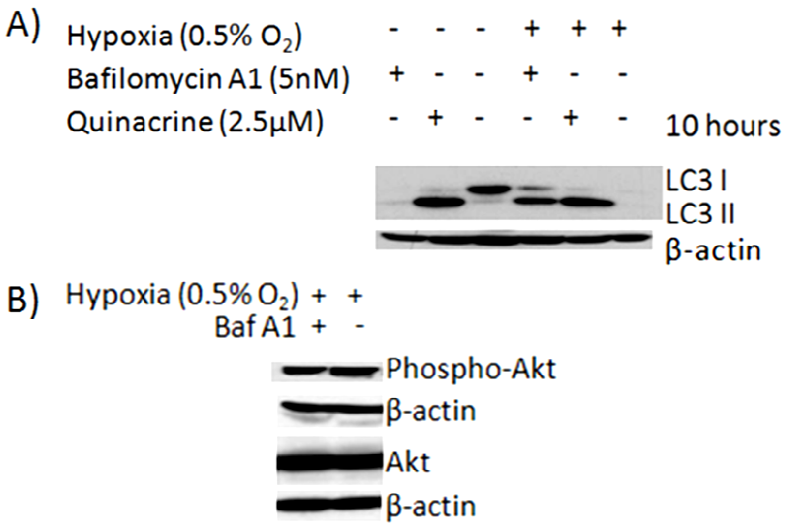


**Figure 2.7. Bafilomycin A1 causes autophagic vacuole accumulation to a lesser extent compared to quinacrine and does not affect Akt activation.** A)Representative LC3 western blots obtained from 4C8 cells grown under normoxic or hypoxic (0.5% $O_2$) conditions for 10 hrs while untreated or exposed to quinacrine (2.5 µM) or bafilomycin A1 (5nM). B) Representative basal Akt and phospho-Akt western blots obtained from 4C8 cells grown under hypoxic (0.5% $O_2$) conditions for 24 hrs while untreated or exposed to bafilomycin A1 (5nM).

To further probe into the differences in cytotoxicity observed with the quinacrine/cediranib and bafilomycin A1/cediranib combinations, we exposed 4C8 cells to bafilomycin A1 and quinacrine using doses that had comparable effects on cell viability. These experiments were conducted under normoxic and hypoxic conditions, to assess the levels of LC3-II accumulation. We observed that under both conditions, quinacrine caused a larger accumulation of LC3-II (Figure 2.7A). We further probed for the levels of phosphorylated Akt kinase in response to bafilomycin A1 treatment and found that there was no change in the activation of Akt kinase (Figure 2.7B). These data

suggest that quinacrine, and not just cediranib, plays an essential role in inducing autophagic flux under hypoxic conditions, creating a stronger cytotoxic effect through the inhibition of degradation and promotion of an extensive accumulation of AVs.

### 2.5 Discussion

Tyrosine kinases are known to play a critical role in the regulation of growth factor signaling in tumor cells. Targeted anticancer therapy through RTK inhibitors have been shown to possess high specificity towards tumor cells, a broad therapeutic window and lesser nonspecific toxicity in comparison to conventional chemotherapy (Arora*, et al.* 2005). With the phenomenal success of Gleevec (imatinib mesylate) in the treatment of patients with chronic myelogenous leukemia (CML), RTK inhibitors have been extensively studied, leading to the FDA approval of several of them including Sunitinib (targets include VEGFR and PDGFR) for the treatment of gastrointestinal stromal tumor and Sorafenib (targets include RAF, PDGFR, VEGFR) for the treatment of advanced renal cell carcinoma, amongst other tumor types. RTK inhibitors, however, have not yet demonstrated efficacy in clinical studies for GBM (De Witt Hamer 2010). This could be due to a number of reasons including a lack of animal glioma models that are a true representation of the pathobiology of glioblastoma in patients, failure of agent to cross the blood brain barrier, and development of treatment resistance in tumors through mechanisms such as autophagy (Gupta*, et al.* 2010, Shingu*, et al.* 2009 Shen*, et al.* 2013, Zhang*, et al.* 2009). Under stressful conditions, as well as in response to commonly used therapeutic agents such as temozolomide and bevacizumab, it has been shown that autophagic flux can be increased in tumor cells to provide a temporary source of energy

and cellular building blocks essential for survival (Shintani*, et al.* 2004). Thus, autophagy contributes to the survival of tumor cells, but a late stage inhibition of the process will inhibit AV degradation and can potentially trigger cell death. Although the precise mechanisms of autophagic cell death are presently unclear, it is known that AV accumulation is associated with mitochondrial and lysosomal membrane permeabilization which may play a role through the release of catabolic enzymes that trigger cell death. This cell death can occur via pathways related to apoptosis or necrosis (Levine*, et al.* 2005). Thus, when autophagic flux has been sufficiently upregulated in tumor cells, they can be very sensitive to lysosomotropic agents, such as chloroquine and quinacrine through the late stage inhibition of the process.

Our results demonstrate that cediranib, an anti-angiogenic RTK inhibitor, has direct cytotoxic effects on glioma cells at micromolar concentrations, which is in agreement with earlier studies (Wedge*, et al.* 2005). Inhibition of the pro-survival Akt pathway through cediranib's action on PDGFR signaling in glioma cells presents a possible mechanism for these effects observed *in vitro* (Figure 2.2A). Quinacrine treatment also resulted in significant reductions in tumor cell viability. It has a polypharmacological nature, and hence in addition to its lysosomotropic effects, its inhibition of nuclear factor-κB (NF-κB), Akt and stabilization of p53 tumor suppressor pathways may also play a role (Gurova 2009). MTS assays revealed that quinacrine and cediranib had a greater than additive effect on tumor cell viability under hypoxic conditions, which correlated well with increased caspase-3 activation (Figure 2.2B). Our study is the first to report that cediranib directly induces autophagy in glioma cells (Figure 2.3). Under hypoxic

conditions, we also found that the combination treatment induced a maximum accumulation of LC3II and hence AVs (Figure 2.3A). By co-administering 3-MA and preventing the formation and accumulation of AVs, we observed a significant decrease in the cytotoxicity of the quinacrine/cediranib combination (Figure 2.4). These data showed that AV accumulation is at least partly required for the enhanced anti-glioma effects reported in Figure 2.2. We also probed 4C8 cells for the levels of phosphorylated Akt kinase and found that cediranib potently inhibits Akt kinase activation (Figure 2.5). Thus, downregulation of the Akt pathway may present a possible mechanism for the increase in autophagic flux in response to cediranib treatment. Also, because agents such as 9-Aminoacridine have been shown to inhibit signaling through the Akt kinase, quinacrine has been proposed to have similar abilities because of its related structure (Ehsanian*, et al.* 2011, Guo*, et al.* 2009). To our knowledge, we are the first to establish that quinacrine strongly inhibits Akt kinase phosphorylation. This suggests that quinacrine not only inhibits the degradation of AVs, but also may induce autophagy. The significance of this contribution of quinacrine to the cytotoxicity of the combination treatment was evident when the enhancement of cediranib cytotoxicity with bafilomycin A1 was not as pronounced as with quinacrine. (Figure 2.6). We found that bafilomycin A1 had no effects on the Akt kinase activation and created a smaller presence of AVs as observed by LC3-II blots (Figure 2.7). These data suggest that activation of autophagy not only occurs with cediranib in tumor cells but it is likely quinacrine as well, thus creating a more potent cytotoxic effect with the inhibition of AV degradation.

Our findings reveal that hypoxic glioma cells are particularly sensitive to quinacrine/cediranib combination treatment. It is possible that hypoxia, cediranib and quinacrine together provide a powerful stimulation to autophagic flux, creating an extensive accumulation of AVs through the inhibition of their degradation. Our results demonstrate that modulating the autophagy pathway can be an effective strategy to enhance the anti-glioma efficacy of cediranib and possibly other related RTK inhibitors. Other mechanisms may also contribute. Recent evidence demonstrates an increased dependence of glioma cells on Akt signaling under hypoxic conditions for growth and survival (Kunz*, et al.* 2003, Polytarchou*, et al.* 2011, Stegeman*, et al.* 2012). An inhibition of Akt signaling has been shown to effectively overcome hypoxia induced treatment resistance in tumors (Polytarchou*, et al.* 2011, Stegeman*, et al.* 2012). Our present study suggests that our novel treatment strategy involving the quinacrine/cediranib combination can effectively sensitize hypoxic tumor cells to apoptotic cell death *in vitro*. Because a wide variety of solid tumors have shown to develop hypoxia (Cairns*, et al.* 2007), this strategy might prove effective in other tumor types as well and might also be exceptionally useful in improving the outcome associated with a range of treatments where hypoxia contributes to resistance, including radiotherapy. Studies in Chapter 3 will probe into the *in vivo* efficacy of this unique drug combination.

# Chapter 3: Quinacrine enhances cediranib anti-angiogenic/anti-tumor efficacy in intracranial mouse glioma

*Merryl R. Lobo, Sarah C. Green, Matthias C Schabel, Yancey G. Gillespie, Randall L. Woltjer, *Martin M. Pike

*Most of the work described in this Chapter has been accepted for publication in Neuro-Oncology. *These authors are the sole contributors to this work.*

## 3.1 Abstract

Despite malignant glioma vascularity, anti-angiogenic therapy is largely ineffective. We hypothesized that efficacy of the anti-angiogenic agent cediranib is synergistically enhanced in intracranial glioma via combination with the late-stage autophagy inhibitor quinacrine. Relative cerebral blood flow and volume (rCBF, rCBV), vascular permeability ($K^{trans}$), and tumor volume were assessed in intracranial 4C8 mouse glioma using a dual-bolus dynamic MRI approach. We found that cediranib or quinacrine treatment alone did not alter tumor growth. Survival was only marginally improved by cediranib, and unchanged by quinacrine. In contrast, combined quinacrine/cediranib reduced tumor growth by over 2-fold ($p < 0.05$), and increased median survival by over 2-fold, compared to untreated ($p < 0.05$). Cediranib or quinacrine treatment alone did not significantly alter mean tumor rCBF or $K^{trans}$ compared to untreated while combined quinacrine/cediranib substantially reduced both ($p < 0.05$), indicating potent tumor

devascularization. Immunohistochemical studies revealed that MVD and necrosis were unchanged by cediranib or quinacrine treatment. In contrast, MVD was reduced by nearly 2-fold ($p < 0.01$), and necrosis increased by 3-fold ($p < 0.05$ one-tailed), in quinacrine/cediranib treated versus untreated. Using electron microscopy, we also confirmed the presence of autophagic vacuoles (AVs) *in vivo* with cediranib treatment suggesting that the mechanistic interactions involving autophagy modulation, elucidated in Chapter 2, may play a role *in vivo*. Collectively, our results demonstrated that combined quinacrine/cediranib treatment synergistically increased anti-vascular/anti-tumor efficacy in intracranial 4C8 mouse glioma, suggesting a promising and facile treatment strategy for malignant glioma.

### 3.2 Introduction

The studies outlined in Chapter 2 show that Cediranib, an anti-angiogenic RTK inhibitor, exerts direct cytotoxic effects on glioma cells. Not only does cediranib, by itself, reduce tumor cell viability in a dose dependant manner, but it also potently induces autophagy, which may be protecting the tumor cells and limiting cediranib efficacy. A detailed investigation of combined treatment with cediranib and the autophagy inhibitor-quinacrine, using glioma cell cultures, revealed that cediranib efficacy can be significantly enhanced through late stage autophagy inhibition, as a result of the toxic accumulation of AVs. Both agents were shown to potently inhibit Akt activation, presenting a mechanism for modulation of the autophagy pathway. Although these *in vitro* studies suggest that the novel quinacrine/cediranib combination has immense potential in glioma treatment, it is essential to determine if this synergistic interaction

translates to therapeutic benefit in the *in vivo* setting as well. Tumors, *in vivo,* tend to be much more complex, presenting a dynamic system consisting of not just tumor cells but also fibroblasts, blood vessels, extracellular matrix, a diverse range of signaling molecules and immune cells. All these factors, together constituting the tumor microenvironment, communicate with the tumor cells and can limit the efficacy of treatment (Swartz*, et al.* 2012). Also, drug pharmacokinetics can compromise therapeutic outcome, particularly if they are unable to adequately access the tumor. This is of particular relevance to brain tumors where many therapeutic agents are unable to cross the blood brain barrier and reach the tumor cells (Westphal*, et al.* 2011). Thus, an effective animal model evaluation of a new treatment strategy requires the assessment of clinically relevant parameters such as tumor growth and survival.

Apart from testing the translatability of the quinacrine/cediranib anti-glioma efficacy from the *in vitro* to the *in vivo* setting, we also sought to determine if the anti-angiogenic effects of cediranib were enhanced through combined treatment. Because angiogenesis involves interaction between tumor and host, and is thus dependant on the surrounding microenvironment, it must be evaluated *in vivo*. For this study, we have employed the syngeneic intracranial mouse 4C8 glioma model, used in studies described in Chapter 2, which fosters a seamless tumor–host interaction in immunocompetent mice (Dyer*, et al.* 1995, Pike*, et al.* 2009). We have utilized a comprehensive, dynamic MRI approach which quantifies key vascular biomarkers noninvasively in this model, measuring both vascular flow and permeability while also monitoring tumor growth (Pike*, et al.* 2009). To accomplish this, we employed dynamic contrast enhanced (DCE-MRI), producing

high resolution maps of $K^{trans}$, an index of vascular permeability, that is a key biomarker of tumor neovasculature. Subsequently, dynamic susceptibility contrast MRI (DSC-MRI) was used to determine cerebral blood flow (CBF) and cerebral blood volume (CBV). This dynamic imaging approach, provides functional vascular parameters difficult to obtain histologically, and has revealed evidence that cediranib works synergistically with the autophagy inhibitor quinacrine to induce anti-vascular/anti-tumor efficacy and improve survival of treated mice. The presence of AVs in response to cediranib treatment, detected by electron micrscopy, are consistent with the concept that direct modulatory effects of cediranib on the autophagy pathway, as described in chapter 2, may play a role. Combined histological analysis of tumor necrosis and blood vessel density provided further evidence for the unique efficacy of the combined treatment.

## 3.3 Materials and methods

### *3.3.1 Cell culture and Tumor Inoculation*

Mouse studies were conducted with the approval of the Oregon Health and Science University Institutional Animal Care and Use Committee and under the supervision of the OHSU Department of Comparative Medicine. The 4C8 mouse glioma cells (provided by Dr. G. Yancey Gillespie, UAB) were grown in Dulbecco's modified Eagle's medium/Ham's F-12 50/50 Mix (Invitrogen, Carlsbad, California), supplemented with 7% fetal bovine serum (FBS) (Hyclone, Logan, Utah) and 1% L-glutamine (Sigma-Aldrich, St. Louis, Missouri). Female C57BL/6 × DBA/2 $F_1$ hybrid mice (B6D2F1) were purchased from Charles River Laboratories (Wilmington, MA). Brain tumors were

induced by the intracerebral injection of ~1 × $10^6$ 4C8 cells, suspended in DMEM/F12 (5-10µl) using a stereotaxic frame as previously described (Pike*, et al.* 2009).

### *3.3.2 Electron Microscopy*

Formalin fixed tumor samples were post fixed in 1% Osmium Tetroxide for 1 hour. Samples were then rinsed in water and dehydrated in a graded series of Acetone for 20 minute intervals, placed in 1:1 Acetone/Epon 812 for 12 hours and embedded in 100% Epon 812 at 60°C for 12 hours. The embedded blocks were sectioned on an ultramicrotome at 60 nanometers and stained with saturated Uranyl Acetate and lead citrate and viewed with the electron microscope (FEI CM120/Biotwin TEM).

### *3.3.3 MRI procedures*

Starting at 10 days after tumor cell inoculation, mice were routinely imaged using contrast-enhanced (Magnevist i.p.) $T_1$ weighted MR imaging to determine when tumor growth initiates. When tumors reached a cross-sectional area of approximately 2 $mm^2$, (generally at 2-3 weeks post inoculation), pretreatment dynamic MRI studies were implemented, after which mice were randomized into four treatment groups with treatments starting within 24 hours: 1) untreated, n = 6 (vehicle: 1% Tween in phosphate buffered saline (PBS), oral gavage, daily); 2) cediranib, n = 6 (AZD2171, 6 mg/kg in 1% Tween/PBS, daily, oral gavage, Selleck Chemicals LLC Houston, TX); 3) quinacrine, n = 5 (50 mg/kg in PBS, daily, oral gavage, Sigma-Aldrich); and 4) cediranib + quinacrine, n = 6 (daily). Biweekly dynamic MRI experiments were discontinued when right brain

displacement by the tumor was reaching a maximum, or when mice showed neurological/behavorial changes, or signs of physical deterioration such as excessive weight loss or skull deformation, at which point mice were sacrificed and their brains were harvested and stored in 10% formalin for histology. For dynamic MRI, mice were initially anesthetized with a ketamine/xylazine mixture (1.5 mg xylazine/10 mg ketamine/100g) and one of the lateral tail veins was cannulated using a 30 gauge needle attached to PE 10 tubing, filled with sterile saline containing 15U heparin/ml. MR imaging employed a Bruker-Biospin 11.75T small animal MR system with a Paravision 4.0 software platform, 9 cm inner diameter gradient set (750 mT/m), and a mouse head (20 mm ID) quadrature RF transceiver coil (M2M Imaging Corp.) The mice were positioned with their heads immobilized with a specially designed head holder with adjustable ear pieces. Body temperature of the mice was monitored and maintained at 37°C using a warm air temperature control system (SA instruments). Isoflurane (0.5–2%) in 100% oxygen was administered and adjusted while monitoring respiration.

A coronal 25 slice $T_1$ weighted image set was obtained using a spoiled gradient echo sequence (Paravision FLASH, 256×256 matrix, 98 μm in-plane resolution, 0.5 mm slice width, TR 500 msec, TE 1.4 msec, FA 60°, 1 average) to determine the dynamic MRI slice position within the tumor, which was matched to that used in any previous imaging sessions using brain/skull anatomical features. A $T_2$ weighted image set (Paravision spin echo RARE, same spatial geometry as for multislice $T_1$ weighted, TR 4000 msec, $TE_{effective}$ 32 msec, RARE factor 8, 1 average) was obtained to assess tumor volume. A fully relaxed ($M_0$) spoiled gradient echo precontrast image (Paravision FLASH, TR 6000

ms, TE 1.2 ms, FA 90°, 128×128 matrix, 1 slice, 1 mm slice thickness, 195 μm in-plane resolution) was obtained at the position of the subsequent DCE $T_1$ weighted image series (450 images) which used the same parameters except with TR 15.6 msec and FA 20° (2.0 s/image), and with Gd-DTPA injection (Magnevist, Berlex Inc, i.v., 10X diluted, 3.0 μl/g, 0.15 mmol/kg). DSC-MRI was then implemented (150 $T_2$* weighted images, Paravision FLASH, TR 8, TE 4.2 ms, FA 5°, 128×128 matrix, 1 slice, 1 mm slice thickness, 195 μm in-plane resolution, 1 s/image) employing Feridex, an SPIO agent (Berlex Inc, 4X diluted, 2.4 μl/g, 26.9ug iron/g). Both injections occurred at 30 s after initiation of the image series, at 1 mL/min, using a 150 μL saline/heparin chase.

*3.3.4 Image processing*

DCE-MRI parameters were computed voxelwise using the Extended Tofts-Kety model (Sourbron*, et al.* 2012, Tofts*, et al.* 1999) using custom pharmacokinetic modeling software (developed by M. C. Schabel) written in MATLAB (MathWorks, Natick, MA). Fully relaxed $M_0$ image intensities were used to compute pre-injection longitudinal relaxation time, enabling quantitative concentration measurement and $K^{trans}$ (in $min^{-1}$) estimates (Pike*, et al.* 2009). The Monte Carlo Blind Estimation (MCBE) algorithm was used to determine the arterial input function directly from measured tumor curves (Schabel*, et al.* 2010, Schabel*, et al.* 2010). Calculation of DSC-MRI perfusion parameters followed the model-independent method described in Ostergaard L. *et al*. (Ostergaard*, et al.* 1996) using the Jim software package (Xinapse Systems LTD, Northants, UK). The AIF was determined from 12 non-tumor brain pixels identified by an automatic scanning and selection routine which targeted brain parenchymal arterial

microvessels (Pike*, et al.* 2009). DSC data analysis was restricted to the first 50 post-contrast images in the series to bracket the susceptibility bolus intensity changes. Parametric maps were generated for cerebral blood flow (CBF in mL blood/100g tissue/ minute), cerebral blood volume (CBV in blood volume percentage of total tissue volume), and mean transit time (MTT in seconds). Analysis of the DCE/DSC-MRI parametric maps, and $T_2$ multislice images employed the Jim software package. Tumor volumes were calculated from the multislice $T_2$ weighted images. The DSC-MRI parameters (rCBF, rCBV, rMTT) were reported relative to contralateral values to reduce measurement error, and minimize effects from alterations in intracranial pressure, blood pressure, and depth of anesthesia.

*3.3.5 Histology*

At the termination of serial MRI studies, mice were sacrificed and brains were stored in 10% Formalin. Fixed tissue samples were paraffin embedded and 7 μm sections were mounted on slides. The slides were then processed and stained with Hemotoxylin (Sigma-Aldrich) and Eosin (Sigma-Aldrich), using standard methodologies. For each tumor sample (n = 4 tumor samples/treatment group) a total of three image fields (4X magnification) were positioned randomly across a minimum of two stained tumor sections and photographed using an Olympus BX50 microscope mounted with a Leica camera DFC320 equipped with Leica Firecam Version 3.4.1. Necrotic regions within the image fields were quantified using the ROI analysis tool of the Jim software package under the supervision of an experienced neuropathogist (RLW) and averaged. In adjacent sections from three mice per treatment group, immunohistochemical vascular staining

was performed after deparaffinized sections were subjected to antigen retrieval (5 min treatment at room temperature with 95% formic acid followed by incubation at 85-90 degrees in citrate buffer, pH 6.0, for 30 min), using mouse monoclonal primary antibody to CD31, clone JC70A (Dako), with hematoxylin counter stain. Slides were prepared using the Mouse-On-Mouse (M.O.M) Peroxidase Kit (Vector Labs) to prevent non-specific background and the presence of CD31 was investigated using the avidin-biotin complex (ABC) method (Vector Labs), with diaminobenzidine. Slides were studied at 40x magnification, and the number of CD31 stained vessels was counted in 10 random fields across 2 sections for each tumor and averaged to obtain mean vessel density (MVD).

### *3.3.6 Statistics*

Values are expressed as mean (± SEM). For dynamic MRI and CD31 immunohistochemistry results, the two-tailed Unpaired Student's t test (NCSS Statistical Software, (Kaysville, UT) was employed to test for differences at 0, 3(±1), 6(±1), and 11(±1) days after tumor growth initiation versus untreated (time points corresponding to ≥ 50% untreated group survival). Differences in median survival were tested using the log-rank test. The Paired Student's *t* test (one-tailed, tumors were paired to tumor cell injection batch) was used for analysis of percent necrosis (MATLAB).

## 3.4 Results

### *3.4.1 Quinacrine/cediranib combination decreases tumor growth rate and increases mouse survival*

The $T_2$ weighted MR images depicted in Figure 3.1 were obtained from mice at 14 days after tumor growth initiation and show clearly delineated tumors. Figures 3.1A-C indicate similar cross sectional areas for untreated tumors in comparison to single agent treatment with cediranib or quinacrine. In contrast, Figure 3.1D indicates that the tumor from the combined quinacrine/cediranib treatment group is substantially smaller.

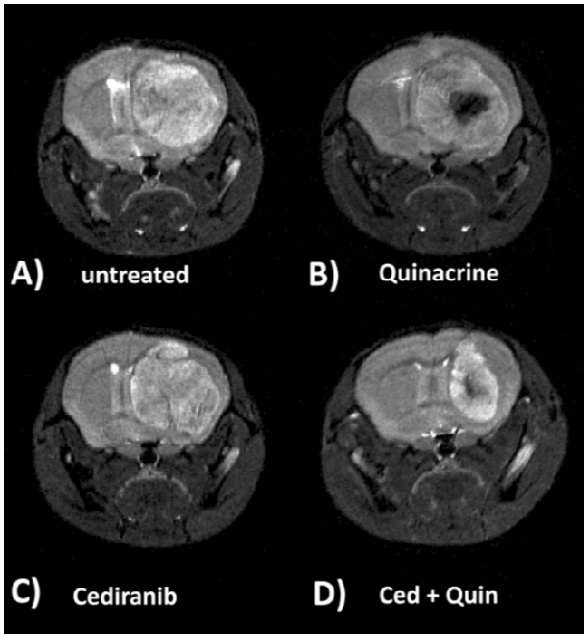


**Figure 3.1. Combined quinacrine/cediranib treatment results in smaller tumor sizes.** Representative $T_2$ weighted coronal mouse brain MR images obtained at 14 days after tumor growth initiation for the four treatment groups: A) untreated, B) quinacrine-treated, C) cediranib-treated, and D) quinacrine/cediranib treated.

Figure 3.2A shows tumor growth curves obtained from the MRI evaluations for the different treatment groups, with tumor volume plotted versus the time from tumor growth

initiation. Rapid tumor growth was observed for untreated mice, increasing to over 70 $mm^3$ over an 11 day period. The growth curves indicated that tumor growth was essentially unaltered by cediranib or quinacrine treatment. In contrast, tumor growth was markedly reduced with combined quinacrine/cediranib throughout the treatment period, ($p < 0.05$ versus untreated), with a 60% lower tumor volume than untreated at 11 days of growth. Consistent with this, exponential curves fit to the individual tumor volume *vs* time data provided mean exponential growth rate constants (in $days^{-1}$), and indicated a substantially lower growth rate constant for combined quinacrine/cediranib ($0.12 \pm 0.01$) versus untreated ($0.26 \pm 0.03$ $p < 0.0014$), with values for quinacrine ($0.21 \pm 0.017$) and cediranib ($0.18 \pm 0.017$) that were not significantly different from untreated.

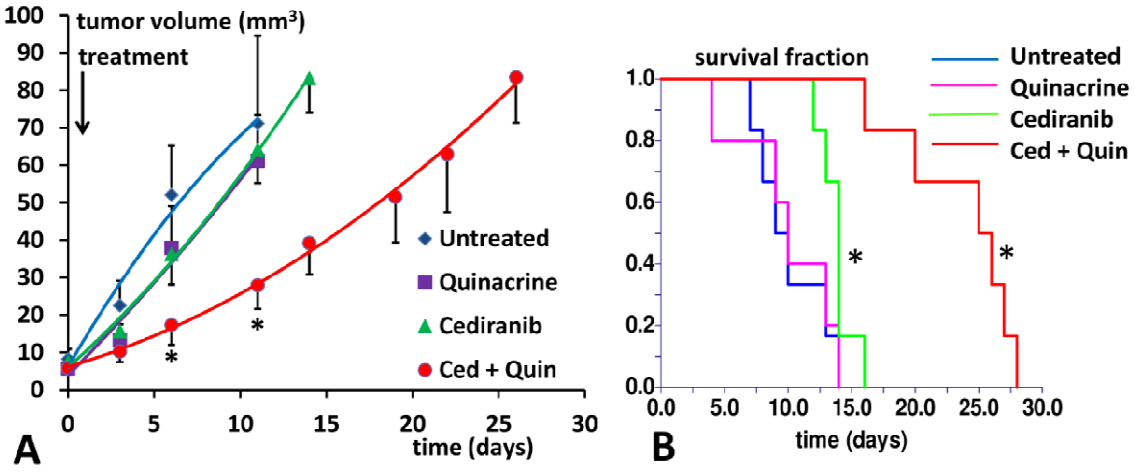


**Figure 3.2. Quinacrine/cediranib treatment delays tumor growth and increases mouse survival.** A) Tumor growth curves are shown for the four treatment groups, in tumor volume versus time after tumor growth initiation. Curves are indicated for time points corresponding to ≥ 50% survival. *: $p < 0.05$ versus untreated. B) Kaplan-Meier survival curves for the four treatment groups (in days from tumor growth initiation) *: $p < 0.05$ versus untreated.

The Kaplan-Meier survival curves in Figure 3.2B indicate that no increase in median survival over untreated ($9.5 \pm 1.1$) occurred with quinacrine-treated mice ($10.0 \pm 1.8$). Cediranib-treated mice indicated only a modest increase in survival ($14 \pm 0.5$, $p < 0.05$ vs

untreated). In contrast, median survival was substantially extended with combined quinacrine/cediranib treatment (25.5 ± 1.9, $p < 0.0001$) versus untreated.

*3.4.2 Quinacrine/cediranib causes substantial and sustained reductions in mean tumor DCE/DSC pharmacokinetic parameters*

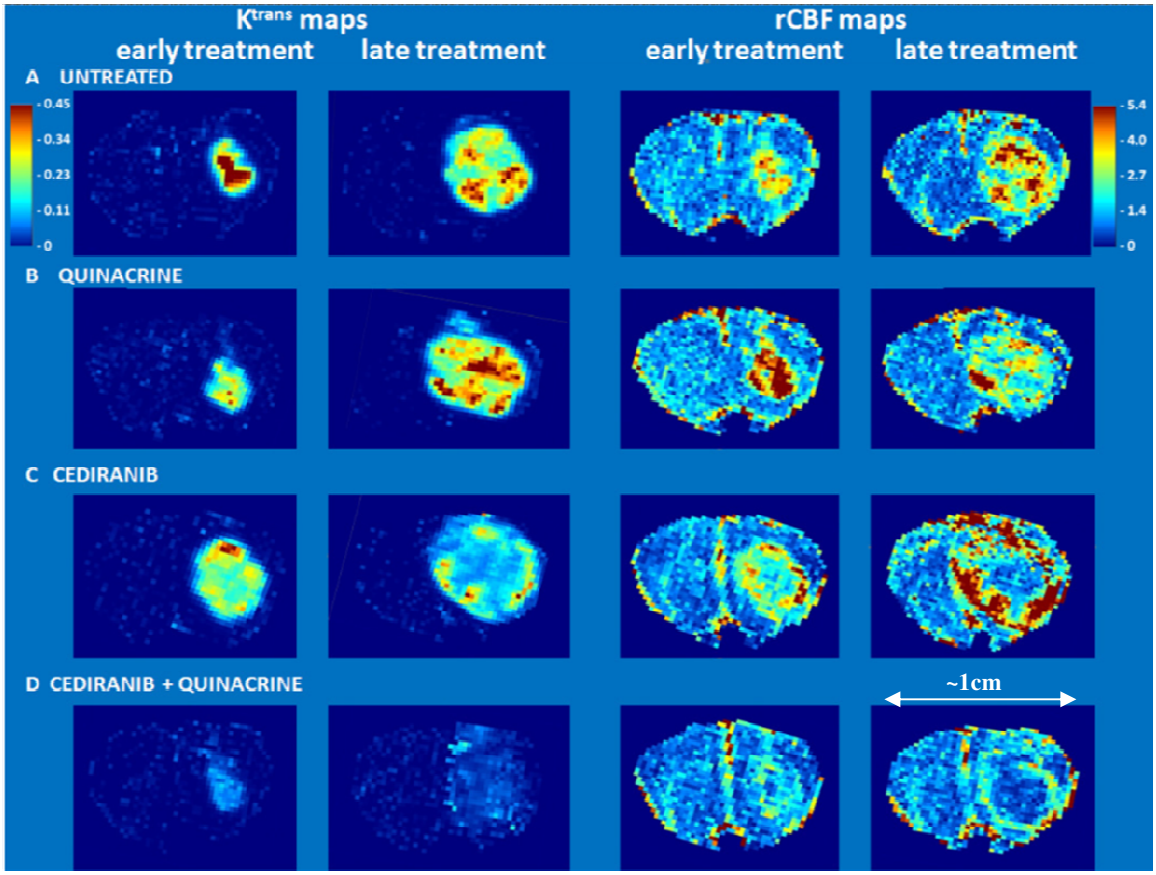


**Figure 3.3. Quinacrine/cediranib treatment causes substantial reductions in $K^{trans}$ and rCBF values in the tumor rim and core regions.** rCBF and $K^{trans}$ ($min^{-1}$) parametric maps (non-brain regions masked) obtained from representative tumors from each treatment group both during the first week after tumor growth initiation, and during the final week of MRI evaluation (CBF color scale is relative: contralateral hues set to ~unity.)

Tumor vascularity was evaluated with the dual bolus-tracking DCE/DSC dynamic MRI approach that we previously validated with intracranial 4C8 mouse glioma (Pike, *et al.*

2009). Figure 3.3 indicates typical rCBF and $K^{trans}$ parametric maps obtained both during the first week after tumor growth initiation, and during the final week of MRI evaluation for representative tumors from each treatment group. While negligible $K^{trans}$ values were observed in non-tumor regions due to the intact blood brain barrier, Figure 3.3A indicates that relatively high and heterogeneous $K^{trans}$ values were observed in untreated tumor. High values of rCBF were also observed, with local "hot spots" exceeding flow in contralateral regions by more than 5-fold, also with a heterogeneous distribution. This pattern, observed throughout the tumor growth period, is consistent with the robust yet heterogeneous and permeable vasculature typical of malignant glioma (Gladson*, et al.* 2010, Rahman*, et al.* 2010). Figure 3.3B shows that similar characteristics are observed in a quinacrine-treated mouse tumor. Figure 3.3C shows parametric maps obtained from a cediranib-treated mouse tumor. Consistent with cediranib's anti-angiogenic mode of action was the development of a very poorly perfused tumor core. Notably however, the tumor clearly retained a well vascularized tumor rim. Persistence of an angiogenic tumor rim, in a continually expanding tumor, demonstrates resilience of gliomas in the face of angiogenic blockade, congruent with clinical observations (Bergers*, et al.* 2008, Rahman*, et al.* 2010). In contrast, Figure 3.3D indicates that with combined quinacrine/cediranib treatment, there was a dramatic reduction in tumor rCBF and $K^{trans}$ in comparison to untreated tumor, starting at the early treatment stage and continuing to the end of treatment. At the latter stage of treatment, the rCBF map indicates an extensive poorly perfused tumor core region, involving a much larger tumor fraction than was observed with cediranib alone. The vascularized rim is also noticeably thinner than that observed following single agent cediranib treatment, with greatly reduced $K^{trans}$ and rCBF values

compared to those observed in cediranib or untreated tumors. The marked reduction in these key flow and permeability vascular biomarkers indicates greatly increased anti-vascular efficacy with combined treatment.

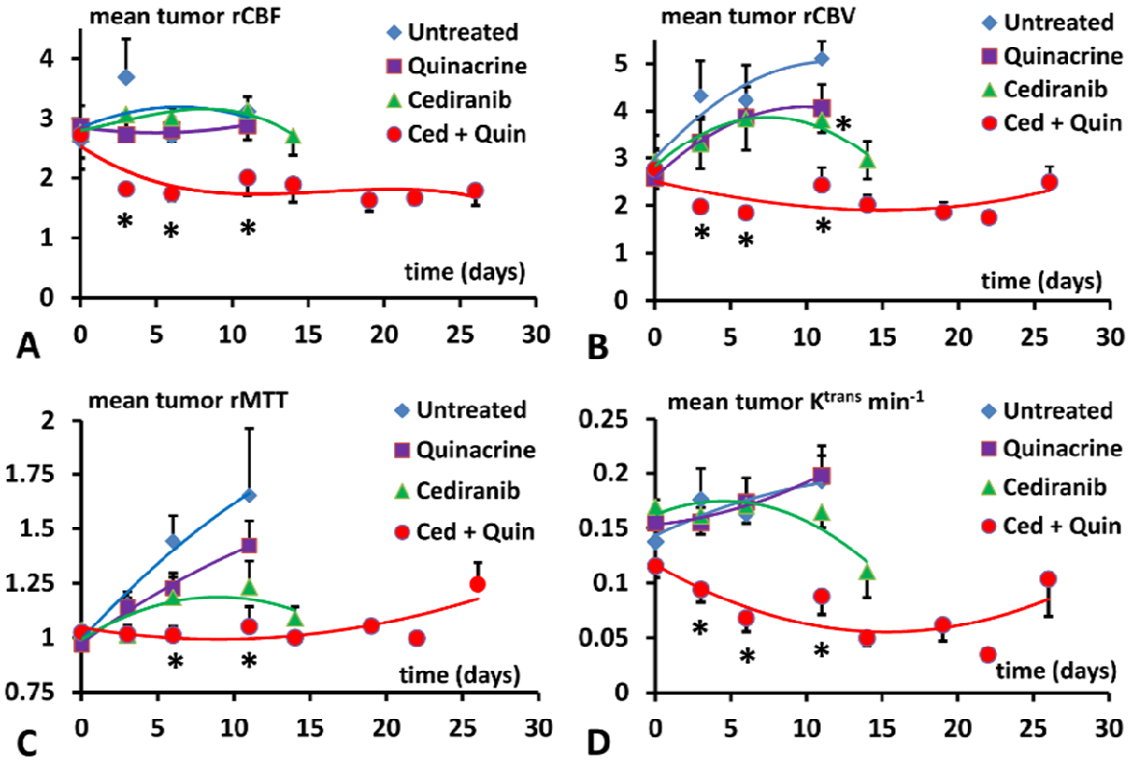


**Figure 3.4. Quinacrine/cediranib treatment induced reductions in mean tumor rCBF, rCBV, rMTT and $K^{trans}$ are consistent throughout the treatment period.** Mean tumor A) rCBF, B) rCBV, C) rMTT and D) $K^{trans}$ ($min^{-1}$) values plotted versus the time from tumor growth initiation for the four different treatment groups. Curves are indicated for time points corresponding to ≥ 50% survival. *: $p < 0.05$ versus untreated.

Figure 3.4 displays mean tumor rCBF, rCBV, rMTT and $K^{trans}$ values plotted versus the time from tumor growth initiation for the four different treatment groups. Figure 3.4A indicates that pre-treatment rCBF levels were uniformly high (~2.8) in the different groups. Consistent with the parametric maps shown in Figure 3.3, in the untreated group, as well as in cediranib-treated and quinacrine-treated groups, mean tumor rCBF remained relatively unchanged at this level during the following period of tumor growth. In

contrast, with combined quinacrine/cediranib treatment, large and sustained decreases in mean rCBF occurred starting at early treatment stages, ($p<0.05$ *vs* untreated). Unlike rCBF, Figure 3.4B indicates that rCBV increased substantially throughout the period of tumor growth in the untreated group. The relatively robust increase in rCBV, in comparison to that of rCBF, suggests the development of a tumor vascular network which is increasingly inefficient, consistent with our previous findings with 4C8 glioma (Pike*, et al.* 2009). Quinacrine treatment did not substantially alter tumor rCBV in comparison to untreated. Cediranib-treatment moderately attenuated the increase in rCBV, indicating lower values in comparison to untreated at 11 days after initiation of tumor growth. Combination of cediranib with quinacrine produced a substantially greater effect however, with rCBV decreasing rather than increasing, to values significantly below that of untreated throughout the treatment period. Figure 3.4C indicates that rMTT, which is inversely related to vascular efficiency, increased substantially with tumor growth for the untreated group, consistent with the robust increase in rCBV in comparison to rCBF. Quinacrine did not substantially alter rMTT in comparison to untreated. Consistent with its effects on rCBV, cediranib tended to attenuate rMTT values below those observed in untreated (non significant versus untreated). Combined quinacrine/cediranib treatment entirely prevented increases in rMTT with tumor growth, resulting in rMTT values that were substantially lower than those observed in the untreated group. Figure 3.4D indicates that mean tumor $K^{trans}$ values gradually increased with tumor growth, consistent with development of permeable tumor neovasculature. Quinacrine-treated mice indicated a similar pattern, while the cediranib-treated group exhibited a tendency toward decreased $K^{trans}$ values in the latter stages of tumor growth (non significant versus

untreated), likely due at least in part to decreased vascular permeability, consistent with cediranib's VEGF receptor inhibition. With combined quinacrine/cediranib treatment, marked decreases in $K^{trans}$ occurred, to levels substantially below that in all the other groups. As $K^{trans}$ is, under most conditions, proportional to the permeability-surface area product per unit volume of tissue, the marked decrease is likely to be primarily due to decreased vessel surface area in conjunction with tumor devascularization, given the substantial reductions in tumor rCBF and rCBV which also occurred, suggesting a greatly reduced vascular network (Barrett, *et al.* 2007). Taken together, the dynamic MRI results indicate that combined quinacrine/cediranib treatment has a profound effect on the tumor vasculature, inducing a synergistic increase in anti-vascular/anti-tumor efficacy, and effectively slowing tumor growth and extending survival in mouse 4C8 glioma.

*3.4.3 Cediranib treatment results in AV formation in vivo.*

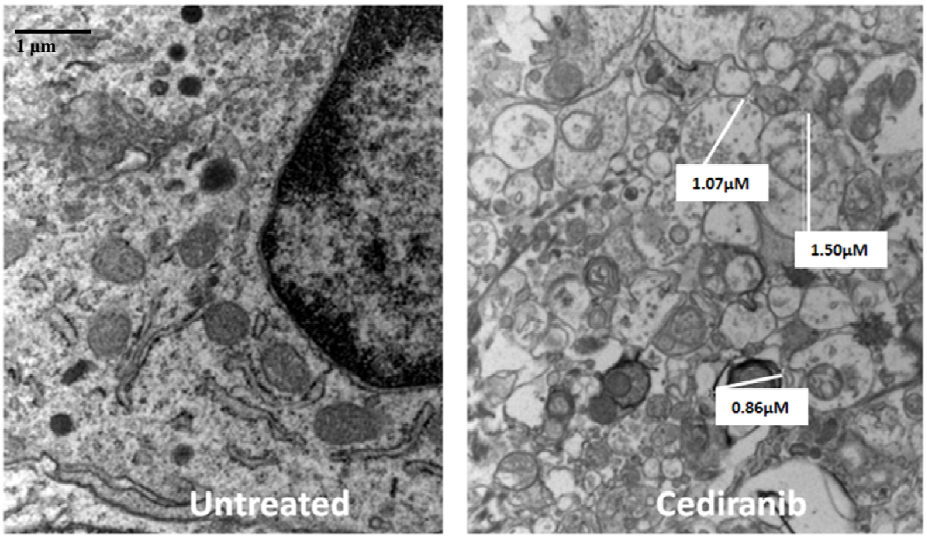


**Figure 3.5. Cediranib treatment causes autophagic vacuole formation *in vivo*.** Representative electron micrographs showing ultrastructure of tumor tissue derived from untreated and cediranib treated mouse 2 weeks post initiation of tumor growth. Diameter measurements associated with some of the autophagic vacuoles in the cediranib treated tumor tissue have been indicated. Mike Webb from the OHSU electron microscopy core assisted in generating these data.

Tumor tissue obtained with and without cediranib treatment was analyzed using electron microscopy for signs of increased autophagic flux (Figure 3.5). Electron microscopy is considered to be the "gold standard" technique in detecting AVs. A number of vacuoles were found to be present in cediranib treated tumor tissue, which generally contained engulfed cytoplasmic material, characteristic of AVs. These results suggest that cediranib induced autophagic flux in intracranial 4C8 tumors.

### *3.4.4 Combined quinacrine/cediranib treatment results in reduced Mean Vessel Density (MVD)*

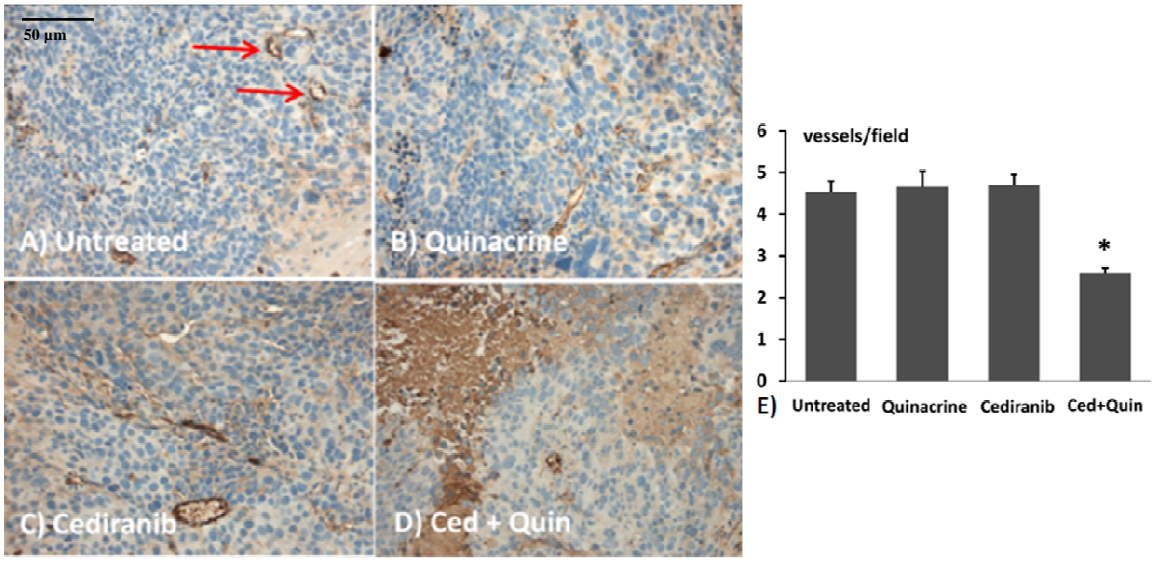


**Figure 3.6. Quinacrine/cediranib treatment reduces mean vessel density in tumors.** A-D) Representative histological tumor sections with CD31 vascular staining (brown) and hematoxylin nuclear counter stain (blue) from the four treatment groups. Discrete staining is associated with vascular endothelial cells, whereas more diffuse and variable staining is nonspecific and associated with tumor necrosis. Microvessel examples are marked by arrows. E) MVD quantified from multiple CD31 stained sections for the four treatment groups. Field area = $2x10^{-3}$ $mm^2$. *: $p<0.01$ versus untreated. Keri Forquer from the OHSU histopathology core assisted in generating these data.

Histological studies performed after completion of the longitudinal MRI studies confirmed the dynamic MRI results, and provided further information regarding tumor pathology. Representative histological tumor sections with CD31 vascular staining are shown in Figures 3.6 A-D, and indicate clearly demarcated tumor vessels (see arrows). Consistent with the dynamic MRI results, we generally observed a greater prevalence of vessels at tumor borders. Multiple vessels are indicated in Figures 3.6A-C, in sections from untreated, quinacrine-treated, and cediranib-treated tumors. In contrast, in Figure 3.6D, a section from a quinacrine/cediranib treated tumor shows substantial necrosis (indicated by nonspecific staining), and fewer vessels. Figure 3.6E indicates mean values of MVD that were quantified from multiple CD31 sections. The MVD values were very similar for the untreated, cediranib, and quinacrine groups. In contrast, MVD was reduced in the quinacrine/cediranib treated group by nearly 2-fold in comparison to the other groups. ($p < 0.01$ versus untreated).

*3.4.5 Treatment with quinacrine/cediranib combination increases tumor necrosis*

In Figure 3.7A-D representative H&E sections from the various treatment groups are shown, and clearly indicate regions of tumor necrosis. While similar levels of necrosis were observed in the sections from untreated, quinacrine-treated, and cediranib-treated tumors, necrosis was comparatively increased in sections from quinacrine/cediranib treated tumors. Figure 3.7E indicates that similar levels of tumor necrosis were observed in the untreated, quinacrine, and cediranib groups. In contrast, necrosis was markedly elevated, by approximately 3-fold, in the quinacrine/cediranib group ($p < 0.05$, one-tailed paired t test). That the marked devascularization and reduced tumor growth shown in

Figures 3.1-3.7 occurs in the context of greatly increased tumor necrosis, further documents the marked anti-tumor efficacy of the combined quinacrine/cediranib treatment.

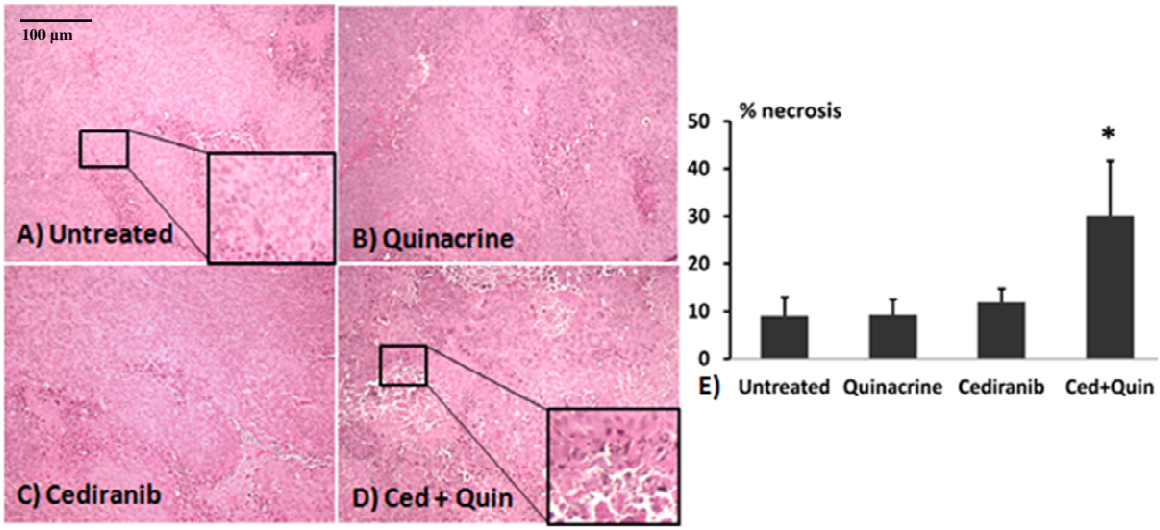


**Figure 3.7. Quinacrine/cediranib treatment induces necrosis in tumors.** A-D) Representative H&E stained sections from the four treatment groups, indicating areas of necrosis, which appear as condensed cells in areas of vacuolated tissue. Insets indicate enlarged areas of the section as indicated. E) Percent necrosis, quantified from multiple H&E stained sections, for the four treatment groups. *: $p<0.05$ versus untreated (one-tailed paired t test). Sarah Green from the Randall Woltjer laboratory assisted in generating these data.

### 3.5 Discussion

Malignant glioma remains a frustratingly difficult disease to treat, characterized by robust angiogenesis, proliferation, and invasion (Gladson, *et al.* 2010, Rahman, *et al.* 2010). It often exhibits marked treatment resistance, and despite its elevated vacularity, anti-angiogenic monotherapy is of limited utility (Bergers, *et al.* 2008, Norden, *et al.* 2009, Rahman, *et al.* 2010). The current study employed the syngeneic intracranial 4C8 mouse glioma model which is characterized by aggressive tumor growth with robust neovasculature, core necrosis (Dyer, *et al.* 1995, Pike, *et al.* 2009) and regions of hypoxia, as shown in Chapter 2. A unique dynamic MRI approach was employed with

the 4C8 glioma model in combination with immunohistological approaches to investigate the effects of separate and combined treatment with cediranib and quinacrine. Our dynamic MRI results demonstrated that while single agent treatment with cediranib in the 4C8 glioma model did not decrease mean tumor rCBF in comparison to untreated tumors, poorly perfused tumor core regions were prevalent in cediranib treated mice, in conjunction with robustly vascularized tumor rim regions. These findings were corroborated by immunohistological determinations of MVD, averaged across the tumor, which were found to be unchanged with cediranib treatment alone. Mean rCBV increases were attenuated with cediranib, in conjunction with a tendency to attenuate mean rMTT increases. In combination with the absence of mean rCBF reduction, this may suggest an augmented vascular efficiency with cediranib, as has been proposed to occur at early stages of anti-angiogenic monotherapy, due to normalization of abnormal and dilated tumor vasculature (Goel*, et al.* 2012, Kamoun*, et al.* 2009, Rahman*, et al.* 2010).

While our study is consistent with previous studies reporting reduced rCBV and vascular permeability in cediranib-treated glioma, to our knowledge the current study is the first to report mean tumor rCBF measurements in a cediranib-treated preclinical glioma model (Bradley*, et al.* 2009, Farrar*, et al.* 2011, Kamoun*, et al.* 2009). Our results clearly demonstrated, with both perfusion MRI and immunohistological approaches, that while cediranib may have limited perfusion in localized regions of the tumor core, it did not prevent a vigorous neovascularization process in the 4C8 mouse glioma model. Cediranib had little effect on tumor growth, and only modest effects on survival,

consistent with previous preclinical and clinical studies indicating that cediranib and other small molecule anti-angiogenic RTK inhibitors with similar molecular targets, have limited efficacy as a single agent cancer therapeutic, particularly with malignant glioma (Batchelor*, et al.* 2007, Bergers*, et al.* 2008, Gotink*, et al.* 2010, Rahman*, et al.* 2010). Our study is the first to document that *in vivo* single agent treatment with quinacrine induces no measureable effects on mean rCBF, rCBV, $K^{trans}$, tumor growth or survival in malignant glioma. Similarly it did not alter tumor necrosis or MVD. In contrast, our study provides dramatic evidence for a strong synergy between cediranib and quinacrine in terms of both anti-vascular and anti-tumor efficacy. Combined cediranib and quinacrine induced markedly reduced tumor perfusion, consistent with the sharply reduced histological determinations of MVD. Consistent with this, tumor necrosis was found to be 3-fold greater in the combined quinacrine/cediranib than in untreated or single agent treated tumors. Tumor growth was slowed by more than a factor of 2, resulting in substantially increased survival.

Given the known pharmokinetics of the therapeutic agents employed in this study, our *in vivo* results are consistent with the cytotoxicity the agents exhibited *in vitro*, as documented in Chapter 2. A study by Wang *et al*. indicates that cediranib reaches micromolar concentrations in the blood plasma: a one-time cediranib dose of 5 mg/kg resulted in a cediranib plasma concentration of 1.13 μM, ~4 hours post drug administration (Wang*, et al.* 2011). Although concentrations in normal brain tissue were found to be much lower, cediranib present in 4C8 tumor tissue is likely to approach micromolar concentrations, given its extremely permeable vasculature and the repetitive

dosing regimen of mice in our studies (6 mg/kg/day). Quinacrine, has been reported to reach brain tissue concentrations (ng/g) of 400-600 and 1500 for doses (mg/Kg/day) of 37.5 and 75, respectively (Yung*, et al.* 2004). These translate to concentrations of 1.3 µM and 3.2 µM in mouse brain tissue (assuming tissue density to be 1g/ml). Thus, quinacrine is likely to be present at micromolar concentrations in 4C8 tumor tissue with the dosing regimen of 50 mg/kg/day used in our studies. The in vitro MTS cell viability assays described in chapter 2 revealed significant enhancement in cytotoxicity with combinations of quinacrine = 2.5 µM and cediranib = 1 µM in hypoxic 4C8 cells. Hence, the *in vivo* therapeutic efficacy may derive from more than just anti-angiogenic effects, but also direct tumor cell cytotoxicity. Our studies described in Chapter 2 indicate that cediranib drives autophagic flux, which in combination with quinacrine's ability to modulate autophagy, promotes AV accumulation and tumor cell death. Autophagy activation by Cediranib may occur via the inhibition of Akt signaling, evidence for which was presented in Chapter 2. Our data would also predict autophagy activation to be particularly prevalent in the hypoxic regions of the tumors (Hoyer-Hansen*, et al.* 2008, Hu*, et al.* 2012). As indicated in Chapter 2, our EF5 histology experiments clearly detected such hypoxic regions in untreated tumors. Our dynamic MRI data also indicate that, consistent with its anti-angiogenic capability, cediranib can reduce perfusion in tumor core regions, and hence would be expected to exacerbate hypoxia *in vivo*, further activating autophagy (Hu*, et al.* 2012). An ultrastructural investigation of tumor tissue in response to cediranib treatment, using electron microscopy, provided evidence for such an *in vivo* induction of autophagy.

In summary, using a novel treatment combination with the intracranial 4C8 mouse glioma model, we documented a synergistic increase in anti-vascular/anti-tumor efficacy, using a comprehensive DCE/DSC perfusion MRI approach and immunohistology. The anti-angiogenic RTK inhibitor cediranib in combination with the autophagy inhibitor quinacrine produced a powerful anti-vascular and anti-tumor effect that far exceeded treatment with either agent alone, with markedly decreased tumor perfusion, increased tumor necrosis, decreased tumor growth, and increased survival. The similarity of cediranib's molecular targets to those of other recently developed RTK anti-angiogenic agents (Gotink*, et al.* 2010), suggests that the novel and effective combination tested in the current study could represent an important new combinational paradigm, which could greatly increase the utility of this class of agent. Our studies reveal a potentially important therapeutic avenue for the treatment of malignant glioma, a disease for which prognosis is extremely poor and therapeutic options are limited.

# Chapter 4: Dynamic MRI investigation of cediranib anti-angiogenic/anti-tumor efficacy when combined with proteasome inhibition

*Merryl R. Lobo, Sarah C. Green, Huong Tran, Matthias C Schabel, Yancey G. Gillespie, Randall L. Woltjer, *Martin M. Pike

*Most of the work described in this Chapter is part of a manuscript in preparation.*

**These authors are the sole contributors to the work.*

## 4.1 Abstract

The limited sensitivity of gliomas to most conventional chemotherapeutic agents contributes to an extremely poor prognosis for this disease. To date, separate anti-angiogenic and proteasome inhibition anti-tumor strategies have produced disappointing results in the treatment of glioblastomas. We hypothesized that the efficacy of the anti-angiogenic receptor tyrosine kinase (RTK) inhibitor, cediranib is enhanced in intracranial glioma by combination with a novel proteasome inhibitor, SC68896. Dynamic MRI techniques comprising DCE-MRI and DSC-MRI were implemented to measure vascular permeability ($K^{trans}$) and relative cerebral blood flow and volume (rCBF, rCBV).Tumor growth was also monitored. We found that while single agent treatment did not alter tumor growth or survival, combined SC68896/cediranib significantly delayed tumor growth and increased median survival by over 2-fold, compared to untreated ($p<0.05$).

This was accompanied by substantially increased tumor necrosis in the combination treatment group, not observed with single agent treatment. Although no changes in vessel density were observed using immunohistochemical investigations of CD31, dynamic MRI revealed that the combination treatment may have exerted a vascular normalizing effect by preventing increases in tumor blood vessel inefficiency and permeability. Our studies provide the first comprehensive assessment of the *in vivo* effects of a combination of anti-angiogenic treatment with proteasome inhibition for glioblastoma and warrant further investigations through clinical trials.

### 4.2 Introduction

Studies outlined in chapters 2 and 3 describe a novel therapeutic approach for malignant glioma, involving the modulation of Akt signaling and its downstream effects on the autophagic pathway. This approach was targeted at improving the anti-angiogenic effects as well as the direct cytotoxic effects of cediranib on glioma cells, through a unique combination with late stage autophagy inhibitor, quinacrine. Experiments in chapter 4 are aimed at investigating the *in vivo* efficacy of another promising strategy that could also exert potent anti-tumor effects through Akt inhibition. Studies presented here assess the effects of a combination of cediranib with a novel proteasome inhibitor, SC68896 in intracranial mouse glioma and reveal that this therapeutic combination significantly delays tumor growth, increases tumor necrosis and improves mouse survival. Furthermore, the dynamic MRI suggested that the combination therapy may induce a vascular normalization effect.

### 4.3 Background

A proteasome is a cylindrical multisubunit protein complex lined with proteolytically active sites that degrade proteins into shorter peptides, to be re-used by the cell. Proteins that need to be degraded are tagged with multiple ubiquitin molecules which are then detected by the proteasome (Mani*, et al.* 2005). This ubiquitin-proteasome pathway, apart from playing a role in protein quality control and turnover, controls the presence of many regulatory proteins that are critical to a number of cellular functions (Kisselev*, et al.* 2012, Mani*, et al.* 2005). This extends the influence of proteasome activity on critical physiological processes such as cell cycle progression, angiogenesis, apoptosis, endoplasmic reticulum (ER) stress, oxidative stress and the activation of signaling molecules such as NF-κB and Akt (Crawford*, et al.* 2011, Kisselev*, et al.* 2012). Thus, proteasomes have been proposed to be an attractive target in cancer therapy, leading to the development of numerous proteasome inhibitors (Crawford*, et al.* 2011). Such agents generally have a peptide moiety and an electrophillic trap which interacts with, and inhibits the proteolytic sites (Kisselev*, et al.* 2012). Proteasome inhibitors such as Bortezomib, a boronic acid dipeptide, have been shown to have significant clinical efficacy in multiple hematologic malignancies such as multiple myeloma and mantle cell lymphoma (Orlowski*, et al.* 2008). Bortezomib, unfortunately, only has limited efficacy in solid tumors, particularly in glioma. Labussiere et al. showed that bortezomib reduced tumor cell growth *in vitro* but failed to have any therapeutic effect in malignant glioma xenografts *in vivo* (Labussiere*, et al.* 2008, Roth*, et al.* 2009, Zhu*, et al.* 2010). A potentially therapeutic strategy would be to combine proteasome inhibition with targeted agents such as RTK inhibitors that can collaborate in the effective inhibition of critical

survival pathways. Research has shown that combinations of RTK inhibitors and proteasome inhibitors have worked well *in vitro* in a number of tumor types, primarily through the combined inhibition of Akt signaling (Chen*, et al.* 2010, Yeramian*, et al.* 2011). Such a combination, to the best of our knowledge, has not been tested *in vivo* for glioblastoma. In the intracranial setting, signaling within glioma cells can be influenced by numerous factors and conditions present in the surrounding microenvironment, including immune cells, fibroblasts, extracellular matrix, growth factors, hypoxia, oxidative stress and pH alterations. These could contribute towards resistance in glioma cells, thus compromising therapeutic outcome (Swartz*, et al.* 2012). The inability of agents to cross the blood brain barrier and access the tumor cells could also limit the efficacy of treatment (Westphal*, et al.* 2011). The aim of the present study is to use noninvasive dynamic magnetic resonance imaging (MRI) techniques to provide an *in vivo* assessment of the effects of such a drug combination on tumor growth and vasculature.

The study uses the syngeneic intracranial mouse 4C8 glioma model, which fosters a seamless tumor–host interaction in immunocompetent mice (Dyer*, et al.* 1995, Pike*, et al.* 2009). The drug combination being tested involves a novel small molecule proteasome inhibitor, SC68896, that induces cell death in glioma cell cultures and to date has been one of the few proteasome inhibitors to show *in vivo* efficacy in a mouse experimental glioblastoma xenograft (Roth*, et al.* 2009). In the studies described below, we assessed the *in vivo* single agent efficacy of SC68896 with the 4C8 mouse glioma model and its combination with the RTK inhibitor, cediranib. Cediranib targets vascular endothelial

growth factor (VEGF), Platelet derived growth factor (PDGF) and stem-cell factor receptor (c-kit) signaling and is in multiple clinical trials for malignant glioma (Dietrich, *et al.* 2009).

The comprehensive dynamic MRI approach we used quantifies key vascular biomarkers noninvasively, measuring vascular flow, volume, permeability and also tumor growth (Pike, *et al.* 2009). It employs dynamic contrast enhanced MRI (DCE-MRI), which produces high resolution maps of $K^{trans}$, an index of vascular permeability. Subsequently dynamic susceptibility contrast MRI (DSC-MRI) is implemented to determine cerebral blood flow (CBF) and cerebral blood volume (CBV).

## 4.4 Materials and methods

### *4.4.1 Cell culture and Tumor Inoculation*

Mouse studies were conducted with the approval of the Oregon Health and Science University Institutional Animal Care and Use Committee and under the supervision of the OHSU department of Comparative Medicine. The 4C8 mouse glioma cells (provided by Dr. G. Yancey Gillespie, UAB) were grown in Dulbecco's modified Eagle's medium/Ham's F-12 50/50 Mix (Invitrogen, Carlsbad, California), supplemented with 7% fetal bovine serum (FBS) (Hyclone, Logan, Utah) and 1% L-glutamine (Sigma-Aldrich, St. Louis, Missouri). Female C57BL/6 × DBA/2 $F_1$ hybrid mice (B6D2F1) were purchased from Charles River Laboratories (Wilmington, MA). Brain tumors were induced by the intracerebral injection of ~$1 \times 10^6$ 4C8 cells, suspended in DMEM/F12 (5-10µl) using a stereotaxic frame as previously described (Pike, *et al.* 2009).

*4.4.2 MRI procedures*

Starting at 10 days after tumor cell inoculation, mice were routinely imaged using contrast-enhanced (Magnevist i.p.) $T_1$ weighted MR imaging to determine when tumor growth initiates. When tumors exceeded a volume of approximately 2 $mm^3$, (generally at 2-3 weeks post inoculation), pretreatment perfusion MRI studies were implemented, after which mice were randomized into four treatment groups with treatments starting within 24 hours: 1) untreated, n = 4 (vehicle: 1% Tween in phosphate buffered saline (PBS), oral gavage, daily); 2) cediranib, n = 5 (AZD2171, 6 mg/kg in 1% Tween/PBS, daily, oral gavage, Selleck Chemicals LLC Houston, TX); 3: SC68896, n = 4 (150 mg/kg in PBS/DMSO 1:2.5, daily, i.p. injection, ViroLogik, Erlangen, Germany); and 4) cediranib + SC68896, n = 5 (daily). Dynamic MRI experiments were conducted on days ~ 0, 10 and 25, and mice were sacrificed when right brain displacement by the tumor was reaching a maximum, or when mice showed neurological/behavioral changes, or signs of physical deterioration such as excessive weight loss or skull deformation. Mouse brains were harvested and stored in 10% formalin for histology. For dynamic MRI, mice were initially anesthetized with a ketamine/xylazine mixture (1.5 mg xylazine/10 mg ketamine/100g) and one of the lateral tail veins was cannulated using a 30 gauge needle attached to PE 10 tubing, filled with sterile saline containing 15U heparin/ml. MR imaging employed a Bruker-Biospin 11.75T small animal MR system with a Paravision 4.0 software platform, 9 cm inner diameter gradient set (750 mT/m), and a mouse head (20 mm ID) quadrature RF transceiver coil (M2M Imaging Corp.) The mice were positioned with their heads immobilized with a specially designed head holder with

adjustable ear pieces. Body temperature of the mice was monitored and maintained at 37°C using a warm air temperature control system (SA instruments). Isoflurane (0.5–2%) in 100% oxygen was administered and adjusted while monitoring respiration.

A coronal 25 slice $T_1$ weighted image set was obtained using a spoiled gradient echo sequence (Paravision FLASH, 256×256 matrix, 98 μm in-plane resolution, 0.5 mm slice width, TR 500 msec, TE 1.4 msec, FA 60°, 1 average) to determine the dynamic MRI slice position within the tumor, which was matched to that used in any previous imaging sessions using brain/skull anatomical features. A $T_2$ weighted image set (Paravision spin echo RARE, same spatial geometry as for multislice $T_1$ weighted, TR 4000 ms, $TE_{effective}$ 32 ms, RARE factor 8, 1 average) was obtained to assess tumor volume. A fully relaxed ($M_0$) spoiled gradient echo precontrast image (Paravision FLASH, TR 6000 ms, TE 1.2 ms, FA 90°, 128×128 matrix, 1 slice, 1 mm slice thickness, 195 μm in-plane resolution) was obtained at the position of the subsequent DCE $T_1$ weighted image series (450 images) which used the same parameters except with TR 15.6 msec and FA 20° (2.0s/image), and with tail-vein Gd-DTPA injection (Magnevist, Berlex Inc, i.v., 10X diluted, 3.0 μL/g, 0.15 mmol/kg). DSC-MRI was then implemented (150 $T_2$* weighted images, Paravision FLASH, TR 8, TE 4.2 ms, FA 5°, 128×128 matrix, 1 slice, 1 mm slice thickness, 195 μm in-plane resolution, 1 s/image) employing i.v. Feridex, an SPIO agent (Berlex Inc, 4X diluted, 2.4 μl/g, 26.9ug iron/g). Both injections occurred at 30s after initiation of the image series, at 1 mL/min, using a 150 μL saline/heparin chase.

*4.4.3 Image processing*

DCE-MRI parameters were computed voxelwise using the Extended Tofts-Kety model (Sourbron*, et al.* 2012, Tofts*, et al.* 1999) using custom pharmacokinetic modeling software (developed by M. C. Schabel) written in MATLAB (MathWorks, Natick, MA). Fully relaxed $M_0$ image intensities were used to compute pre-injection longitudinal relaxation time, enabling quantitative contrast agent concentration measurement and $K^{trans}$ (in $min^{-1}$) estimates (Pike*, et al.* 2009). The Monte Carlo Blind Estimation (MCBE) algorithm was used to determine the arterial input function directly from measured tumor curves (Schabel*, et al.* 2010, Schabel*, et al.* 2010). Calculation of DSC-MRI perfusion parameters followed the model-independent method described in Ostergaard L. *et al* (Ostergaard*, et al.* 1996), using the Jim software package (Xinapse Systems LTD, Northants, UK). The AIF was determined from 12 non-tumor brain pixels identified by an automatic scanning and selection routine which targeted brain parenchymal arterial microvessels (Pike*, et al.* 2009). DSC data analysis was restricted to the first 50 post-contrast images in the series to bracket the susceptibility bolus intensity changes. Parametric maps were generated for cerebral blood flow (CBF in mL blood/100g tissue/ minute), cerebral blood volume (CBV in blood volume percentage of total tissue volume), and mean transit time (MTT in seconds). Analysis of the DCE/DSC-MRI parametric maps, and $T_2$ multislice images employed the Jim software package. Tumor volumes were calculated from the multislice $T_2$ weighted images. The DSC-MRI parameters (rCBF, rCBV, rMTT) were reported relative to contralateral values to reduce measurement error, and minimize effects from alterations in intracranial pressure, blood pressure, and depth of anesthesia.

*4.4.4 Histology*

At the termination of serial MRI studies, mice were sacrificed and brains were stored in 10% Formalin. Fixed tissue samples were paraffin embedded and 7 μm sections were mounted on slides. The slides were then processed and stained with Hemotoxylin (Sigma-Aldrich) and Eosin (Sigma-Aldrich), using standard methodologies. For each tumor sample (at least 3 tumor samples/treatment group) a total of three image fields (4X magnification) were positioned randomly across a minimum of two stained tumor sections and photographed using an Olympus BX50 microscope mounted with a Leica camera DFC320 equipped with Leica Firecam Version 3.4.1. Necrotic regions within the image fields were quantified using the ROI analysis tool of the Jim software package under the supervision of an experienced neuropathogist (RLW) and averaged. In adjacent sections from a minimum of three mice per treatment group, immunohistochemical vascular staining was performed after deparaffinized sections were subjected to antigen retrieval (5 min treatment at room temperature with 95% formic acid followed by incubation at 85-90 degrees in citrate buffer, pH 6.0, for 30 min), using mouse monoclonal primary antibody to CD31, clone JC70A (Dako), with hematoxylin counter stain. Slides were prepared using the Mouse-On-Mouse (M.O.M) Peroxidase Kit (Vector Labs) to prevent non-specific background and the presence of CD31 was investigated using the avidin-biotin complex (ABC) method (Vector Labs), with diaminobenzidine. Slides were studied at 40x magnification, and the number of CD31 stained vessels was counted in 10 random fields across 2 sections for each tumor and averaged to obtain mean vessel density (MVD).

*4.4.5 Cell viability assays*

Cells were plated in 96-well plates at a density of 3000 cells/well and were exposed to a range of treatment conditions. To assess cell viability in response to treatment, MTS solution (CellTiter 96® AQueous MTS Reagent) was added to cells in 96 well plates (20 µL/well) and left for 1 hour at 37°C. A negative control of MTS solution and medium alone was also included. The absorbance was measured using ELX800 Micro Plate Reader (Bio-Tek Instruments, Inc.) at 490 nm.

*4.4.6 Statistics*

Values are expressed as mean (± SEM). For H&E histology results and dynamic MRI parameters (except $K^{trans}$), the two-tailed Student's t test (NCSS Statistical Software, (Kaysville, UT) was employed to test for differences at 0, 10(±2) days after tumor growth initiation versus untreated (time points corresponding to ≥ 3 surviving mice). The one-tailed Students t test was employed in the statistical analysis for $K^{trans}$. Differences in median survival were tested using the log-rank test.

## 4.5 Results

*4.5.1 SC68896/cediranib combination delays tumor growth and improves mouse survival*

Figure 4.1 shows $T_2$ weighted mouse MR images obtained after 7 days of tumor growth initiation. Tumor volume assessment using $T_2$ weighted MRI revealed much smaller tumor sizes in response to SC68896/cediranib combination treatment whereas each agent alone did not alter tumor growth in comparison to untreated mice.

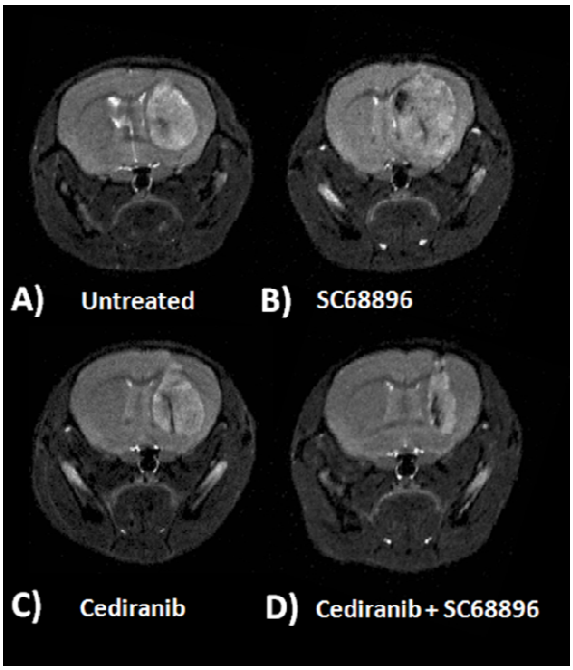


**Figure 4.1. Combined SC68896/cediranib treatment results in smaller tumor sizes.** Representative $T_2$ weighted coronal mouse brain MR images obtained at 7 days after tumor growth initiation for the four treatment groups: A) untreated, B) SC68896, C) cediranib, and D) SC68896/cediranib treated.

Tumor growth curves derived from multislice $T_2$ weighted images obtained biweekly are shown in Figure 4.2A, with tumor volume plotted against time from initiation of tumor growth. Treatment of mice began on Day 1. These plots indicate rapidly growing tumors with untreated mice and no therapeutic effects of cediranib or SC68896 treatment on tumor growth. Mice treated with SC68896/cediranib combination however had significant delays in tumor growth. An increase of ~830% in tumor volume within the first 10 days of growth observed in untreated mice was restricted to ~350% in the combination treated mice. Mean exponential growth rate constants, $(\text{days})^{-1}$ obtained from exponential fits to individual tumor growth curves we 0.21 ± 0.02, 0.19 ± 0.03, 0.21 ± 0.01 and 0.14 ± 0.01 for untreated, cediranib, SC68896 and combination treated mice, respectively ($p < 0.05$, for combination group versus untreated). Mice given the

SC68896/cediranib combination also survived much longer than other treatment groups (Figure 4.2B), with a median survival (days) of 26 ± 0.91 ($p < 0.05$, versus untreated) compared to mice treated with cediranib (13 ± 0.75), SC68896 (13 ± 1.49) or untreated (13.5 ± 0.47).

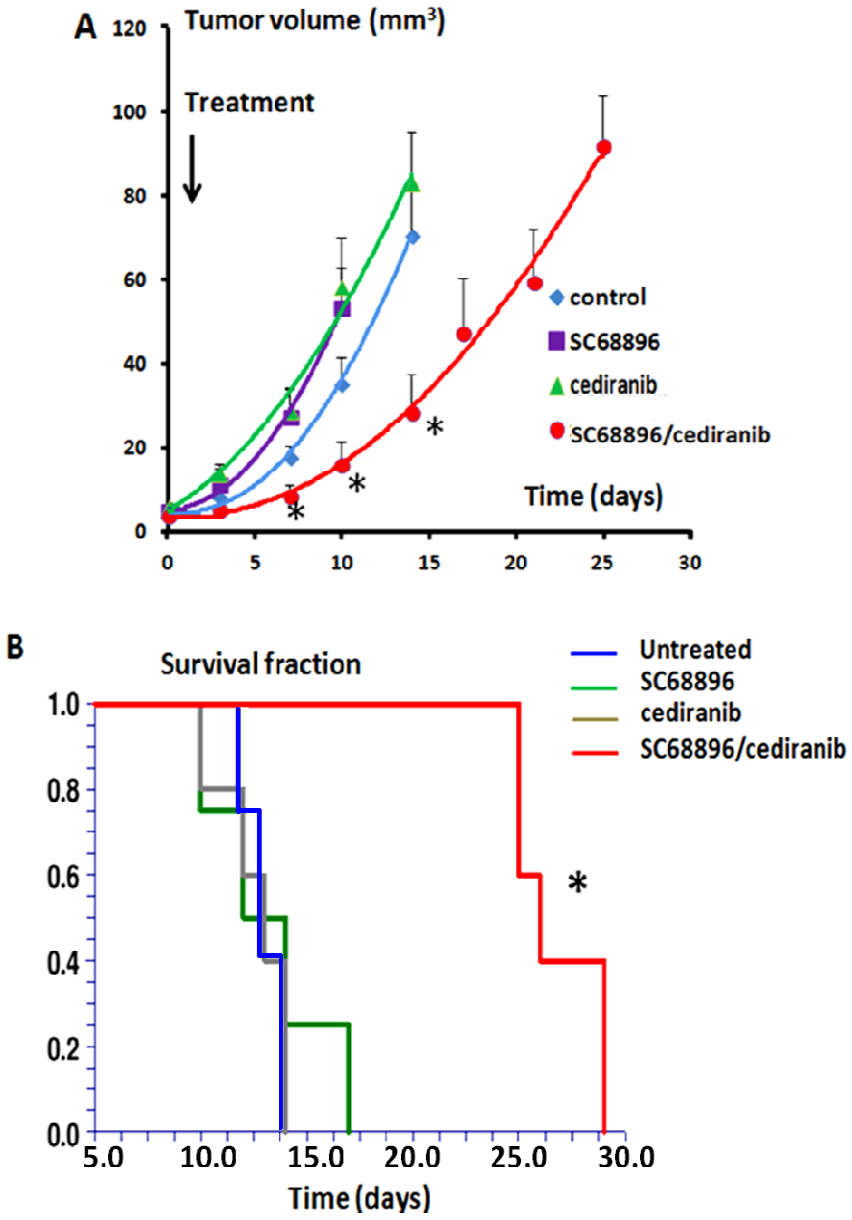


**Figure 4.2. SC68896/cediranib treatment delays tumor growth and increases mouse survival.** A) Tumor growth curves are shown for the four treatment groups, in tumor volume versus time after tumor growth initiation. Curves are indicated for time points corresponding to ≥ 3 surviving mice. *: $p < 0.05$ versus untreated. B) Kaplan-Meier survival curves for the four treatment groups (in days from tumor growth initiation) *: $p < 0.05$ versus untreated.

*4.5.2 Combined SC68896/cediranib prevents increases in mean tumor DCE/DSC pharmacokinetic parameters with tumor growth.*

Figure 4.3 shows representative $K^{trans}$ and rCBF mouse brain parametric maps using the dual bolus-tracking DCE/DSC perfusion MRI approach, obtained from the 4 treatment groups at the final MRI evaluation time point. In the normal brain tissue, the intact blood brain barrier prevented contrast agent extravasation, resulting in negligibly small $K^{trans}$ values. In contrast, tumor tissue exhibited elevated and heterogeneously distributed $K^{trans}$ values, indicating a compromised blood brain barrier integrity (Figure 4.3A). The areas of elevated $K^{trans}$ were particularly prevalent within tumors in SC68896 treated mice. Cediranib treatment generally decreased $K^{trans}$ values in the tumor core, but failed to have an effect along the rim, consistent with our previous studies. In contrast, the combined administration of SC68896/cediranib resulted in substantially lower $K^{trans}$ values. Figure 4.3B indicates that as with $K^{trans}$, the tumor rCBF maps also exhibited elevated and heterogeneously distributed values, in contrast to normal brain. Analogous to what was observed on the $K^{trans}$ maps, the rCBF maps indicated the presence of a resistive angiogenic tumor rim in response to cediranib treatment. Both single agent SC68896 treatment and the combined SC68896/cediranib treatment decreased overall tumor rCBF.

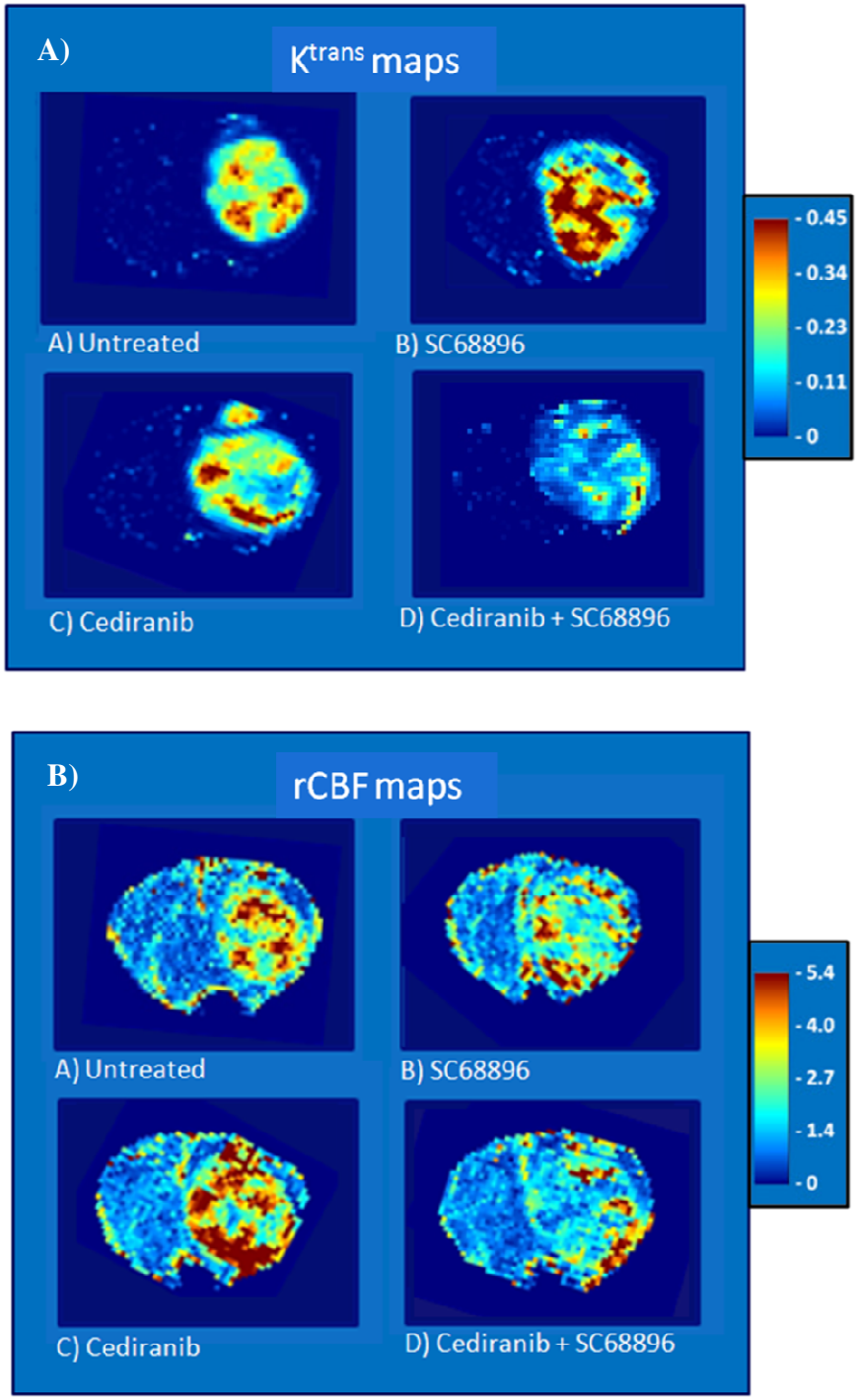


**Figure 4.3. SC68896/cediranib treatment prevents increases in $K^{trans}$ and rCBF values across the tumor section. A)**$K^{trans}$ ($min^{-1}$) and B) rCBF parametric maps (non-brain regions masked) obtained from representative tumors from each treatment group during the final week of MRI evaluation (CBF color scale is relative: contralateral hues set to ~unity.)

Figure 4.4 shows the variation of mean tumor rCBF, rCBV, rMTT and $K^{trans}$ with time from the start of tumor growth, for the four treatment groups. On day 0, mean tumor rCBF values of between 2.2-2.6 were observed for the four treatment groups, which in untreated mice continued to increase with tumor growth (Figure 4.4A). Figure 4.4B shows that the rCBV increased faster than rCBF in untreated tumors, which suggests a progression to a more chaotic and inefficient vascular network. Further supporting this is that rMTT, a parameter which is inversely related to vascular efficiency, also increased over time (Figure 4.4C). Also consistent with a progressive development of abnormal tumor neovasculature is the increasing $K^{trans}$ (Figure 4.4D) observed in untreated tumors. As $K^{trans}$ is proportional to the permeability-surface area product per unit volume of tissue, an increasing $K^{trans}$ is indicative of an increasing vascular permeability, and/or an increasing vessel surface area. We found that cediranib treatment alone did not produce significant changes in mean rCBF, rCBV, or rMTT, from those observed in vehicle treated mice. Consistent with our previous findings, cediranib also tended to decrease mean tumor $K^{trans}$, which is likely due at least in part to a decreased vascular permeability, consistent with its anti-angiogenic action. Notably, single agent SC68896 treatment significantly decreased rCBF in comparison to untreated. This occurred without concomitant reductions in rCBV, a trend consistent with an exacerbation of vessel inefficiency, as further suggested by the large increase in rMTT. In contrast the combined SC68896/cediranib treatment largely restricted increases in mean tumor rCBF, rCBV, rMTT and $K^{trans}$, suggesting a prevention of the transition to an irregular tumor phenotype.

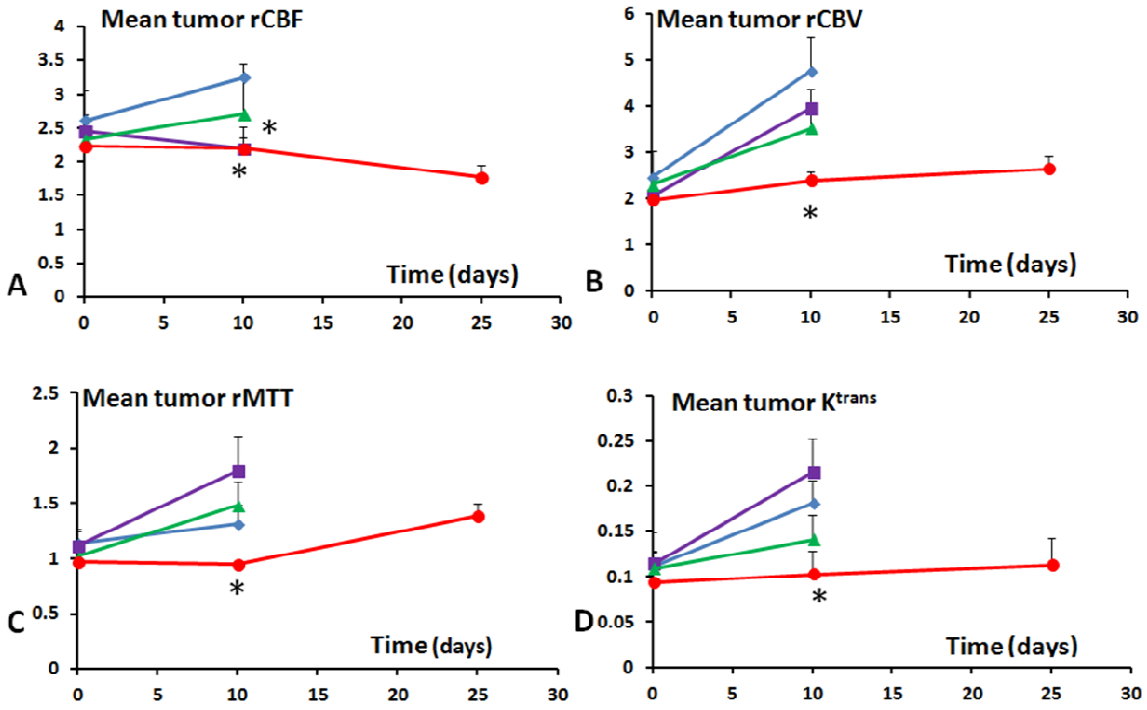


**Figure 4.4. SC68896/cediranib treatment prevents increases in mean tumor rCBF, rCBV, rMTT and $K^{trans}$.** Mean tumor A) rCBF, B) rCBV, C) rMTT and D) $K^{trans}$ ($min^{-1}$) values plotted versus the time from tumor growth initiation for the four different treatment groups ( ■-Untreated, ■-SC68896, ■-cediranib , ■-SC68896/cediranib). Curves are indicated for time points corresponding to ≥ 3 surviving mice. *: $p < 0.05$ versus untreated.

*4.5.3 Combined SC68896/cediranib treatment has no effects on Mean Vessel Density (MVD)*

Figure 4.5A and B show the results of immunohistochemical investigations of CD31 expression in tumor sections derived from mice belonging to the 4 treatment groups, after the completion of the longitudinal MRI studies. CD31 positive tumor vessels were equally prevalent in tumor sections from all treatment groups and no significant difference was observed in MVD.

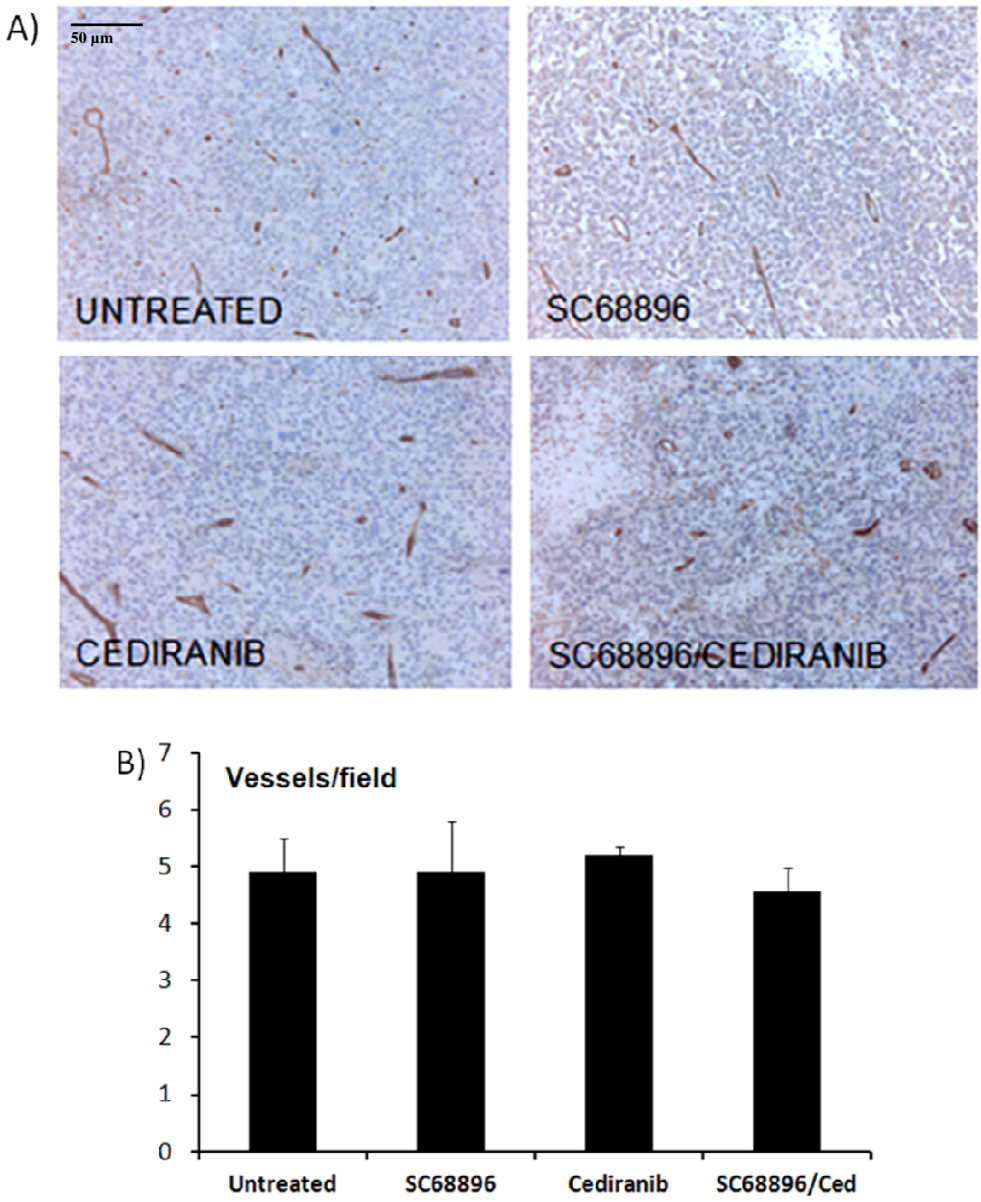


**Figure 4.5. SC68896/cediranib treatment causes no change in tumor mean vessel density.** A) Representative histological tumor sections with CD31 vascular staining (brown) and hematoxylin nuclear counter stain (blue) from the four treatment groups. B) MVD quantified from multiple CD31 stained sections for the four treatment groups. Field area = $2x10^{-3}$ $mm^2$. Keri Forquer from the OHSU histopathology core assisted in generating these data.

*4.5.4 Treatment with SC68896/cediranib combination increases tumor necrosis*

Representative H&E sections from the various treatment groups indicate regions of tumor necrosis in all tumor sections (Figure 4.6 A). While similar levels of necrosis were

observed in the sections from untreated, SC68896, and cediranib treated mice, the SC68896/cediranib combination resulted in significant increases in tumor necrosis (Figure 4.6 A and B).

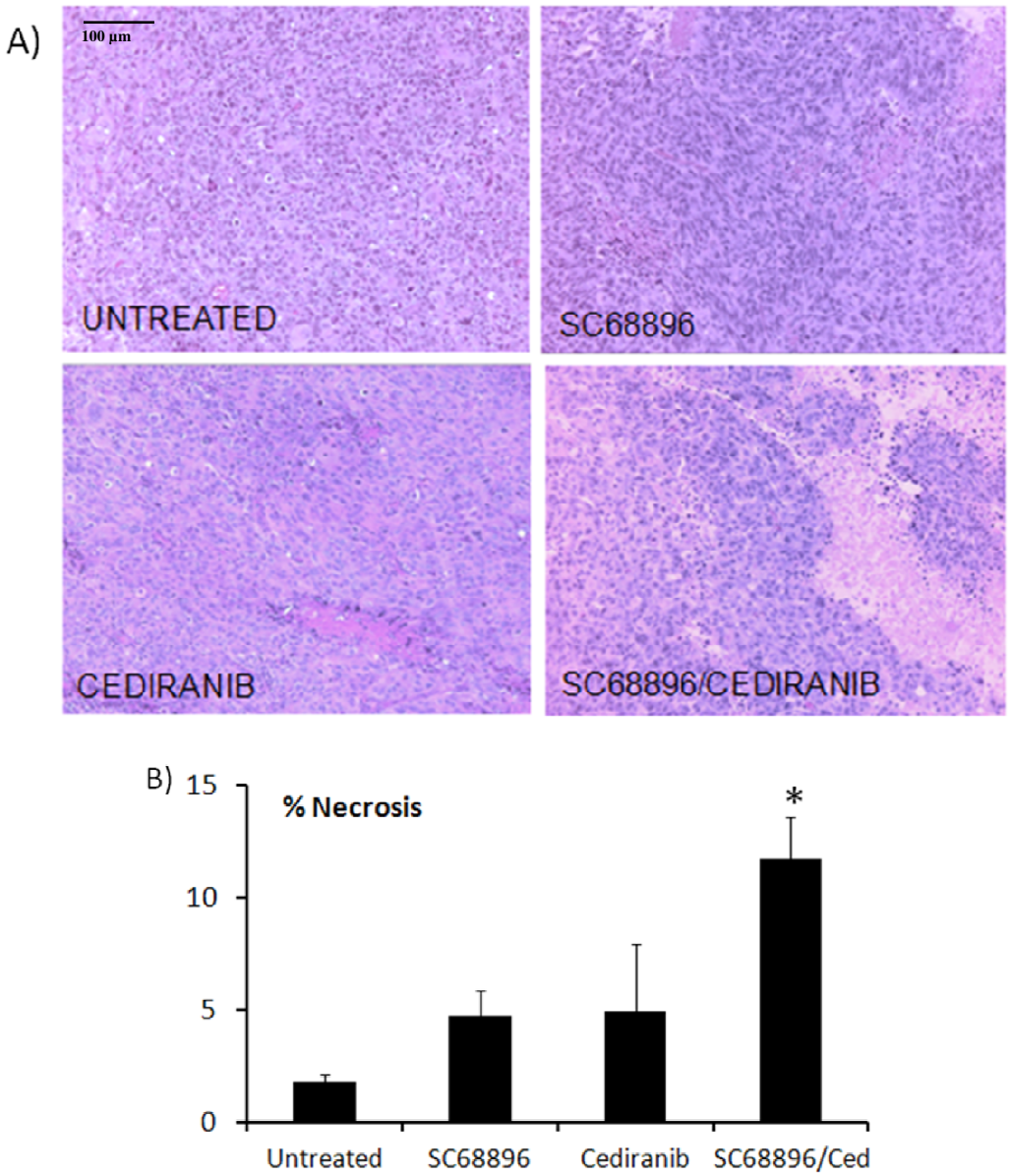


**Figure 4.6. SC68896/cediranib treatment induces necrosis in tumors.** A) Representative H&E stained sections from the four treatment groups, indicating areas of necrosis, which appear as condensed cells in areas of vacuolated tissue. B) Percent necrosis, quantified from multiple H&E stained sections, for the four treatment groups. *: $p<0.05$ versus untreated. Huong Tran from the Randall Woltjer laboratory assisted in generating these data.

*4.5.5 SC68896 in vitro cytotoxicity and combined treatment efficacy with cediranib is modulated by hypoxia.*

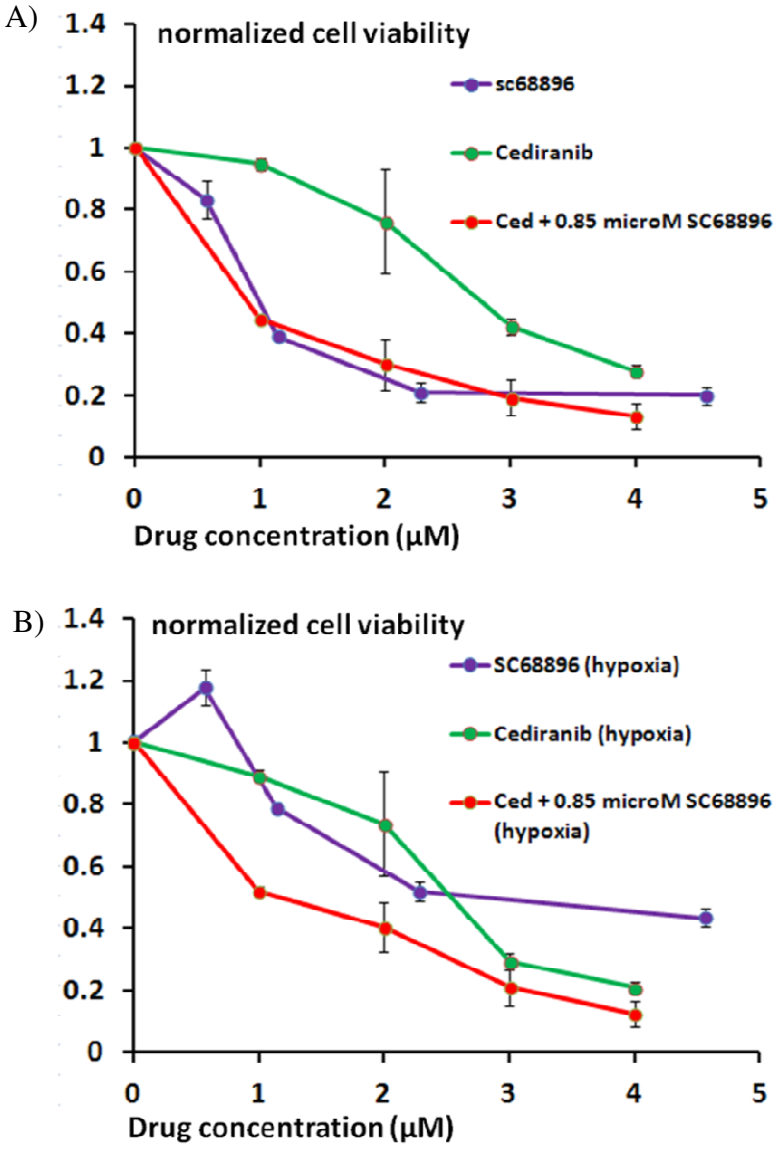


**Figure 4.7. Hypoxia decreases SC68896 cytotoxicity but promotes a greater than additive interaction with cediranib.** Results from MTS cell viability assays showing mean 4C8 cell viability in response to treatment, normalized to untreated samples. Assays were performed after cells were exposed to treatment for 72 hours, under A) normoxic or B) hypoxic (0.5% $O_2$) conditions. Results are mean ± SEM of three independent experiments, performed in triplicate.

A preliminary study to assess the direct anti-glioma effects of SC68896 and the SC68896/cediranib combination was conducted using MTS cell viability assays (Figure

4.7). 4C8 cells were exposed to varying concentrations of SC68896, cediranib and the combination of both agents under normoxic and hypoxic conditions. SC68896 had a dose dependant cytotoxic effect on 4C8 cells with a half maximal inhibitory concentration ($IC_{50}$) of ~1μM under normoxic conditions, which increased to ~3 μM under hypoxic conditions. These data suggest that hypoxia compromises SC68896 glioma cytotoxicity. One of the important mechanisms through which proteasome inhibitors exert their anti-tumor effects is through the generation of reactive oxygen species (ROS) (Ling*, et al.* 2003, Ohshima-Hosoyama*, et al.* 2011, Perez-Galan*, et al.* 2006). A reduction in ROS production under hypoxic conditions could explain the reduced toxicity of SC68896 in Figure 4.7B. As observed in Chapter 2, hypoxia did not affect cediranib anti-glioma effects. Despite the reduced SC68896 cytotoxicity under hypoxic conditions, we observed that the combined SC68896/cediranib efficacy was relatively unchanged between the normoxic and hypoxic conditions. The more than additive interaction demonstrated at lower drug concentrations under hypoxic conditions suggests an enhancement of treatment effects with the combination.

**4.5 Discussion**

The ubiquitin-proteasome system has been shown to be a useful target for cancer therapy as it regulates the degradation of a number of cellular proteins involved in proliferation, cell cycle and apoptosis (Crawford*, et al.* 2011, Kisselev*, et al.* 2012, Mani*, et al.* 2005). A particular advantage to such an approach is an increased dependence of neoplastic cells on intact and functional proteasomes, which confers unique sensitivity among tumor cells to proteasome degradation while mostly sparing normal or non-transformed cells. This

increased dependence has been attributed to high proliferation rates among tumor cells which require an increased amount of protein synthesis and turnover (Crawford*, et al.* 2011).

Although Bortezomib has had excellent success rates in hematological malignancies, proteasome inhibitors have yet to show promising results among solid tumors (Honma*, et al.* 2013). SC68896 belongs to the family of peptide aldehydes and presents an exciting addition to the new generation of proteasome inhibitors (Kisselev*, et al.* 2012, Leban*, et al.* 2008, Roth*, et al.* 2009). A study by Roth et al. in 2009 showed that treatment of glioma cell cultures with SC68896 resulted in the accumulation of p21 and p27, cell cycle arrest and induction of apoptosis. Moreover, the study also showed smaller tumors and an improvement in survival in response to treatment with SC68896, asserting the agent to be the first proteasome inhibitor to exert antiglioma activity in an experimental glioma model *in vivo* (Roth*, et al.* 2009).

Recent studies have reported synergistic interactions between proteasome inhibitors and the RTK inhibitor, Sorafenib (targets include raf, PDGFR, VEGFR) in a variety of solid tumor models *in vitro* including renal cell carcinoma, breast cancer and glioma (Yu*, et al.* 2006). Chen et al. have shown that this combination also causes a delay in tumor growth *in vivo* in hepatocellular carcinoma (Chen*, et al.* 2010). Another study found that the RTK inhibitor, Sunitinib (targets include PDGFR, VEGFR) can effectively sensitize metastatic melanoma cell cultures to Bortezomib treatment and cause a synergistic reduction in cell viability (Yeramian*, et al.* 2011). Each of these studies has shown that a

combined inhibition of the pro-survival Akt signaling pathway by the two agents plays an important role in synergistic activity. We proposed to assess the *in vivo* efficacy of a related, yet novel therapeutic combination, SC68896 and cediranib, for the treatment of malignant glioma. We used the syngeneic intracranial 4C8 mouse glioma model and a unique dynamic MRI approach to quantitatively investigate the *in vivo* anti-tumor and anti-vascular effects of the SC68896/cediranib combination.

We found that SC68896 treatment alone had no observable effects on 4C8 tumor growth and mouse survival. Our results are in contrast with those from Roth et al. who have demonstrated an increase in median survival of ~10 days with SC68896 treatment (Roth*, et al.* 2009). The discrepancy between the observations made in the two studies could be related to the difference in the tumor model chosen. While the 4C8 cell line is a syngeneic glioma model and utilizes immunocompetent mice, the induction of LNT-229 tumors used in the studies of Roth. et al requires athymic nude mice. Since untreated mice inoculated with LNT-229 cells seemed to survive much longer than mice with 4C8 gliomas, it is possible that the 4C8 glioma model is much more aggressive, with higher vascularization and growth rate. Also, in the study by Roth et al., survival was expressed in terms of days from glioma implantation, which does not account for the generally variable period of time taken post implantation for the tumor to start growing (Roth*, et al.* 2009). We also observed no significant delays in tumor growth with cediranib treatment, which is in agreement with previous clinical and preclinical studies (Kamoun*, et al.* 2009, Rahman*, et al.* 2010). Our study is the first to demonstrate that while treatment with SC68896 or cediranib individually did not show significant therapeutic effects *in vivo*,

combined treatment resulted in substantial delays in tumor growth and a 2 fold increase in mouse survival (Figure 4.2).

Dynamic MRI revealed that SC68896 treated tumors had reduced blood flow and also showed a tendency towards increased vascular permeability, suggesting an increase in vascular inefficiency. The precise mechanisms underlying these effects require further study but could be related to the inhibitory action of proteasome inhibitors on vascular remodeling, in connection to their effects on NF-κB and VEGF signaling (Wang*, et al.* 2013). While cediranib treated tumors showed only a tendency towards reduced blood volume and permeability, the combination of the two agents completely prevented the increases in all dynamic MRI perfusion parameters throughout the period of tumor growth (Figure 4.4). Because our immunohistochemical investigations of CD31 in tumor tissue revealed no reductions in MVD with combined treatment, it is possible that the main anti-vascular action of the SC68896/cediranib combination could be directed towards vascular normalization, by enabling the tumor vascular network to adopt a more normal phenotype, by being more efficient and less permeable.

Previous reports have shown that apart from anti-vascular therapeutics such as bevacizumab and cediranib, cytotoxic agents such as trastuzumab (antibody against human epidermal growth factor receptor-2 [HER2]) can also have normalizing effects on the tumor vasculature through an indirect anti-angiogenic effect (Fukumura*, et al.* 2007, Izumi*, et al.* 2002). A number of studies have shown that proteasome inhibitors have an indirect inhibitory effect on VEGF signaling (Boccadoro*, et al.* 2005, Orlowski*, et al.*

2008, Zhu, *et al.* 2010) and it is possible that cediranib and SC68896 together exert a stronger normalizing effect on the tumor vasculature as evidenced by a combined reduction in vascular permeability, tumor blood flow and improvement in vascular efficiency. Measurements of rMTT suggest that the tumor vasculature efficiency remained comparable to normal brain vasculature up to at least 10 days of treatment. Further studies are required to validate the presence of normalized tumor vessels through features such as increased pericyte coverage and reduced intratumor hypoxia levels as well as to accurately determine the exact duration during which normalization may have occurred (Fukumura, *et al.* 2007). Such a process may have contributed to the observed increased survival in the SC68896/cediranib treatment group through a reduction of peritumor edema and intracranial pressure. Less permeable tumor vasculature could have prevented increases in interstitial fluid pressure, which, accompanied by improved vascular efficiency, may have facilitated improved interstitial penetration of the drugs (Fukumura, *et al.* 2007, Winkler, *et al.* 2004). This could have allowed for a stronger effect of the two agents resulting in an increase in necrosis seen through H&E staining of tumor tissue with combined treatment, not observed with single agent treatment or untreated mice (Figure 4.6).

The *in vitro* experiments with SC68896 and cediranib revealed interesting effects which in some ways differed from the patterns observed *in vivo*. Potent cytotoxicity was documented with SC68896 *in vitro*. However, under normoxic conditions the efficacy of the SC68896/cediranib combination appeared to be less than additive. In contrast, under hypoxic conditions, single agent SC68896 treatment efficacy markedly decreased, but

notably, its combination with cediranib induced a greater than additive effect. Thus, the overall combined efficacy of the agents was relatively unchanged between with normoxia and hypoxia. The differences in levels of synergistic interaction observed *in vitro* and *in vivo* are at least partly related to the fact that *in vitro* systems are not a completely accurate representation of the *in vivo* tumor microenvironment. These data further justify the use of intracranial tumor models for an effective preclinical assessment of therapy. These data could also suggest that the effects of the drugs on tumor vasculature through vascular normalization and the possible improved penetration of drugs within the tumor may be criticial to the *in vivo* efficacy observed. Future studies will probe into the mechanistic effects of the agents on glioma cells and endothelial cells, required for a synergistic interaction between SC68896 and cediranib.

Collectively, our results suggest that combined SC68896/cediranib treatment effectively reduced tumor growth, improved survival and increased tumor necrosis *in vivo*. While a potent devascularization was not observed, the therapeutic combination may have exerted a normalizing effect on the tumor vascular network by preventing increases in leakiness and vascular inefficiency. Our studies provide a rationale for further exploration of this unique therapeutic approach in the clinical setting for malignant glioma.

# Chapter 5: Conclusions and Future Directions

## 5.1 Thesis summary and conclusions

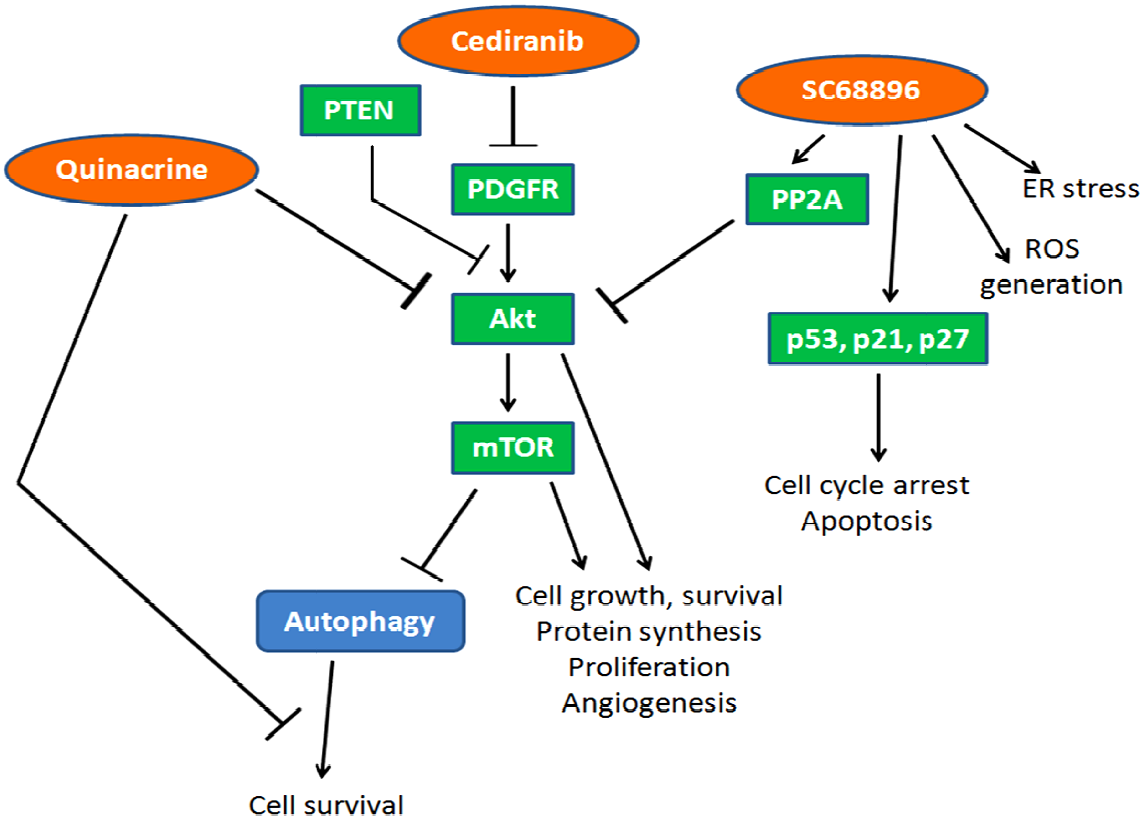


**Figure 5.1. Interactions between quinacrine, cediranib and SC68896, and the Akt signaling pathway.** Activated receptor tyrosine kinases phosphorylate and activate the Akt kinase which regulates a number of cellular processes through or independent of mTOR activation, such as cell proliferation, survival, protein synthesis and angiogenesis. A critical survival promoting process also regulated by the pathway is autophagy. Quinacrine and cediranib, together, exert an enhanced anti-tumor and anti-vascular effect in glioma which is associated with inhibition of Akt and the modulation of its downstream effects on autophagy (Chapters 2 and 3). SC68896 and cediranib also exhibit significantly improved anti-glioma effects (Chapter 4) and future studies described in section 5.3 will investigate involvement of the Akt pathway in the synergistic interaction.

Studies described in this thesis were aimed at improving the anti-tumor and anti-angiogenic efficacy of the receptor tyrosine kinase (RTK) inhibitor cediranib in the treatment of the worst form of brain tumor, glioblastoma multiforme, for which prognosis has remained extremely poor (Westphal, *et al.* 2011). Cediranib is a small molecule RTK inhibitor targeting all vascular endothelial growth factor receptors (VEGFR), platelet derived growth factor receptors (PDGFR) and c-kit (Rahman, *et al.* 2010). Research efforts were focused on two novel therapeutic combinations with cediranib, which exhibited enhanced therapeutic effects, possibly through the inhibition of certain critical survival promoting mechanisms in tumor cells such as the Akt signaling pathway (Chen, *et al.* 2010, Yeramian, *et al.* 2011, Yu, *et al.* 2006). The Akt pathway (Figure 5.1) receives activating signals from PDGFR expressed in glioma cells, among other growth factor receptors such as VEGFR and epidermal growth factor receptor (EGFR). It plays important roles in regulating autophagy, tumor cell survival, proliferation and angiogenesis through several downstream targets including mammalian target of rapamycin (mTOR) (Burris 2013). This thesis centers on studying two innovative treatment combinations, each of which can collaboratively inhibit this pathway and its downstream targets to create a synergistic anti-glioma effect. The 4C8 syngeneic glioma model was used for all studies described in this thesis.

The first therapeutic strategy studied in Chapters 2 and 3 evaluated a combination of cediranib with the late stage autophagy inhibitor quinacrine in the treatment of malignant glioma. We observed a synergistic increase in glioma cell death with the treatment combination under hypoxic conditions. These same conditions produced the maximum

levels of autophagic vacuole (AV) formation and accumulation (Figures 2.2 and 2.3). Experiments were also conducted to establish that AV accumulation plays a causal role in the observed cytotoxicity (Figure 2.4). Both agents were found to potently inhibit Akt phosphorylation in hypoxic glioma cells, presenting a mechanism for cediranib induced autophagy and also suggesting that quinacrine may not only block AV degradation through its lysosomotropic action, but may also trigger autophagy in the tumor cells (Figure 2.5). The potential importance of this unique capability of quinacrine was evident when, unlike with quinacrine, potentiation of glioma cytotoxic effects was not observed under hypoxic conditions with the Bafilomycin A1/cediranib combination. Bafilomycin A1 was shown to have no effects on Akt (Figure 2.6 and Figure 2.7). An *in vivo* evaluation of this treatment strategy described in Chapter 3 revealed an over 2 fold reduction in tumor growth, increased median survival (2 fold) and increased tumor necrosis (3 fold), in comparison to untreated and single agent treatment groups. We also documented a potent devascularization indicated by strong reductions in dynamic magnetic resonance imaging (MRI) parameters such as vascular permeability, cerebral blood flow and blood volume as well as mean vessel density (MVD) measured through immunohistochemical detection of CD31.

The second therapeutic strategy studied in chapter 4 assesses the *in vivo* efficacy of a combination of cediranib with the proteasome inhibitor, SC68896, in the treatment of malignant glioma. Proteasome inhibitors have been shown to inhibit Akt phosphorylation, which may be through the stabilization of the protein phosphatase, PP2A (Chen*, et al.* 2008, Lin*, et al.* 2012). Further studies are required to assess the

effects of SC68896 on Akt. Combinations of proteasome inhibitors and anti-angiogenic RTK inhibitors studied so far have been shown to exert anti-tumor effects through the combined inhibition of Akt (Chen, *et al.* 2010, Yeramian, *et al.* 2011, Yu, *et al.* 2006). Because such a combination to date has not been evaluated *in vivo* for glioblastoma, experiments in chapter 4 aimed at assessing the efficacy of the SC68896/cediranib combination in intracranial mouse glioma. We observed a significant delay in tumor growth using the 4C8 intracranial glioma model, accompanied by a substantial increase in tumor necrosis and improvement in survival. In the absence of a decrease in tumor vascularization, a stabilization of dynamic MRI parameters during the period of tumor growth indicated a possible normalizing effect on the tumor vasculature, as exhibited by restriction of the increases in vascular permeability and inefficiency. Future studies will be dedicated to dissecting underlying mechanistic interactions as mentioned in Section 5.3, verifying the involvement of the Akt pathway in the improved efficacy of the therapeutic combination.

The two therapeutic combinations studied in this thesis present novel and innovative strategies to overcome resistance mechanisms involving the Akt pathway and its downstream effects that compromise the efficacy of RTK inhibitors such as cediranib. Despite the extensive vascularization of such tumors and the development of potent and specific anti-angiogenic agents, patients with glioblastoma only have an average survival of 12-14 months (Lim, *et al.* 2011). The treatment strategies studied here cause not only an over 2 fold increase in mouse survival but also substantially slow down tumor growth and progression, and could potentially provide new hope to glioblastoma patients through

significant improvements in clinical outcome. The therapeutic concepts of autophagy and proteasome inhibition could possibly be used to improve the efficacy of a range of other RTK inhibitors as well and can also be extended to other tumor types known to be resistive to treatment. Taken together, the preclinical studies described in this thesis provide a rationale for the clinical evaluation of two novel treatment combinations that have shown considerable efficacy in a tumor type which is resistive to most conventional forms of therapy.

### 5.2 Evaluate the efficacy of EGFR inhibition with autophagy modulation

In chapters 2 and 3, experiments demonstrated that although 4C8 tumors were mostly resistant to cediranib treatment, a modulation of the autophagic pathway using quinacrine significantly improved the anti-vascular and anti-tumor efficacy. Since autophagy has been shown to contribute to resistance to a range of treatments, it would be very useful to test if this strategy can enhance the therapeutic efficacy of other potentially promising agents that glioma cells are known to be relatively resistant towards.

Signaling through the epidermal growth factor receptor (EGFR) in tumor cells, has been shown to contribute towards proliferation, invasion, angiogenesis and evasion of apoptosis through certain critical survival promoting pathways such as the Akt/mTOR pathway (Figure 1.1) (Rich*, et al.* 2004). The EGFR gene is altered in over 40% of glioblastomas and has been proposed to get tumors "addicted" to the extent that blocking this signal triggers tumor cell death (Joshi*, et al.* 2012, Mellinghoff*, et al.* 2005). RTK inhibitors designed to target the EGFR receptors, such as Erlotinib (Tarceva, Genentech)

and Gefitinib (Iressa, AstraZeneca), have been successfully incorporated into standard clinical treatments for non-small cell lung cancer but have failed Phase II trials for glioblastoma as monotherapy (Han*, et al.* 2011, Kesavabhotla*, et al.* 2012, Rich*, et al.* 2004). Thus, despite the deregulation of this pathway in a majority of malignant gliomas, the EGFR target has not been very therapeutically useful so far. Recently, glioma cells treated with an EGFR kinase inhibitor were shown to exhibit signs of autophagy (Ghildiyal*, et al.* 2012) and in other tumor types, autophagy was shown to contribute to resistance to this treatment (Fung*, et al.* 2012, Han*, et al.* 2011, Li*, et al.* 2010, Zou*, et al.* 2013). Han et al. also showed that human lung cancer cell lines that were relatively resistant to EGFR RTK inhibition had increased autophagic flux relative to sensitive cell lines, suggesting that autophagy could impair the sensitivity of cancer cells to EGFR targeting. We hypothesize that an inhibition of autophagy using the late stage autophagic inhibitor, quinacrine will sensitize glioma cells to EGFR inhibition and trigger a synergistic increase in tumor cell death. We propose to initially test this hypothesis using the 4C8 cell line which was developed through the over-expression of the c-neu oncogene. Since the neu oncogene encodes a tyrosine kinase receptor which exhibits considerable homology to EGFR, the 4C8 glioma model serves as a relevant platform to test the proposed treatment combination (Ross*, et al.* 1998).

Preliminary studies were conducted to test the sensitivity of 4C8 glioma cells to two EGFR inhibitors: erlotinib and gefitinib, through MTS cell viability assays (Figure 5.2). The results suggest that these agents are cytotoxic to 4C8 cells in culture, providing a sensitive system to test for treatment effects. Future studies will be designed to test for

the presence of autophagy in these glioma cells, in response to treatment, and determine if a combination with quinacrine further sensitizes 4C8 cells to EGFR inhibition. The involvement of the Akt/mTOR signaling pathways will also be assessed. Experiments will also be conducted using several patient derived glioblastomas known to have an over-expression of EGFR. Testing of the combination using orthotopic implantations will provide insights into the translatability of treatment effects from the *in vitro* to the *in vivo* setting.

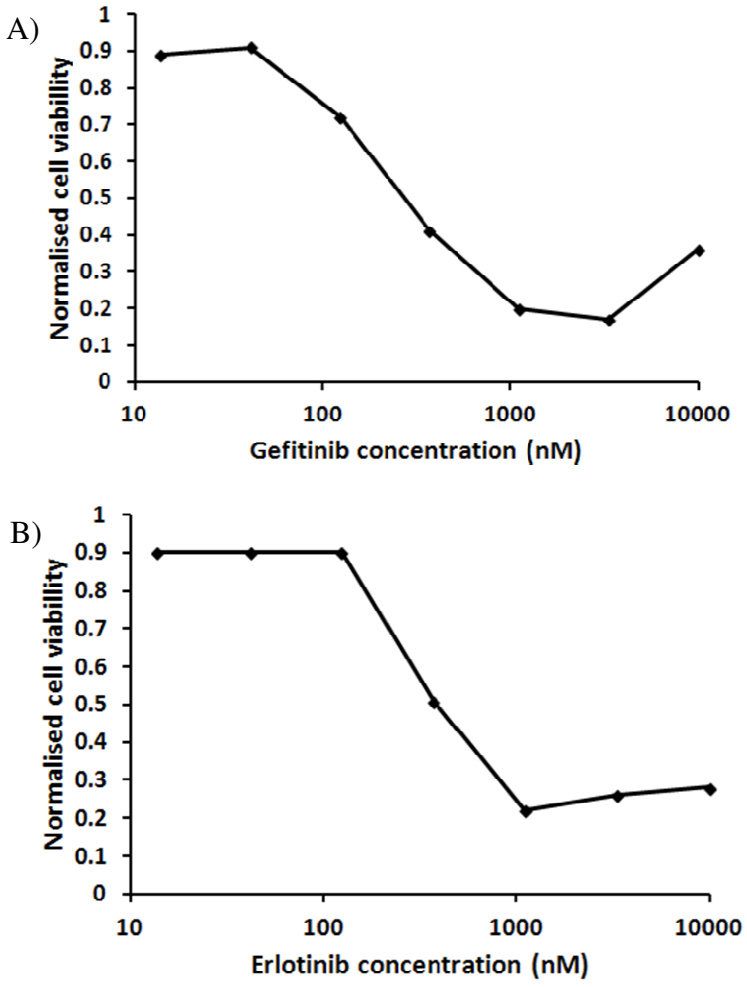


**Figure 5.2. 4C8 cells are sensitive to EGFR inhibition *in vitro*.** Results from MTS cell viability assays showing mean 4C8 cell viability in response to treatment, normalized to untreated samples. Assays were performed after cells were exposed to treatment for 72 hours, under hypoxic (0.5% $O_2$) conditions. Results are from a single preliminary experiment, performed in triplicate. Jeffrey Tyner from the Knight Cancer Institute assisted in generating these data.

These studies will determine if the innovative strategy of autophagy modulation to improve therapeutic outcome, used in chapters 2 and 3, can be expanded to other forms of targeted therapy. Since EGFR is the most commonly activated growth stimulating molecule in malignant glioma, an improvement in treatment efficacy of EGFR inhibitors will prove to be highly advantageous to improving the prognosis of patients.

### 5.3 Determine the mechanistic interactions underlying the synergy between SC68896 and cediranib

Studies described in chapter 4 demonstrated a potent *in vivo* anti-tumor and possibly vascular normalizing effect of the SC68896/cediranib in malignant glioma. While our studies provide an understanding of the potential of this innovative drug combination as a new therapy for malignant glioma, experiments to establish some of the underlying mechanistic interactions are yet to be conducted.

Proteasome inhibition has been maintained as an attractive therapeutic strategy for cancer because of its wide array of anti-tumor effects (Boccadoro, *et al.* 2005, Zhu, *et al.* 2010). Proteasome inhibition has been shown to inhibit the NF-κB pathway and stabilize the p53 tumor suppressor pathway instead. It has been shown to trigger cell cycle arrest and apoptosis through stabilizing proteins such as p21 and p27. Proteasome inhibitors have also shown to potently inhibit the Akt pathway and its downstream effects (Figure 5.1). They can aggravate endoplasmic reticulum (ER) stress by preventing the degradation of unfolded and misfolded proteins as well (Zhu, *et al.* 2010). An increase in oxidative

stress is another anti-tumor effect of proteasome inhibition (Ling, *et al.* 2003, Perez-Galan, *et al.* 2006). Although glioma cells are relatively resistant to proteasome inhibitors as monotherapy (Labussiere, *et al.* 2008), we have shown in chapter 4 that a combination of cediranib and SC68896 can have synergistic anti-glioma effects. Preclinical studies evaluating a combination of Bortezomib with RTK inhibitors such as Sunitinib or Sorafenib in other tumor models have shown that a combined inhibition of the Akt signaling pathway plays a role in anti-tumor effects (Chen, *et al.* 2010, Yeramian, *et al.* 2011, Yu, *et al.* 2006).

Preliminary studies have revealed a dose dependant cytotoxic effect of SC68896 on 4C8 cells in culture, with a half maximal inhibitory concentration of ~1μM under normoxic conditions (Figure 4.7A). Future studies will determine if these effects are mediated through Akt inhibition or the other pleiotropic effects of proteasome inhibitors (Figure 5.1). Future experiments will also probe into changes in ROS generation, in relation to reduced SC68896 cytotoxicity observed under hypoxic conditions (Figures 4.7B and 5.1). Since the protein phosphatase PP2A, which dephosphorylates Akt, is sensitive to proteasomal degradation, a possible mechanism through which SC68896 might block Akt signaling is through the stabiliziation of PP2A. In support of this argument, recent evidence shows that OP449 (Oncotide Pharmaceuticals, NC), a PP2A activator, inhibits Akt in multiple pancreatic tumor cell lines (Figure 5.3). Future experiments will thus determine if SC68896 cytotoxic effects are PP2A dependant. Experiments will also be designed to assess the involvement of PP2A, the Akt pathway and other pleiotropic effects in the synergistic anti-glioma effects of the SC68896/cediranib combination

described in chapter 4. Also, the therapeutic combination will be further tested in patient derived glioblastomas to assess the sensitivity of this treatment strategy in a wide range of glial tumors.

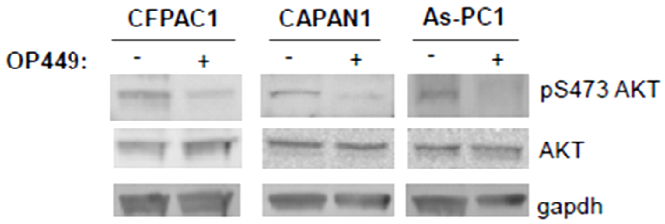


**Figure 5.3. PP2A activator represses Akt activation in tumors.** Representative western blots obtained from 3 pancreatic cancer cell lines after cells were treated for 24 hrs with OP449 (2 μM). Data was generated by Amy Farrell of the Rosalie Sears laboratory.

These future studies may not only provide a mechanistic rationale for the increased tumor necrosis, among other anti-tumor effects seen in Chapter 4, but will also provide new insights into designing better therapeutic combinations that can more effectively overcome treatment resistance in gliomas.

### 5.4 Determine the effects of quinacrine/cediranib and SC68896/cediranib combinations on endothelial cells.

Experiments described in chapters 2, 3 and 4 demonstrated a significant change in tumor dynamic in response to treatment with the quinacrine/cediranib and SC68896/cediranib combinations. With the quinacrine/cediranib combination, we found potent tumor devascularization with substantial reductions in tumor blood flow, blood volume and vascular permeability. The mean vessel density quantified through immunohistochemical analysis of tumor tissue also revealed a 2 fold reduction with combination treatment. On the other hand, with the SC68896/cediranib combination, there was no change in the mean vessel density and the perfusion parameters were maintained at constant levels and

prevented from increasing, as opposed to untreated and single agent treatment groups, suggesting a vascular normalizing effect. We have shown that 4C8 glioma cells are sensitive to quinacrine, cediranib and SC68896 (Figure 2.2 and Figure 4.7). Because there are strong communication links between tumor cells and endothelial cells *in vivo* (Swartz*, et al.* 2012), it is presently unclear if the anti-angiogenic effects documented for these combinations are caused indirectly through a toxicity to glioma cells or a direct toxic insult to the tumor vascular endothelium.

Typical human endothelial cells are mostly quiescent and tend to proliferate only once in many months. Tumor endothelial cells, on the other hand, constantly receive mitogenic signals from the surrounding environment and are stimulated to form new blood vessels (Drexler*, et al.* 2000). Thus therapeutic strategies that can selectively target proliferating endothelial cells would be extremely useful for targeting tumor angiogenesis. It is already known that endothelial cell proliferation is inhibited by cediranib treatment at nanomolar concentrations (Wedge*, et al.* 2005). It has also been shown that endothelial cells are sensitive to proteasome inhibitors as well as to lysosomotropic agents similar to quinacrine such as chloroquine (Belloni*, et al.* 2009, Drexler*, et al.* 2000, Inyang*, et al.* 1990). We hypothesize that both therapeutic combinations: quinacrine/cediranib and SC68896/cediranib exert direct cytotoxic effects on proliferating endothelial cells and that these effects play a role in the enhanced *in vivo* efficacy. Future studies will use human umbilical vein endothelial cells (HUE; ATCC CRL-1730) in culture, to test this hypothesis. Cytotoxic effects of each drug and the combinations will be assessed on quiescent endothelial cells (contact-inhibited or confluent), naturally proliferating cells

(subconfluent) and fibroblast growth factor (FGF) triggered proliferating cells in culture (Belloni, *et al.* 2009). These studies will involve the use of cell viability assays and caspase 3 western blotting. The involvement of the Akt/mTOR signaling pathway and its downstream effects will also be assessed. These studies will provide a clearer understanding of the specific anti-angiogenic effects of the two novel therapeutic combinations and provide further insights into the role of these effects in the overall *in vivo* anti-tumor efficacy documented in Chapters 3 and 4.

**5.5 Determine if loss of PTEN function in glioblastoma contributes to resistance to quinacrine/cediranib or SC68896/cediranib combination treatment.**

Studies described in this thesis focus on two novel therapeutic combinations with cediranib which exhibit enhanced therapeutic effects, possibly through the inhibition of the Akt signaling pathway (Chen, *et al.* 2010, Yu, *et al.* 2006). In tumors that have an activated Akt pathway through the over-expression of growth factors, the tumor suppressor, phosphatase and tensin homolog (PTEN) can effectively reverse this effect and regulate Akt activation (Figure 5.1). Inactivating mutations or deletions of PTEN can contribute to oncogenesis (Burris 2013). Studies have shown that even a 20% reduction in PTEN gene dosage can increase susceptibility to cancer (Alimonti, *et al.* 2010). The PTEN gene is altered in 37% of glioblastomas (Joshi, *et al.* 2012). Alterations in PTEN signaling can cause a hyperactivation of Akt and an uncoupling of the Akt pathway from upstream growth factors including PDGFR and EGFR (She, *et al.* 2003). This can greatly limit the efficacy of therapeutic agents that target such growth factors (Chen, *et al.* 2011, Fenton, *et al.* 2012, Mahimainathan, *et al.* 2004, Mellinghoff, *et al.* 2005, Morgillo, *et al.*

2011, She, *et al.* 2003). Because the two therapeutic combinations, quinacrine/cediranib and SC68896/cediranib involve the RTK inhibition of PDGFR, it is essential to determine if the efficacy of these combinations is compromised in tumors that lack a functional PTEN.

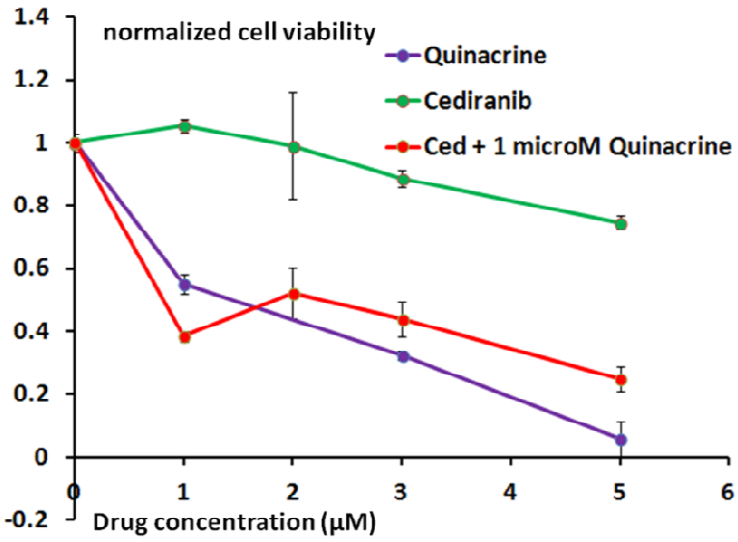


**Figure 5.4. The quinacrine/cediranib combination does not have enhanced glioma cytotoxicity in the PTEN null U87 glioma model, under hypoxic conditions.** Results from MTS cell viability assays showing mean U87 cell viability in response to treatment, normalized to untreated samples. Assays were performed after cells were exposed to treatment for 72 hours, under hypoxic (0.5% $O_2$) conditions. Results are mean ± SEM of three independent experiments, performed in triplicate.

Experiments in chapters 2, 3 and 4 utilized the 4C8 glioma model which has a wild-type PTEN protein expression and demonstrated an enhanced anti-tumor and anti-vascular efficacy with both therapeutic combinations. Preliminary studies were conducted to test the sensitivity of a PTEN null glioma cell line, U87, to the quinacrine/cediranib combination using MTS cell viability assays (Figure 5.4). These experiments were performed under hypoxic (0.5% $O_2$) conditions and reveal a dose dependant reduction in cell viability in response to cediranib and quinacrine treatment. The U87 glioma cells, however, were less sensitive to cediranib treatment compared to the 4C8 glioma cell line

(Figures 2.2 and 5.4). We also observed that the combination of the two agents exhibited no potentiation of cytotoxic effects under hypoxic conditions (Figure 5.4). These results are in contrast to the significantly enhanced anti-glioma efficacy observed with the 4C8 glioma model under hypoxic conditions (Figure 2.2). These preliminary results suggest that the lack of functional PTEN protein expression in U87 glioma cells could be compromising the efficacy of the quinacrine/cediranib combination. Further studies will be performed to assess the sensitivity of other PTEN null tumor models such as U251, U373 and also PTEN wild type tumor models such as LN229 to this treatment combination. Studies will also be conducted to determine the levels of Akt phosphorylation and autophagic vacuole (AV) accumulation in response to treatment. The efficacy of the SC68896/cediranib therapeutic combination will also be investigated using these glioma models.

These future studies may not only provide a better understanding of the mechanistic effects of these novel therapeutic combinations, but will also help assess their limitations. If these future experiments reveal that treatment efficacy is limited in the absence of a functional PTEN protein, and that this is brought about by a constitutive activation of the Akt pathway, studies would be conducted to test for improved efficacy through co-treatment with specific inhibitors of the Akt pathway, downstream of PTEN (She*, et al.* 2003). In the clinical setting, the incorporation of these treatment strategies for glioblastoma might warrant a personalized medicine approach, involving a screening of patient tumor biopsies for the PTEN protein.

**5.6 Obtain a more sensitive assessment of microvascular permeability compared to $K^{trans}$.**

Studies described in this thesis focus on two novel therapeutic combinations with cediranib that exert strong effects on $K^{trans}$, a measure of vascular permeability-surface area product per unit volume of the tissue. The quantification of $K^{trans}$ using the DCE-MRI technique revealed significant decreases in this parameter as a result of quinacrine/cediranib and SC68896/cediranib treatment, while single agent treatment did not cause any substantial differences from untreated mice (Figure 3.4D and 4.4D). The reductions in $K^{trans}$ values could be a result of a decreased presence of tumor vasculature (reduced blood vessel surface area) and/or decreased microvascular permeability.

$$K^{trans} = P_{CA}.S \qquad (5.1)$$

where $P_{CA}$ is microvascular permeability to contrast agent and $S$ is the capillary surface area per unit volume of tissue. To determine if microvascular permeability specifically was affected by treatment, we propose to use a ratio of $K^{trans}$ to rCBV as a more sensitive assessment of changes in endothelial permeability, using the following derivation by our collaborator, Dr. Charles Springer (Senior scientist, Advanced Imaging Research Center, Oregon Health & Science University, Portland, OR):

Assume capillaries are cylinders of radius r and length L

$$A = 2\pi rl \qquad (5.2)$$

$$V = \pi r^2 L \qquad (5.3)$$

where $A$ and $V$ refer to capillary surface area and volume. Using equations 5.2 and 5.3,

$$A = \frac{2}{r}V \qquad (5.4)$$

$$S = \left(\frac{n}{Vt}\right)A = \rho A \qquad (5.5)$$

where $n$ is the number of capillaries, $Vt$ is the volume of tissue and $\rho$ is the capillary density number.

Using equations 5.4 and 5.5,

$$(5.7): \qquad S = \frac{2}{r}\rho V$$

$$(5.8): \qquad CBV = \rho V$$

Using equations 5.7 and 5.8,

$$(5.9): \qquad S = \frac{2}{r}CBV$$

Thus,

$$(5.10): \qquad CBV = \frac{2}{r}S$$

Using equations 5.1 and 5.10,

$$(5.11): \qquad \frac{K^{trans}}{CBV} = \frac{r}{2}P_{CA}$$

Thus,

$$(5.12): \qquad \frac{K^{trans}}{CBV} = C.P_{CA}$$

where $C$ is a coefficient that depends on the mean tumor vascular $r$ value.

Figure 5.5 A and B show the variations of mean tumor $K^{trans}$/rCBV during the treatment period in response to treatment with single agent or combination of quinacrine and cediranib, and SC68896 and cediranib, respectively. Figure 5.5A reveals that cediranib treatment resulted in significant reductions in ratios of $K^{trans}$ to rCBV, suggesting that microvascular permeability was reduced by cediranib. This is in agreement with the anti-angiogenic action of cediranib, through the inhibition of VEGFR signaling.

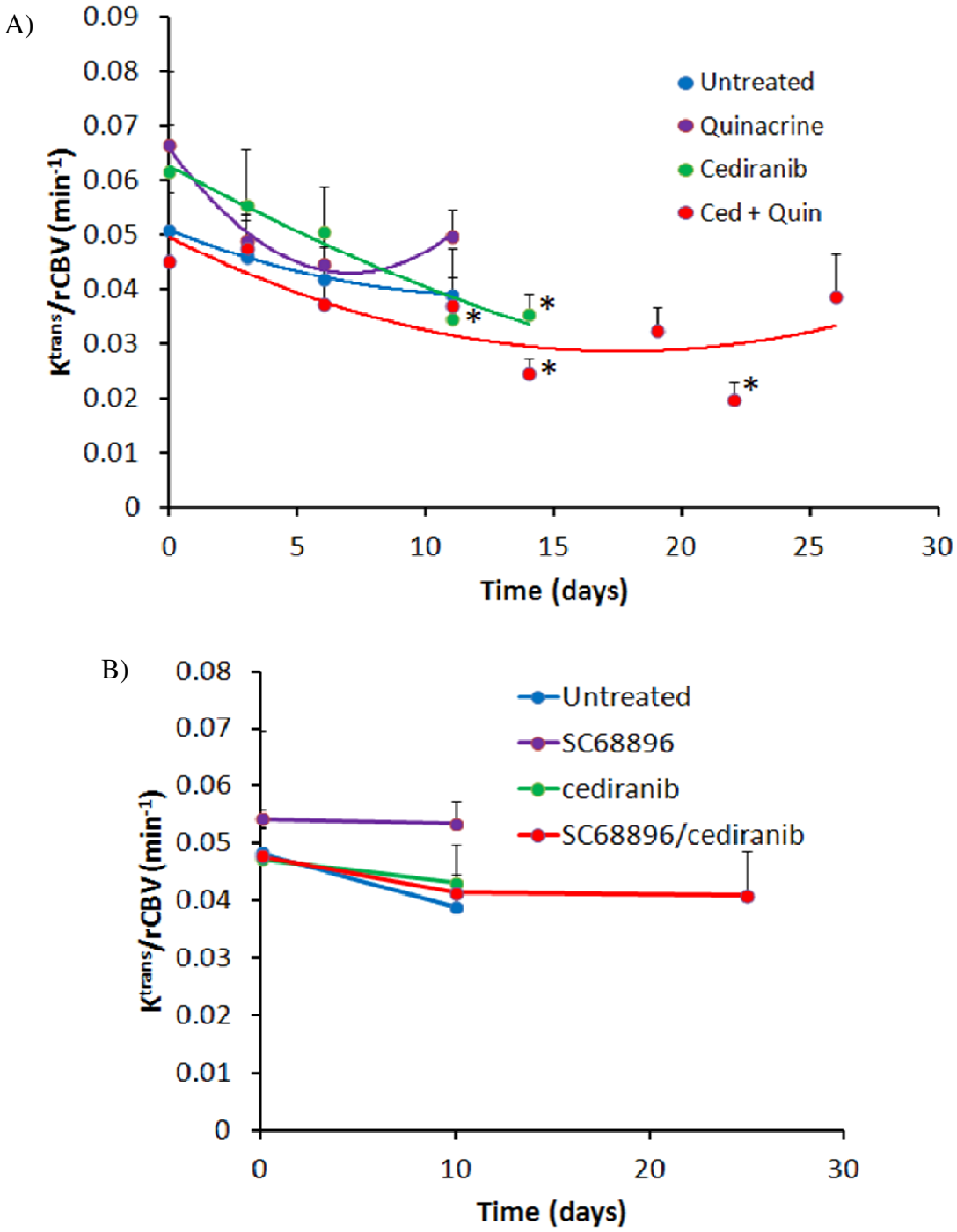


**Figure 5.5. Assessment of treatment effects of quinacrine/cediranib and SC68896/cediranib combinations on microvascular permeability, as assessed by ratios of $K^{trans}$ to rCBV.** Mean tumor $K^{trans}$/rCBV in response to treatment with single agent and combination of A) quinacrine and cediranib, and B) SC68896 and cediranib. Values plotted versus the time from tumor growth initiation for the four different treatment groups. The two-tailed Unpaired Student's t test (NCSS Statistical Software, (Kaysville, UT) was employed to test for differences from the pre-treatment time-point within each group. *: $p < 0.05$ versus untreated.

Quinacrine/cediranib treatment may have also resulted in reductions in microvascular permeability, but these changes were not consistent throughout the treatment period. Treatment with SC68896/cediranib did not cause any changes in microvascular permeability. These data suggest that the significant reductions in $K^{trans}$ in response to quinacrine/cediranib and SC68896/cediranib combination treatment, seen in Chapters 3 and 4, were most likely due to reductions in capillary surface area.

We propose that future studies employing the ratio of $K^{trans}$ to rCBV will provide a more accurate assessment of changes in endothelial permeability. The quantification of this parameter provides an excellent assessment of blood brain barrier integrity. Microvascular permeability has been shown to correlate with brain tumor grade and is also used to monitor treatment effects. It is known that reductions in tumor microvascular permeability has a number of advantages such as reduction in edema, inflammation, intravasation and metastatic spread of tumor cells, and tumor interstitial fluid pressure. Since changes in $K^{trans}$ may not always reflect changes in microvascular permeability, the more specific assessment of changes in this parameter through ratios of $K^{trans}$ to rCBV may prove to be very useful.

# References


Akella NS, Twieg DB, Mikkelsen T, Hochberg FH, Grossman S, Cloud GA and Nabors LB. Assessment of brain tumor angiogenesis inhibitors using perfusion magnetic resonance imaging: quality and analysis results of a phase I trial. *J Magn Reson Imaging*. 2004;20:913-22.

Alimonti A, Carracedo A, Clohessy JG, Trotman LC, Nardella C, Egia A, Salmena L, Sampieri K, Haveman WJ, Brogi E, Richardson AL, Zhang J and Pandolfi PP. Subtle variations in Pten dose determine cancer susceptibility. *Nat Genet*. 2010;42:454-8.

Amaravadi R. Autophagy can contribute to cell death when combining targeted therapy. *Cancer Biol Ther*. 2009;8:130-3.

Amberger-Murphy V. Hypoxia helps glioma to fight therapy. *Curr Cancer Drug Targets*. 2009;9:381-90.

Arora A and Scholar EM. Role of tyrosine kinase inhibitors in cancer therapy. *J Pharmacol Exp Ther*. 2005;315:971-9.

Barrett T, Brechbiel M, Bernardo M and Choyke PL. MRI of tumor angiogenesis. *J Magn Reson Imaging*. 2007;26:235-49.

Batchelor TT, Sorensen AG, di Tomaso E, Zhang WT, Duda DG, Cohen KS, Kozak KR, Cahill DP, Chen PJ, Zhu M, Ancukiewicz M, Mrugala MM, Plotkin S, Drappatz J, Louis DN, Ivy P, Scadden DT, Benner T, Loeffler JS, Wen PY and Jain RK. AZD2171, a pan-VEGF receptor tyrosine kinase inhibitor, normalizes tumor vasculature and alleviates edema in glioblastoma patients. *Cancer Cell*. 2007;11:83-95.

Belloni D, Veschini L, Foglieni C, Dell'Antonio G, Caligaris-Cappio F, Ferrarini M and Ferrero E. Bortezomib induces autophagic death in proliferating human endothelial cells. *Exp Cell Res*. 2009;316:1010-8.

Bergers G and Hanahan D. Modes of resistance to anti-angiogenic therapy. *Nat Rev Cancer*. 2008;8:592-603.

Boccadoro M, Morgan G and Cavenagh J. Preclinical evaluation of the proteasome inhibitor bortezomib in cancer therapy. *Cancer Cell Int*. 2005;5:18.

Boya P and Kroemer G. Lysosomal membrane permeabilization in cell death. *Oncogene*. 2008;27:6434-51.

Bradley DP, Tessier JJ, Lacey T, Scott M, Jurgensmeier JM, Odedra R, Mills J, Kilburn L and Wedge SR. Examining the acute effects of cediranib (RECENTIN, AZD2171) treatment in tumor models: a dynamic contrast-enhanced MRI study using gadopentate. *Magn Reson Imaging*. 2009;27:377-84.

Brat DJ and Mapstone TB. Malignant glioma physiology: cellular response to hypoxia and its role in tumor progression. *Ann Intern Med*. 2003;138:659-68.

Burris HA, 3rd. Overcoming acquired resistance to anticancer therapy: focus on the PI3K/AKT/mTOR pathway. *Cancer Chemother Pharmacol*. 2013;71:829-42.

Cairns RA, Papandreou I, Sutphin PD and Denko NC. Metabolic targeting of hypoxia and HIF1 in solid tumors can enhance cytotoxic chemotherapy. *Proc Natl Acad Sci U S A*. 2007;104:9445-50.

Calamante F. Bolus dispersion issues related to the quantification of perfusion MRI data. *J Magn Reson Imaging*. 2005;22:718-22.

Cao Y and Langer R. A review of Judah Folkman's remarkable achievements in biomedicine. *Proc Natl Acad Sci U S A*. 2008;105:13203-5.

Chen KF, Yeh PY, Yeh KH, Lu YS, Huang SY and Cheng AL. Down-regulation of phospho-Akt is a major molecular determinant of bortezomib-induced apoptosis in hepatocellular carcinoma cells. *Cancer Res*. 2008;68:6698-707.

Chen KF, Yu HC, Liu TH, Lee SS, Chen PJ and Cheng AL. Synergistic interactions between sorafenib and bortezomib in hepatocellular carcinoma involve PP2A-dependent Akt inactivation. *J Hepatol*. 2010;52:88-95.

Chen KF, Chen HL, Tai WT, Feng WC, Hsu CH, Chen PJ and Cheng AL. Activation of phosphatidylinositol 3-kinase/Akt signaling pathway mediates acquired resistance to sorafenib in hepatocellular carcinoma cells. *J Pharmacol Exp Ther*. 2011;337:155-61.

Crawford LJ, Walker B and Irvine AE. Proteasome inhibitors in cancer therapy. *J Cell Commun Signal*. 2011;5:101-10.

Dalby KN, Tekedereli I, Lopez-Berestein G and Ozpolat B. Targeting the prodeath and prosurvival functions of autophagy as novel therapeutic strategies in cancer. *Autophagy*. 2010;6:322-9.

De Witt Hamer PC. Small molecule kinase inhibitors in glioblastoma: a systematic review of clinical studies. *Neuro Oncol*. 2010;12:304-16.

Degtyarev M, De Maziere A, Orr C, Lin J, Lee BB, Tien JY, Prior WW, van Dijk S, Wu H, Gray DC, Davis DP, Stern HM, Murray LJ, Hoeflich KP, Klumperman J, Friedman LS and Lin K. Akt inhibition promotes autophagy and sensitizes PTEN-null tumors to lysosomotropic agents. *J Cell Biol*. 2008;183:101-16.

Dietrich J, Wang D and Batchelor TT. Cediranib: profile of a novel anti-angiogenic agent in patients with glioblastoma. *Expert Opin Investig Drugs*. 2009;18:1549-57.

Drexler HC, Risau W and Konerding MA. Inhibition of proteasome function induces programmed cell death in proliferating endothelial cells. *FASEB J*. 2000;14:65-77.

Dyer CA and Philibotte T. A clone of the MOCH-1 glial tumor in culture: multiple phenotypes expressed under different environmental conditions. *J Neuropathol Exp Neurol*. 1995;54:852-63.

Ehsanian R, Van Waes C and Feller SM. Beyond DNA binding - a review of the potential mechanisms mediating quinacrine's therapeutic activities in parasitic infections, inflammation, and cancers. *Cell Commun Signal*. 2011;9:13.

Eichhorn ME, Kleespies A, Angele MK, Jauch KW and Bruns CJ. Angiogenesis in cancer: molecular mechanisms, clinical impact. *Langenbecks Arch Surg*. 2007;392:371-9.

Evans SM, Judy KD, Dunphy I, Jenkins WT, Hwang WT, Nelson PT, Lustig RA, Jenkins K, Magarelli DP, Hahn SM, Collins RA, Grady MS and Koch CJ. Hypoxia is important in the biology and aggression of human glial brain tumors. *Clin Cancer Res*. 2004;10:8177-84.

Farrar CT, Kamoun WS, Ley CD, Kim YR, Catana C, Kwon SJ, Rosen BR, Jain RK and Sorensen AG. Sensitivity of MRI tumor biomarkers to VEGFR inhibitor therapy in an orthotopic mouse glioma model. *PLoS One*. 2011;6:e17228.

Fenton TR, Nathanson D, Ponte de Albuquerque C, Kuga D, Iwanami A, Dang J, Yang H, Tanaka K, Oba-Shinjo SM, Uno M, Inda MM, Wykosky J, Bachoo RM, James CD, DePinho RA, Vandenberg SR, Zhou H, Marie SK, Mischel PS, Cavenee WK and Furnari FB. Resistance to EGF receptor inhibitors in glioblastoma mediated by phosphorylation

of the PTEN tumor suppressor at tyrosine 240. *Proc Natl Acad Sci U S A*. 2012;109:14164-9.

Fukumura D and Jain RK. Tumor microvasculature and microenvironment: targets for anti-angiogenesis and normalization. *Microvasc Res*. 2007;74:72-84.

Fung C, Chen X, Grandis JR and Duvvuri U. EGFR tyrosine kinase inhibition induces autophagy in cancer cells. *Cancer Biol Ther*. 2012;13:1417-24.

Geng Y, Kohli L, Klocke BJ and Roth KA. Chloroquine-induced autophagic vacuole accumulation and cell death in glioma cells is p53 independent. *Neuro Oncol*. 2010;12:473-81.

Ghildiyal R, Dixit D and Sen E. EGFR inhibitor BIBU induces apoptosis and defective autophagy in glioma cells. *Mol Carcinog*. 2012.

Gladson CL, Prayson RA and Liu WM. The pathobiology of glioma tumors. *Annu Rev Pathol*. 2010;5:33-50.

Goel S, Wong AH and Jain RK. Vascular normalization as a therapeutic strategy for malignant and nonmalignant disease. *Cold Spring Harb Perspect Med*. 2012;2:a006486.

Gotink KJ and Verheul HM. Anti-angiogenic tyrosine kinase inhibitors: what is their mechanism of action? *Angiogenesis*. 2010;13:1-14.

Grepin R and Pages G. Molecular mechanisms of resistance to tumour anti-angiogenic strategies. *J Oncol*. 2010;2010:835680.

Guo C, Gasparian AV, Zhuang Z, Bosykh DA, Komar AA, Gudkov AV and Gurova KV. 9-Aminoacridine-based anticancer drugs target the PI3K/AKT/mTOR, NF-kappaB and p53 pathways. *Oncogene*. 2009;28:1151-61.

Gupta A, Roy S, Lazar AJ, Wang WL, McAuliffe JC, Reynoso D, McMahon J, Taguchi T, Floris G, Debiec-Rychter M, Schoffski P, Trent JA, Debnath J and Rubin BP. Autophagy inhibition and antimalarials promote cell death in gastrointestinal stromal tumor (GIST). *Proc Natl Acad Sci U S A*. 2010;107:14333-8.

Gurova K. New hopes from old drugs: revisiting DNA-binding small molecules as anticancer agents. *Future Oncol*. 2009;5:1685-704.

Han W, Pan H, Chen Y, Sun J, Wang Y, Li J, Ge W, Feng L, Lin X, Wang X and Jin H. EGFR tyrosine kinase inhibitors activate autophagy as a cytoprotective response in human lung cancer cells. *PLoS One*. 2011;6:e18691.

Hardee ME and Zagzag D. Mechanisms of glioma-associated neovascularization. *Am J Pathol*. 2012;181:1126-41.

Honma Y, Shimizu S, Takehara T and Harada M. Sorafenib enhances proteasome inhibitor-induced cell death via inactivation of Akt and stress-activated protein kinases. *J Gastroenterol*. 2013.

Hoyer-Hansen M and Jaattela M. Autophagy: an emerging target for cancer therapy. *Autophagy*. 2008;4:574-80.

Hu YL, DeLay M, Jahangiri A, Molinaro AM, Rose SD, Carbonell WS and Aghi MK. Hypoxia-induced autophagy promotes tumor cell survival and adaptation to antiangiogenic treatment in glioblastoma. *Cancer Res*. 2012;72:1773-83.

Huang W, Li X, Morris EA, Tudorica LA, Seshan VE, Rooney WD, Tagge I, Wang Y, Xu J and Springer CS. The magnetic resonance shutter speed discriminates vascular properties of malignant and benign breast tumors in vivo. *Proc Natl Acad Sci U S A*. 2008;105:17943-8.

Inyang AL, Bikfalvi A, Lu H and Tobelem G. Chloroquine's modulation of endothelial cell activity induced with basic fibroblast growth factor and human serum: effect on mitogenesis, protease production and cell migration. *Cell Biol Int Rep*. 1990;14:35-46.

Izuishi K, Kato K, Ogura T, Kinoshita T and Esumi H. Remarkable tolerance of tumor cells to nutrient deprivation: possible new biochemical target for cancer therapy. *Cancer Res*. 2000;60:6201-7.

Izumi Y, Xu L, di Tomaso E, Fukumura D and Jain RK. Tumour biology: herceptin acts as an anti-angiogenic cocktail. *Nature*. 2002;416:279-80.

Jackson A, Jayson GC, Li KL, Zhu XP, Checkley DR, Tessier JJ and Waterton JC. Reproducibility of quantitative dynamic contrast-enhanced MRI in newly presenting glioma. *Br J Radiol*. 2003;76:153-62.

Jackson A, O'Connor JP, Parker GJ and Jayson GC. Imaging tumor vascular heterogeneity and angiogenesis using dynamic contrast-enhanced magnetic resonance imaging. *Clin Cancer Res*. 2007;13:3449-59.

Jiang BH, Zheng JZ, Aoki M and Vogt PK. Phosphatidylinositol 3-kinase signaling mediates angiogenesis and expression of vascular endothelial growth factor in endothelial cells. *Proc Natl Acad Sci U S A*. 2000;97:1749-53.

Joshi AD, Loilome W, Siu IM, Tyler B, Gallia GL and Riggins GJ. Evaluation of tyrosine kinase inhibitor combinations for glioblastoma therapy. *PLoS One*. 2012;7:e44372.

Jung CH, Ro SH, Cao J, Otto NM and Kim DH. mTOR regulation of autophagy. *FEBS Lett*. 2010;584:1287-95.

Kamoun WS, Ley CD, Farrar CT, Duyverman AM, Lahdenranta J, Lacorre DA, Batchelor TT, di Tomaso E, Duda DG, Munn LL, Fukumura D, Sorensen AG and Jain RK. Edema control by cediranib, a vascular endothelial growth factor receptor-targeted kinase inhibitor, prolongs survival despite persistent brain tumor growth in mice. *J Clin Oncol*. 2009;27:2542-52.

Kesavabhotla K, Schlaff CD, Shin B, Mubita L, Kaplan R, Tsiouris AJ, Pannullo SC, Christos P, Lavi E, Scheff R and Boockvar JA. Phase I/II study of oral erlotinib for treatment of relapsed/refractory glioblastoma multiforme and anaplastic astrocytoma. *J Exp Ther Oncol*. 2012;10:71-81.

Kisselev AF, van der Linden WA and Overkleeft HS. Proteasome inhibitors: an expanding army attacking a unique target. *Chem Biol*. 2012;19:99-115.

Kunz M and Ibrahim SM. Molecular responses to hypoxia in tumor cells. *Mol Cancer*. 2003;2:23.

Labussiere M, Pinel S, Delfortrie S, Plenat F and Chastagner P. Proteasome inhibition by bortezomib does not translate into efficacy on two malignant glioma xenografts. *Oncol Rep*. 2008;20:1283-7.

Leban J, Blisse M, Krauss B, Rath S, Baumgartner R and Seifert MH. Proteasome inhibition by peptide-semicarbazones. *Bioorg Med Chem*. 2008;16:4579-88.

Lemasters JJ. Modulation of mitochondrial membrane permeability in pathogenesis, autophagy and control of metabolism. *J Gastroenterol Hepatol*. 2007;22 Suppl 1:S31-7.

Levine B and Yuan J. Autophagy in cell death: an innocent convict? *J Clin Invest*. 2005;115:2679-88.

Li PX, Kong F, Hu CL, Zhao N and Mao JG. A series of new phases containing three different asymmetric building units. *Inorg Chem*. 2010;49:5943-52.

Lim SK, Llaguno SR, McKay RM and Parada LF. Glioblastoma multiforme: a perspective on recent findings in human cancer and mouse models. *BMB Rep*. 2011;44:158-64.

Lin YC, Chen KC, Chen CC, Cheng AL and Chen KF. CIP2A-mediated Akt activation plays a role in bortezomib-induced apoptosis in head and neck squamous cell carcinoma cells. *Oral Oncol*. 2012;48:585-93.

Ling YH, Liebes L, Zou Y and Perez-Soler R. Reactive oxygen species generation and mitochondrial dysfunction in the apoptotic response to Bortezomib, a novel proteasome inhibitor, in human H460 non-small cell lung cancer cells. *J Biol Chem*. 2003;278:33714-23.

Loges S, Schmidt T and Carmeliet P. Mechanisms of resistance to anti-angiogenic therapy and development of third-generation anti-angiogenic drug candidates. *Genes Cancer*. 2010;1:12-25.

Mahimainathan L and Choudhury GG. Inactivation of platelet-derived growth factor receptor by the tumor suppressor PTEN provides a novel mechanism of action of the phosphatase. *J Biol Chem*. 2004;279:15258-68.

Mani A and Gelmann EP. The ubiquitin-proteasome pathway and its role in cancer. *J Clin Oncol*. 2005;23:4776-89.

Mathew R, Karantza-Wadsworth V and White E. Role of autophagy in cancer. *Nat Rev Cancer*. 2007;7:961-7.

Mellinghoff IK, Wang MY, Vivanco I, Haas-Kogan DA, Zhu S, Dia EQ, Lu KV, Yoshimoto K, Huang JH, Chute DJ, Riggs BL, Horvath S, Liau LM, Cavenee WK, Rao PN, Beroukhim R, Peck TC, Lee JC, Sellers WR, Stokoe D, Prados M, Cloughesy TF, Sawyers CL and Mischel PS. Molecular determinants of the response of glioblastomas to EGFR kinase inhibitors. *N Engl J Med*. 2005;353:2012-24.

Mirzoeva OK, Hann B, Hom YK, Debnath J, Aftab D, Shokat K and Korn WM. Autophagy suppression promotes apoptotic cell death in response to inhibition of the PI3K-mTOR pathway in pancreatic adenocarcinoma. *J Mol Med (Berl)*. 2011;89:877-89.

Mizushima N. The pleiotropic role of autophagy: from protein metabolism to bactericide. *Cell Death Differ*. 2005;12 Suppl 2:1535-41.

Morgillo F, Martinelli E, Troiani T, Orditura M, De Vita F and Ciardiello F. Antitumor activity of sorafenib in human cancer cell lines with acquired resistance to EGFR and VEGFR tyrosine kinase inhibitors. *PLoS One*. 2011;6:e28841.

Norden AD, Drappatz J and Wen PY. Antiangiogenic therapies for high-grade glioma. *Nat Rev Neurol*. 2009;5:610-20.

O'Connor JP, Jackson A, Parker GJ and Jayson GC. DCE-MRI biomarkers in the clinical evaluation of antiangiogenic and vascular disrupting agents. *Br J Cancer*. 2007;96:189-95.

O'Connor JP, Jackson A, Parker GJ, Roberts C and Jayson GC. Dynamic contrast-enhanced MRI in clinical trials of antivascular therapies. *Nat Rev Clin Oncol*. 2012;9:167-77.

Ohshima-Hosoyama S, Davare MA, Hosoyama T, Nelon LD and Keller C. Bortezomib stabilizes NOXA and triggers ROS-associated apoptosis in medulloblastoma. *J Neurooncol*. 2011;105:475-83.

Orlowski RZ and Kuhn DJ. Proteasome inhibitors in cancer therapy: lessons from the first decade. *Clin Cancer Res*. 2008;14:1649-57.

Ostergaard L, Weisskoff RM, Chesler DA, Gyldensted C and Rosen BR. High resolution measurement of cerebral blood flow using intravascular tracer bolus passages. Part I: Mathematical approach and statistical analysis. *Magn Reson Med*. 1996;36:715-25.

Perez-Galan P, Roue G, Villamor N, Montserrat E, Campo E and Colomer D. The proteasome inhibitor bortezomib induces apoptosis in mantle-cell lymphoma through generation of ROS and Noxa activation independent of p53 status. *Blood*. 2006;107:257-64.

Pike MM, Stoops CN, Langford CP, Akella NS, Nabors LB and Gillespie GY. High-resolution longitudinal assessment of flow and permeability in mouse glioma vasculature: Sequential small molecule and SPIO dynamic contrast agent MRI. *Magn Reson Med*. 2009;61:615-25.

Polytarchou C, Iliopoulos D, Hatziapostolou M, Kottakis F, Maroulakou I, Struhl K and Tsichlis PN. Akt2 regulates all Akt isoforms and promotes resistance to hypoxia through induction of miR-21 upon oxygen deprivation. *Cancer Res*. 2011;71:4720-31.

Populo H, Lopes JM and Soares P. The mTOR Signalling Pathway in Human Cancer. *Int J Mol Sci*. 2012;13:1886-918.

Preusser M, de Ribaupierre S, Wohrer A, Erridge SC, Hegi M, Weller M and Stupp R. Current concepts and management of glioblastoma. *Ann Neurol*. 2011;70:9-21.

Rabinowitz JD and White E. Autophagy and metabolism. *Science*. 2009;330:1344-8.

Rahman R, Smith S, Rahman C and Grundy R. Antiangiogenic therapy and mechanisms of tumor resistance in malignant glioma. *J Oncol*. 2010;2010:251231.

Rausch V, Liu L, Apel A, Rettig T, Gladkich J, Labsch S, Kallifatidis G, Kaczorowski A, Groth A, Gross W, Gebhard MM, Schemmer P, Werner J, Salnikov AV, Zentgraf H, Buchler MW and Herr I. Autophagy mediates survival of pancreatic tumour-initiating cells in a hypoxic microenvironment. *J Pathol*. 2012;227:325-35.

Ribatti D. Judah Folkman, a pioneer in the study of angiogenesis. *Angiogenesis*. 2008;11:3-10.

Rich JN, Reardon DA, Peery T, Dowell JM, Quinn JA, Penne KL, Wikstrand CJ, Van Duyn LB, Dancey JE, McLendon RE, Kao JC, Stenzel TT, Ahmed Rasheed BK, Tourt-Uhlig SE, Herndon JE, 2nd, Vredenburgh JJ, Sampson JH, Friedman AH, Bigner DD and Friedman HS. Phase II trial of gefitinib in recurrent glioblastoma. *J Clin Oncol*. 2004;22:133-42.

Rong Y, Durden DL, Van Meir EG and Brat DJ. 'Pseudopalisading' necrosis in glioblastoma: a familiar morphologic feature that links vascular pathology, hypoxia, and angiogenesis. *J Neuropathol Exp Neurol*. 2006;65:529-39.

Ross JS and Fletcher JA. The HER-2/neu Oncogene in Breast Cancer: Prognostic Factor, Predictive Factor, and Target for Therapy. *Oncologist*. 1998;3:237-252.

Roth P, Kissel M, Herrmann C, Eisele G, Leban J, Weller M and Schmidt F. SC68896, a novel small molecule proteasome inhibitor, exerts antiglioma activity in vitro and in vivo. *Clin Cancer Res*. 2009;15:6609-18.

Schabel MC, DiBella EV, Jensen RL and Salzman KL. A model-constrained Monte Carlo method for blind arterial input function estimation in dynamic contrast-enhanced MRI: II. In vivo results. *Phys Med Biol*. 2010;55:4807-23.

Schabel MC, Fluckiger JU and DiBella EV. A model-constrained Monte Carlo method for blind arterial input function estimation in dynamic contrast-enhanced MRI: I. Simulations. *Phys Med Biol*. 2010;55:4783-806.

She QB, Solit D, Basso A and Moasser MM. Resistance to gefitinib in PTEN-null HER-overexpressing tumor cells can be overcome through restoration of PTEN function or pharmacologic modulation of constitutive phosphatidylinositol 3'-kinase/Akt pathway signaling. *Clin Cancer Res*. 2003;9:4340-6.

Shen C, Wang W, Tao L, Liu B, Yang Z and Tao H. Chloroquine blocks the autophagic process in cisplatin-resistant osteosarcoma cells by regulating the expression of p62/SQSTM1. *Int J Mol Med*. 2013.

Shimizu S, Takehara T, Hikita H, Kodama T, Tsunematsu H, Miyagi T, Hosui A, Ishida H, Tatsumi T, Kanto T, Hiramatsu N, Fujita N, Yoshimori T and Hayashi N. Inhibition of autophagy potentiates the antitumor effect of the multikinase inhibitor sorafenib in hepatocellular carcinoma. *Int J Cancer*. 2011;131:548-57.

Shingu T, Fujiwara K, Bogler O, Akiyama Y, Moritake K, Shinojima N, Tamada Y, Yokoyama T and Kondo S. Inhibition of autophagy at a late stage enhances imatinib-induced cytotoxicity in human malignant glioma cells. *Int J Cancer*. 2009;124:1060-71.

Shintani T and Klionsky DJ. Autophagy in health and disease: a double-edged sword. *Science*. 2004;306:990-5.

Sorensen AG. Magnetic resonance as a cancer imaging biomarker. *J Clin Oncol*. 2006;24:3274-81.

Sourbron S, Heilmann M, Biffar A, Walczak C, Vautier J, Volk A and Peller M. Bolus-tracking MRI with a simultaneous T1- and T2*-measurement. *Magn Reson Med*. 2009;62:672-81.

Sourbron SP and Buckley DL. Tracer kinetic modelling in MRI: estimating perfusion and capillary permeability. *Phys Med Biol*. 2012;57:R1-33.

Stegeman H, Kaanders JH, Wheeler DL, van der Kogel AJ, Verheijen MM, Waaijer SJ, Iida M, Grenman R, Span PN and Bussink J. Activation of AKT by hypoxia: a potential target for hypoxic tumors of the head and neck. *BMC Cancer*. 2012;12:463.

Swartz MA, Iida N, Roberts EW, Sangaletti S, Wong MH, Yull FE, Coussens LM and DeClerck YA. Tumor microenvironment complexity: emerging roles in cancer therapy. *Cancer Res*. 2012;72:2473-80.

Tabatabai G and Stupp R. Primetime for antiangiogenic therapy. *Curr Opin Neurol*. 2009;22:639-44.

Thomas DL, Lythgoe MF, Pell GS, Calamante F and Ordidge RJ. The measurement of diffusion and perfusion in biological systems using magnetic resonance imaging. *Phys Med Biol*. 2000;45:R97-138.

Tofts PS, Brix G, Buckley DL, Evelhoch JL, Henderson E, Knopp MV, Larsson HB, Lee TY, Mayr NA, Parker GJ, Port RE, Taylor J and Weisskoff RM. Estimating kinetic parameters from dynamic contrast-enhanced T(1)-weighted MRI of a diffusable tracer: standardized quantities and symbols. *J Magn Reson Imaging*. 1999;10:223-32.

Tschan MP and Simon HU. The role of autophagy in anticancer therapy: promises and uncertainties. *J Intern Med*. 2010;268:410-8.

Van Meir EG, Hadjipanayis CG, Norden AD, Shu HK, Wen PY and Olson JJ. Exciting new advances in neuro-oncology: the avenue to a cure for malignant glioma. *CA Cancer J Clin*. 2010;60:166-93.

Wang T, Oberoi RK and Elmquist WF. Determination of cediranib in mouse plasma and brain tissue using high-performance liquid chromatography-mass spectrometry. *J Chromatogr B Analyt Technol Biomed Life Sci*. 2011;879:3812-7.

Wang YY, Luan Y, Zhang X, Lin M, Zhang ZH, Zhu XB, Ma Y and Wang YB. Proteasome inhibitor PS-341 attenuates flow-induced pulmonary arterial hypertension. *Clin Exp Med*. 2013.

Wedge SR, Kendrew J, Hennequin LF, Valentine PJ, Barry ST, Brave SR, Smith NR, James NH, Dukes M, Curwen JO, Chester R, Jackson JA, Boffey SJ, Kilburn LL, Barnett S, Richmond GH, Wadsworth PF, Walker M, Bigley AL, Taylor ST, Cooper L, Beck S, Jurgensmeier JM and Ogilvie DJ. AZD2171: a highly potent, orally bioavailable, vascular endothelial growth factor receptor-2 tyrosine kinase inhibitor for the treatment of cancer. *Cancer Res*. 2005;65:4389-400.

Westphal M and Lamszus K. The neurobiology of gliomas: from cell biology to the development of therapeutic approaches. *Nat Rev Neurosci*. 2011;12:495-508.

Winkler F, Kozin SV, Tong RT, Chae SS, Booth MF, Garkavtsev I, Xu L, Hicklin DJ, Fukumura D, di Tomaso E, Munn LL and Jain RK. Kinetics of vascular normalization by VEGFR2 blockade governs brain tumor response to radiation: role of oxygenation, angiopoietin-1, and matrix metalloproteinases. *Cancer Cell*. 2004;6:553-63.

Yamamoto A, Tagawa Y, Yoshimori T, Moriyama Y, Masaki R and Tashiro Y. Bafilomycin A1 prevents maturation of autophagic vacuoles by inhibiting fusion between autophagosomes and lysosomes in rat hepatoma cell line, H-4-II-E cells. *Cell Struct Funct*. 1998;23:33-42.

Yeramian A, Sorolla A, Velasco A, Santacana M, Dolcet X, Valls J, Abal L, Moreno S, Egido R, Casanova JM, Puig S, Vilella R, Llombart-Cussac A, Matias-Guiu X and Marti RM. Inhibition of activated receptor tyrosine kinases by Sunitinib induces growth arrest and sensitizes melanoma cells to Bortezomib by blocking Akt pathway. *Int J Cancer*. 2011;130:967-78.

Yu C, Friday BB, Lai JP, Yang L, Sarkaria J, Kay NE, Carter CA, Roberts LR, Kaufmann SH and Adjei AA. Cytotoxic synergy between the multikinase inhibitor sorafenib and the proteasome inhibitor bortezomib in vitro: induction of apoptosis through Akt and c-Jun NH2-terminal kinase pathways. *Mol Cancer Ther*. 2006;5:2378-87.

Yung L, Huang Y, Lessard P, Legname G, Lin ET, Baldwin M, Prusiner SB, Ryou C and Guglielmo BJ. Pharmacokinetics of quinacrine in the treatment of prion disease. *BMC Infect Dis*. 2004;4:53.

Zhang J, Yang PL and Gray NS. Targeting cancer with small molecule kinase inhibitors. *Nat Rev Cancer*. 2009;9:28-39.

Zhao YW, Jin L, Li ZM, Zhao CJ, Wei YQ and Yang HS. Enhanced antitumor efficacy by blocking activation of the phosphatidylinositol 3-kinase/Akt pathway during anti-angiogenesis therapy. *Cancer Sci*. 2011;102:1469-75.

Zhu K, Dunner K, Jr. and McConkey DJ. Proteasome inhibitors activate autophagy as a cytoprotective response in human prostate cancer cells. *Oncogene*. 2010;29:451-62.

Zou Y, Ling YH, Sironi J, Schwartz EL, Perez-Soler R and Piperdi B. The autophagy inhibitor chloroquine overcomes the innate resistance of wild-type EGFR non-small-cell lung cancer cells to erlotinib. *J Thorac Oncol*. 2013;8:693-702.